DISSERTATION

Ab initio theory of electric transport in nanostructures

ausgeführt zum Zwecke der Erlangung des akademischen Grades eines
Doktors der technischen Wissenschaften
unter der Leitung von

Univ.Prof. Dr.phil. Peter Weinberger
Institutsnummer: E 134
Institut für Allgemeine Physik

eingereicht an der Technischen Universität Wien
an der Technisch-Naturwissenschaftlichen Fakultät

von

Krisztián Palotás
Matrikelnummer: 0027589
A-1010 Wien, Führichgasse 10/411.

Wien, am 26. Mai 2004

Kurzfassung

In der vorliegenden Dissertation ein Verfahren geeignet für Beschreibung der elektronischen Transporteigenschaften in Nanostrukturen ist dargestellt und ist implementiert geworden. Eine Einbettungstechnik bezogen auf die vollrelativistische spinpolarisierte Korringa-Kohn-Rostoker Methode und auf die Approximation des kohärenten Potentials ist kombiniert mit einer Realraum-Formulierung der Kubo-Greenwood Gleichung. Es sind Berechnungen durchgeführt worden für Ag(001) Oberfläche, Ag Bulk, zwei Arten von CuPt und $Ni_{0.15}Fe_{0.85}$ Bulk Legierungen in dem "grossen Cluster" Limes um die Vertrauenswürdigkeit der Methode zu erläutern. Ausserdem der verbleibende und der anisotropische Widerstand in NiFe Legierungen in dem Ni-reichen Bereich sind berechnet. Als echte Nanostrukturen endliche Fe und Co Ketten eingebettet in die Oberflächenschicht des Ag(001) sind erforscht, sowie eine detaillierte Untersuchung des elektronischen Transports durch atomarskalierten Au Kontakt zwischen halbunendlichen Au(001) Systemen ist präsentiert. Der Fremdatomeinfluss aus Übergangsmetallen (Fe, Co und Pd) in verschiedenen Positionen in der Nähe des Zentrums eines bestimmten Kontakts ist auch ermittelt.

1

Abstract

In the present work a method suitable to characterize electrical transport properties of nanostructures is described and has been implemented. A real-space embedding technique based on the fully relativistic spin-polarized Korringa-Kohn-Rostoker method and the Coherent Potential Approximation is combined with a real-space formulation of the Kubo-Greenwood equation. Calculations are presented for the Ag(001) surface, Ag bulk, two types of CuPt and $Ni_{0.15}Fe_{0.85}$ bulk alloys in the "large cluster" limit in order to illustrate the reliability of this approach. Moreover, the residual resistivity and the anisotropic magnetoresistance of bulk NiFe alloys are calculated in the Ni-rich regime. As real nanostructures, finite Fe and Co chains embedded into the surface layer of Ag(001) are investigated as well as a detailed study of the electric transport through atomic-scaled Au contacts between two semi-infinite Au(001) systems is given. The influence of transition metal impurities (Fe, Co and Pd) placed on various positions near the center of a particular contact is also studied.

Contents

Introduction

Ab-initio investigations of electric transport in solids attracted considerable interest in the last decades (see, e.g., Ref. [1]). This interest was stimulated on the one hand by a spectacular progress in the field of ab-initio band structure calculations, and on the other hand by a growing demand of experimental physics and technology, partly, by intensive studies and applications of various complex devices which utilize the anisotropy of the resistivity in magnetically ordered alloys [2, 3, 4, 5, 6] and heterostructures. Since in complex artificial structures (like spin-valves) there are several possible contributions to the resistivity and its dependence on the direction of the current or the external magnetic field (e.g., random impurities, interfaces and their roughness, phonon scattering etc.), it is often difficult to estimate theoretically their relative contributions [7, 8, 9, 10, 11]. An accurate account of the residual resistivities and anisotropic (or spontaneous) magnetoresistance (AMR) ratios of the random magnetic alloys is, therefore, a rather promising, though still challenging task for ab-initio theories [12, 13, 14]. An ab-initio study of the residual resistivity and the AMR of Ni-rich NiFe bulk alloys is presented in Chapter 7, focusing, in particular, on the concentration dependence of these quantities.

The main goal of this work is to describe electric transport in nanostructures. The increasing interest for investigating atomic-sized conductors is driven by the possibility of using such systems in future nanoelectronic technologies. Magnetic nanostructures, especially on surfaces are of special interest for the production of high-density magnetic recording devices. It is therefore an important issue to investigate the magnetic and electrical transport properties of such structures [15, 16]. The fully relativistic screened Korringa-Kohn-Rostoker (SKKR) Green's function method has been successfully applied in the past to layered systems and reliable results have been provided for the magnetic properties of such systems [17, 18, 19]. This ap-

proach was then extended in terms of the coherent potential approximation (CPA), and, in order to describe electrical transport properties of such systems, the Kubo-Greenwood formula [20, 21] was reformulated using one-particle Green's functions [22, 23]. This combination of methods has been successfully applied to various disordered layered systems with the aim of investigating giant magnetoresistance (GMR) effects [7, 8] as well as evaluating residual resistivities [24]. In order to be able to determine transport properties of nanostructures, the so-called embedding technique based on the multiple scattering theory [17, 25] is used, presented in Refs. [26, 27], which provides the description of the scattering properties of a specific region of a surface, interface or bulk (called cluster), and which can easily be combined with a real-space formulation of the Kubo-Greenwood equation [20, 21].

In Chapter 6 the reliability of the presented real space method is tested in the "large cluster" limit with, in particular, calculating residual resistivities of well studied alloy systems. In addition, it should be noted that further theoretical challenges can be investigated such as the change of electric properties from a nanostructure scale to thin films or even bulk systems, as well as comparing for low dimensional disordered structures configurational averages in real space with CPA-averages [22, 28].

As first application, the in-plane transport properties of the surface layer of Ag(001) are investigated in Chapter 8 by embedding single impurities and finite chains (length of 2-10 atoms) of Fe and Co along the (110) direction (x) into the surface layer. The influence of the direction of the magnetization in the nanostructures is also studied.

As second application, gold nanocontacts between two semi-infinite Au(001) systems are investigated in different geometries as well as the influence of transition metal impurities on the conductance is studied in Chapter 9. At sufficiently low temperatures the measurements revealed a quantized conductance for atomic sized nanocontacts made of various materials, not only pure metals but also alloys [29, 30]. Nanocontacts made of gold are presumably the most studied systems in the literature both theoretically and experimentally. A dominant peak very close to the conductance quantum, 1 $G_0 = 2e^2/h$, has been reported for gold (and other noble metals) in the conductance histogram [31, 32], attributed to the highly transmitting sp–channel across a linear chain connecting the two electrodes. It was also found that the chain formation is in close connection with surface reconstruction phenom-

ena [33]. For a comprehensive review of the field of atomic-sized conductors, see Ref. [34].

In order to understand the mechanism of nanocontact formation, electronic structure and transport, different theoretical methods have been developed. Some theoretical studies use tight–binding methods [35, 36], others are based on ab initio density functional theory [37, 38, 39]. Most of the transport studies rely on the Landauer-Büttiker approach [40, 41], although Baranger and Stone adopted the more sophisticated Kubo-Greenwood formula [20, 21, 22, 42] for calculating the conductance between free electron leads [43]. By using this approach a recent study [38] focused on the effect of transition metal imperfections inserted into an infinite Cu wire showing that the conductance of the wire decreased due to the different conductance for the two spin channels (spin-filter effect). This finding was the motivation to investigate the change of the conductance of a finite contact in the presence of transition metal impurities in the system.

Fabrication of nanostructures

The experimental investigation of atomic- or nano-scaled systems demands tools for manipulation and characterization of structures at this scale. In the first part of this Section the principle of one possible experimental technique for preparing nanostructures on surfaces is briefly described, namely the atomic manipulation by scanning tunnelling microscopy (STM). STM was developed by G. Binnig and H. Rohrer, and it was initially intended for imaging surfaces down to atomic resolution. The developers won the Nobel prize in 1986. It was soon realized that the STM tip often influences the surface due to tip-induced migration of surface particles. This is an evident disadvantage if one would like to image the surface but this property of the STM tip provides also a benefit, namely, the position of the surface atoms can be modified through the tip, thus, it is no more impossible to build nanostructures on surfaces.

Three different parameters influence the surface modification by means of a STM tip: the electrical field between tip and substrate, the tunneling current and the forces between tip and surface. On working with single atoms and molecules, vertical and lateral manipulation modes are distinguished. In the former mode, a particle

is intentionally picked up to the tip and then released back to the surface, while in the latter mode a particle is moved along the surface without losing contact to the substrate. In the lateral mode, three kinds of motions are possible: 1. pulling where the adparticle discontinuously follows the tip from one adsorption site to another due to attractive forces, 2. pushing with the same type of motion but here repulsive forces are applied, and 3. sliding where the adparticle is trapped under the tip and follows its motion continuously and instantly. All these tools demand a higher stability and lower thermal drift of the STM than necessary for imaging surfaces.

Widely applied methods for fabricating nanocontacts between macroscopic electrodes are the mechanically controllable break junction (MCBJ) technique [31, 33, 44, 45] and scanning tunneling microscopy (STM) [32, 46, 47] by pushing the tip intentionally into the surface. The crucial problem for both methods is the presence of contaminants, adsorbates, oxides on the contacting surfaces because it can prevent the formation of small metallic contacts, and also produce false experimental results. The second problem is the mechanical stability where MCBJ techniques are better than STM.

The dissertation is organized as follows: The applied theoretical methods can be found in Part I, while the results are in Part II. Part III is an appendix.

Chapter 1

Transport theories

In this Chapter a few methods describing electric transport in solid matter are presented with emphasis on the Kubo-Greenwood approach which has been used in this work to calculate transport properties of nanostructures.

Given a system of N interacting electrons moving in the electrostatic potential of the nuclei, the Hamilton operator can be transformed to an effective one-electron Hamiltonian by means of density functional theory (see Appendix A) which has the form,

$$\hat{H}_0 = -\frac{\hbar^2}{2m} \sum_{i=1}^{N} \nabla_i^2 + \sum_{i=1}^{N} u_{eff}(\mathbf{r}; \sigma, \mathcal{M}), \qquad (1.1)$$

where the first term is the kinetic energy and the second one is the effective one-electron potential depending on the spin of the electrons (σ) as well as on the magnetic configuration of the system ($\mathcal{M}$). The corresponding one-electron Schrödinger equation can be written as

$$\hat{H}_0 \phi_{k,\sigma}(\mathbf{r}) = E_{k,\sigma} \phi_{k,\sigma}(\mathbf{r}) \qquad (1.2)$$

with notation $k = (\nu, \mathbf{k})$, where ν denotes the band index, $\mathbf{k}$ is the momentum, while $E_{k,\sigma}$ and $\phi_{k,\sigma}(\mathbf{r})$ denote the one-electron energies and states, respectively. As it is well known, a translationally invariant system would not cause any resistivity. For this reason a perturbed system with Hamilton operator

$$\hat{H} = \hat{H}_0 + \hat{H}_{perturbation} \qquad (1.3)$$

is taken, where the perturbation can be, e.g. some scattering potential arising due to impurities present in the system.

1.1 Boltzmann formalism

In this Section, a quasi-classical approach of transport based on the Boltzmann equation is briefly discussed where the transport coefficients stem from a microscopic level. Boltzmann theory assumes the existence of a distribution function, $f_{k,\sigma}(\mathbf{r})$ which measures the probability of charge carriers with spin σ in the state k being in the neighborhood of $\mathbf{r}$. The change of $f_k(\mathbf{r}) = \sum_{\sigma} f_{k,\sigma}(\mathbf{r})$ is described by the Boltzmann equation,

$$\left(\frac{\partial f_k(\mathbf{r},t)}{\partial t}\right) + \left(\frac{\partial f_k(\mathbf{r})}{\partial t}\right)_{diffusion} + \left(\frac{\partial f_k(\mathbf{r})}{\partial t}\right)_{field} = -\left(\frac{\partial f_k(\mathbf{r})}{\partial t}\right)_{scattering} \quad , \quad (1.4)$$

where the terms above correspond to different effects, namely from the left: an explicit time dependence, diffusion, the influence of external fields and scattering. Stationarity implies that the total time dependence of $f_k(\mathbf{r})$ vanishes, see Eq. (1.4). It should be noted that in the following the $\mathbf{r}$-dependence of the distribution function will be neglected and the formulas will correspond to a magnetic system. Let us now analyse the scattering term. The local change of electrons resulted from elastic scattering of independent particles can be connected to the microscopic scattering probability,

$$P_{k\sigma,k'\sigma'} = \begin{pmatrix} P_{k\uparrow,k'\uparrow} & P_{k\uparrow,k'\downarrow} \\ P_{k\downarrow,k'\uparrow} & P_{k\downarrow,k'\downarrow} \end{pmatrix} \quad (1.5)$$

by

$$\left(\frac{\partial f_k}{\partial t}\right)_{scattering} = \sum_{\sigma}\sum_{k'\sigma'} [f_{k',\sigma'}(1 - f_{k,\sigma})P_{k'\sigma',k\sigma} - (1 - f_{k',\sigma'})f_{k,\sigma}P_{k\sigma,k'\sigma'}]. \quad (1.6)$$

The first term is called scattering-in term and describes the scattering of electrons from occupied states (k',σ') into an empty state (k,σ), while the second term typifies the reverse process, namely the scattering of an electron from an occupied state (k,σ) into empty states (k',σ') and is called scattering-out term. It is reasonable to separate the distribution function into two parts,

$$f_{k,\sigma} = f^0_{k,\sigma} + g_{k,\sigma} \, , \quad (1.7)$$

where

$$f^0_{k,\sigma} = \frac{1}{e^{\beta\left(E_{k,\sigma} - E_F\right)} + 1} \quad (1.8)$$

is the Fermi-Dirac distribution function with $E_{k,\sigma}$ being one-electron energies, see
·Eq. (1.2), E_F the Fermi energy, and $\beta = 1/k_B T$ with k_B the Boltzmann constant and
T temperature, while $g_{k,\sigma}$ denotes the deviation from the equilibrium distribution
function. Making use of the principle of microscopic reversibility implying
$P_{k\sigma,k'\sigma'} = P_{k'\sigma',k\sigma}$ for the microscopic scattering probabilities and the separation of
$f_{k,\sigma}$ in Eq. (1.7), the scattering term in Eq. (1.6) can be rewritten as

$$\left(\frac{\partial f_k}{\partial t}\right)_{scattering} = \sum_\sigma \sum_{k'\sigma'} P_{k\sigma,k'\sigma'}(g_{k',\sigma'} - g_{k,\sigma}). \tag{1.9}$$

Neglecting the terms with explicit time dependence of the distribution function and
change caused by diffusion in Eq. (1.4) and keeping only the change of f_k coming from
a homogeneous external electric field, **E**, the following expression can be obtained,

$$e \sum_\sigma \left(\frac{\partial f^0_{k,\sigma}}{\partial E_{k,\sigma}}\right) \mathbf{v}_{k,\sigma} \mathbf{E} = \sum_\sigma \sum_{k'\sigma'} P_{k\sigma,k'\sigma'}(g_{k',\sigma'} - g_{k,\sigma}), \tag{1.10}$$

where $\mathbf{v}_{k,\sigma}$ is the velocity of the electrons with spin σ, which can be defined with
help of the one-electron energies as

$$\mathbf{v}_{k,\sigma} = \frac{1}{\hbar}\frac{\partial E_{k,\sigma}}{\partial \mathbf{k}}. \tag{1.11}$$

Assuming that $g_{k,\sigma}$ depends linearly on the external electric field, the following
ansatz is made,

$$g_{k,\sigma} = -e \left(\frac{\partial f^0_{k,\sigma}}{\partial E_{k,\sigma}}\right) \Lambda_{k,\sigma} \mathbf{E}, \tag{1.12}$$

where $\Lambda_{k,\sigma}$ is the so-called mean free path vector of electrons with spin σ. The mag-
·nitude of $\Lambda_{k,\sigma}$ measures the path of the electron with spin σ between two scattering
events. Defining the so-called relaxation time, $\tau_{k,\sigma}$, which denotes the time that an
electron stays in the state (k,σ) until the next scattering event (scattering life time),
as

$$\tau^{-1}_{k,\sigma} = \sum_{k'\sigma'} P_{k\sigma,k'\sigma'} \quad, \tag{1.13}$$

Eq. (1.10) can be solved with the ansatz of Eq. (1.12) to give

$$\Lambda_{k,\sigma} = \tau_{k,\sigma}\left(\mathbf{v}_{k,\sigma} + \sum_{k'\sigma'} P_{k\sigma,k'\sigma'}\Lambda_{k',\sigma'}\right). \tag{1.14}$$

This is a system of coupled integral equations for magnetic systems. The different spin-components can be decoupled by ignoring spin-flip scattering processes, namely assuming that $P_{k\uparrow,k'\downarrow} = 0$ and $P_{k\downarrow,k'\uparrow} = 0$ in Eq. (1.5). In this case a relatively simple integral equation applies,

$$\Lambda_{k,\sigma} = \tau_{k,\sigma} \left(\mathbf{v}_{k,\sigma} + \sum_{k'} P_{k\sigma,k'\sigma} \Lambda_{k',\sigma} \right), \tag{1.15}$$

from which $\Lambda_{k,\sigma}$ can, in principle be obtained.

Let us now write the current density assuming that the total current density is split into spin-dependent contributions,

$$\mathbf{j} = \sum_{\sigma} \mathbf{j}_\sigma = \frac{e}{V} \sum_{k,\sigma} f_{k,\sigma} \mathbf{v}_{k,\sigma}, \tag{1.16}$$

where V is the volume of the system. The conductivity tensor $\underline{\underline{\sigma}}$ at $T = 0$ is obtained by using Ohm's law, $\mathbf{j}_\sigma = \underline{\underline{\sigma}}_\sigma \mathbf{E}$ and Eqs. (1.7), (1.12), (1.16),

$$\underline{\underline{\sigma}} = \sum_{\sigma} \underline{\underline{\sigma}}_\sigma = \frac{e^2}{V} \sum_{k,\sigma} \delta(E_{k,\sigma} - E_F) \mathbf{v}_{k,\sigma} \circ \Lambda_{k,\sigma}, \tag{1.17}$$

where $\circ$ denotes a dyadic product (resulting in a 3×3 tensor), and the contributions to the total conductivity come from the independent majority ($\uparrow$) and minority ($\downarrow$) spin channels according to the two current model [48], where spin-flip scattering is also ignored. Neglecting the scattering-in term in Eq. (1.14), the conductivity becomes

$$\underline{\underline{\sigma}} = \sum_{\sigma} \underline{\underline{\sigma}}_\sigma = \frac{e^2}{V} \sum_{k,\sigma} \delta(E_{k,\sigma} - E_F) \tau_{k,\sigma} \mathbf{v}_{k,\sigma} \circ \mathbf{v}_{k,\sigma}. \tag{1.18}$$

It is important to note that $\sum_{k,\sigma} \delta(E_{k,\sigma} - E_F)$ defines the density of states, $n(E_F)$ at the Fermi energy, thus it can be concluded that the conductivity tensor is affected by three factors: the density of states, the velocities, and the relaxation times of the electrons at the Fermi surface. The first two are completely determined by the electronic structure of the system, while the last one is determined by defects or impurities present in the solid. Moreover, different approximations can be applied on the relaxation time in Eq. (1.18), e.g. isotropic τ, or only spin-dependent τ_σ, resulting thus in simplified conductance expression. The applicability of them are,

however, strongly limited depending on the system under consideration.

It should be mentioned that the Boltzmann equation can easily be implemented within traditional bandstructure methods, since in the quasi-classical interpretation the velocity is given by the energy dispersion, see Eq. (1.11). As disadvantages can be mentioned that it is a semi-classical theory, in the form of Eq. (1.18) it is applicable only for bulk systems, since the knowledge of the Fermi surface is supposed and the exact form of the relaxation time, $\tau_{k,\sigma}$ is unknown.

1.2 Landauer formalism

The Landauer-Büttiker theory [40, 41] is an effective tool for describing transport in mesoscopic systems where the problem is viewed from the aspect of scattering theory. Let us shortly sketch the most general model system which can be considered. A multiprobe structure is taken which consists of a finite region connected to N_L leads where each lead is attached to an ideal "reservoir". The electrons are scattered in the finite region (scattering or interaction region) which can be caused by disorder or particular geometry characteristics. The transport throughout the scattering region is completely coherent, no phase breaking is taken into account and inelastic scattering processes are to be negligible due to low temperature supposed. The leads are used to inject and drain current or measure voltage, whereas the reservoirs are assumed to fulfil certain conditions: a reservoir for the nth lead is in equilibrium at a chemical potential

$$\mu_n = E_F + eV_n \tag{1.19}$$

with V_n being the applied potential on it and E_F is the Fermi energy. Furthermore, a steady-state current flowing from/into the reservoir does not change μ_n which means that the reservoir is large enough relative to the scattering region. Moreover, it is assumed that no additional resistance is produced by the interface between a reservoir and the scattering region. The last assumption implies that an electron entering a reservoir must be scattered inelastically before returning to the coherent scattering region providing a phase-randomization. The current going through the

nth lead can be written as

$$I_n = \sum_{m \neq n} g_{nm} V_m \, , \tag{1.20}$$

where the sum is carried out for all leads except the nth one, and g_{nm} are the conductance coefficients of the system. Introducing incoming and outgoing scattering channels which play the same role as incoming and outgoing Bloch states in scattering theory, the conductance can be expressed with the transmission probability $(T_{ni,mj})$ or the S-matrix $(S_{ni,mj})$ as

$$g_{nm} = \frac{2e^2}{h} \sum_{ij} T_{ni,mj} = \frac{2e^2}{h} \sum_{ij} |S_{ni,mj}|^2 \, . \tag{1.21}$$

Here, $T_{ni,mj}$ means the transmission probability from an incoming channel j in lead m to an outgoing channel i in lead n, the factor 2 stands for the two spin directions and the sum has to be carried out for all incoming and outgoing channels in the corresponding leads.

The advantage of using Landauer formalism is first and foremost seen for two-probe structures, where only one conductance coefficient g exists, such as for describing perpendicular transport (current perpendicular to plane-CPP) in layered structures (magnetic multilayers, GMR and TMR devices, spin valve systems, heterojunctions) or even investigating quantum wires or point-contacts connecting two electron reservoirs. The point-contacts can be partitioned depending on the features of the transport processes. The main parameters are the characteristic lengths of the system: the contact diameter (d) and the mean free path for elastic (Λ_e) and inelastic (Λ_i) scatterings. Here, Λ_e (Λ_i) is the length of the electron's path between two elastic (inelastic) scatterings. The so-called *ballistic* point-contact is given if $d \ll \Lambda_e, \Lambda_i$. In this case the electron travels through the contact without any scattering. If $d \gg \Lambda_e$ the point-contact is in the *diffusive* regime which means that the electrons experience a lot of elastic scatterings when travelling through the contact. In both cases the contact diameter must be much larger than the electron's wavelength.

In the case of two-probe structures the conductance of the system can be written according to Eq. (1.21) as

$$g = \frac{2e^2}{h} \sum_{ij} T_{ij}. \tag{1.22}$$

Moreover, T_{ij} is a hermitian matrix, thus it can be diagonalized and the conductance is obtained in eigenchannel basis as

$$g = \frac{2e^2}{h} \sum_{i=1}^{N} T_i \qquad (1.23)$$

with N being the number of conducting channels through the scattering region and T_i's are the real eigenvalues of T_{ij}, where T_i denotes the transmission probability of the ith channel, thus $0 < T_i < 1$ must be satisfied. For an ideal ballistic point-contact as well as for a theoretically interesting infinite periodic wire, $T_{ij} = \delta_{ij}$ which implies that the conductance is quantized in units of the conductance quantum $G_0 = 2e^2/h$,

$$g = N_{ch} G_0 . \qquad (1.24)$$

These quantized conductances have been observed by many experimental groups. It can be concluded that the conductance depends on the number of open eigenchannels, N_{ch}, which in turn depends on the sample geometry. This means that N_{ch} for the entire system is determined by the narrowest cross section of the point-contact or the wire.

1.3 Kubo formalism

In the 1950s, Kubo developed a method of evaluating the response of a quantum mechanical system to an external potential, in particular, the current in response to an electric field [20]. To first order, known as linear response, the two quantities are related by a conductivity (Ohm's law), which is given in terms of the equilibrium properties of the system, i.e., in zero field. Moreover, conductance coefficients can be derived from the conductivity, which describe the total current flowing in and out of the system in response to voltages applied at its boundaries. The conductance can be measured instead of the conductivity, which is an average property of the system and is usually obtained by averaging over the sample volume and over the possible impurity configurations of an ensemble of similar systems. The configurational averaging in disordered systems is discussed in Chapter 3. In this Section the Kubo formalism is presented in some details.

1.3.1 Linear response theory

Linear response and the Green function

Assuming a time-dependent perturbation, $\hat{H}'(t)$ in Eq. (1.3), the Hamilton operator of the perturbed system has the form,

$$\hat{H}(t) = \hat{H}_0 + \hat{H}'(t) .$$ (1.25)

Using grand-canonical ensemble, the density operator of the unperturbed system can be written as

$$\hat{\varrho}_0 = \frac{1}{\mathcal{Z}} e^{-\beta \hat{\mathcal{H}}_0}$$ (1.26)

with

$$\hat{\mathcal{H}}_0 = \hat{H}_0 - \mu \hat{N} ,$$ (1.27)

where μ is the chemical potential, $\hat{N}$ is the total (particle) number operator, and

$$\mathcal{Z} = Tr \left(e^{-\beta \hat{\mathcal{H}}_0} \right)$$ (1.28)

is the grand canonical partition function. It should be noted that the expectation value of a physical observable A, associated with a hermitian operator $\hat{A}$ in the unperturbed system is

$$A_0 = \langle A \rangle = \frac{1}{\mathcal{Z}} Tr \left(\hat{A} e^{-\beta \hat{\mathcal{H}}_0} \right) = Tr \left(\hat{\varrho}_0 \hat{A} \right) .$$ (1.29)

Within the Schrödinger picture the equation of motion for the density operator reads as

$$i\hbar \frac{\partial \hat{\varrho}(t)}{\partial t} = \left[\hat{\mathcal{H}}(t), \hat{\varrho}(t) \right] ,$$ (1.30)

where

$$\hat{\mathcal{H}}(t) = \hat{H}(t) - \mu \hat{N} = \hat{\mathcal{H}}_0 + \hat{H}'(t) .$$ (1.31)

Clearly, in absence of perturbation, $\hat{\varrho}(t) = \hat{\varrho}_0$, therefore, partitioning $\hat{\varrho}(t)$ as

$$\hat{\varrho}(t) = \hat{\varrho}_0 + \hat{\varrho}'(t) ,$$ (1.32)

and making use of $\left[\hat{\mathcal{H}}_0, \hat{\varrho}_0\right] = 0$, we get *to first order in* $\hat{H}'$,

$$i\hbar \frac{\partial \hat{\varrho}'(t)}{\partial t} = \left[\hat{\mathcal{H}}_0, \hat{\varrho}'(t)\right] + \left[\hat{H}'(t), \hat{\varrho}_0\right] . \tag{1.33}$$

It is now worth to switch to the interaction (or Dirac) picture,

$$\hat{\varrho}_D(t) = \hat{\varrho}_0 + \hat{\varrho}'_D(t) , \quad \hat{\varrho}'_D(t) = e^{\frac{i}{\hbar}\hat{\mathcal{H}}_0 t}\hat{\varrho}'(t)e^{-\frac{i}{\hbar}\hat{\mathcal{H}}_0 t} , \tag{1.34}$$

since

$$i\hbar \frac{\partial \hat{\varrho}'_D(t)}{\partial t} = \left[\hat{\varrho}'_D(t), \hat{\mathcal{H}}_0\right] + \underbrace{e^{\frac{i}{\hbar}\hat{\mathcal{H}}_0 t}i\hbar\frac{\partial \hat{\varrho}'(t)}{\partial t}e^{-\frac{i}{\hbar}\hat{\mathcal{H}}_0 t}}_{\left[\hat{\mathcal{H}}_0, \hat{\varrho}'_D(t)\right] + \left[\hat{H}'_D(t), \hat{\varrho}_0\right]} = \left[\hat{H}'_D(t), \hat{\varrho}_0\right] . \tag{1.35}$$

This equation has to be solved with some initial condition. If we turn on the external field at $t = -\infty$ then it is clear that at $t = -\infty$ the density operator of the system must represent an ensemble of systems in thermal equilibrium, $\hat{\varrho}(t = -\infty) = \hat{\varrho}_0$. Taking, therefore, the boundary condition $\hat{\varrho}'_D(t) \xrightarrow[t \to -\infty]{} 0$ results the following integral equation,

$$\hat{\varrho}'_D(t) = -\frac{i}{\hbar} \int\limits_{-\infty}^{t} dt' \left[\hat{H}'_D(t'), \hat{\varrho}_0\right] , \tag{1.36}$$

thus, returning back to Schrödinger picture, the density operator can be approximated to first order as

$$\hat{\varrho}(t) \approx \hat{\varrho}_0 - \frac{i}{\hbar} \int\limits_{-\infty}^{t} dt' e^{-\frac{i}{\hbar}\hat{\mathcal{H}}_0 t} \left[\hat{H}'_D(t'), \hat{\varrho}_0\right] e^{\frac{i}{\hbar}\hat{\mathcal{H}}_0 t} . \tag{1.37}$$

Considering the time evolution of the physical observable $A(t)$, one gets

$$A(t) = Tr\left(\hat{\varrho}(t)\hat{A}\right) = A_0 - \frac{i}{\hbar} \int\limits_{-\infty}^{t} dt' \, Tr\left(e^{-\frac{i}{\hbar}\hat{\mathcal{H}}_0 t} \left[\hat{H}'_D(t'), \hat{\varrho}_0\right] e^{\frac{i}{\hbar}\hat{\mathcal{H}}_0 t}\hat{A}\right)$$

$$= A_0 - \frac{i}{\hbar} \int\limits_{-\infty}^{t} dt' \, Tr\left(\left[\hat{H}'_D(t'), \hat{\varrho}_0\right] \hat{A}_D(t)\right) , \tag{1.38}$$

where A_0 is defined by Eq. (1.29) and the Dirac representation of operator $\hat{A}$,

$$\hat{A}_D(t) = e^{\frac{i}{\hbar}\hat{\mathcal{H}}_0 t}\hat{A}e^{-\frac{i}{\hbar}\hat{\mathcal{H}}_0 t} \tag{1.39}$$

is used. Applying the identity,

$$Tr\left(\left[\hat{A},\hat{B}\right]\hat{C}\right) = Tr\left(\hat{A}\hat{B}\hat{C} - \hat{B}\hat{A}\hat{C}\right) = Tr\left(\hat{B}\hat{C}\hat{A} - \hat{B}\hat{A}\hat{C}\right) = Tr\left(\hat{B}\left[\hat{C},\hat{A}\right]\right),$$

we get

$$\delta A(t) = A(t) - A_0 = -\frac{i}{\hbar}\int\limits_{-\infty}^{t}dt'\,Tr\left(\hat{\varrho}_0\left[\hat{A}_D(t),\hat{H}'_D(t')\right]\right). \tag{1.40}$$

Assuming that the perturbation $\hat{H}'(t)$ has the form,

$$\hat{H}'(t) = \hat{B}F(t), \tag{1.41}$$

where $\hat{B}$ is a hermitian operator and $F(t)$ is a complex function (classical field), Eq. (1.40) transforms into

$$\delta A(t) = -\frac{i}{\hbar}\int\limits_{-\infty}^{t}dt'F(t')Tr\left(\hat{\varrho}_0\left[\hat{A}_D(t),\hat{B}_D(t')\right]\right), \tag{1.42}$$

which can be written in terms of the *retarded Green function*,

$$G_{AB}^{ret}(t,t') = -i\Theta(t-t')Tr\left(\hat{\varrho}_0\left[\hat{A}_D(t),\hat{B}_D(t')\right]\right) \tag{1.43}$$

or the so-called *generalized susceptibility*,

$$\chi_{AB}(t,t') = \frac{1}{\hbar}G_{AB}^{ret}(t,t') \tag{1.44}$$

as

$$\delta A(t) = \frac{1}{\hbar}\int\limits_{-\infty}^{\infty}dt'F(t')G_{AB}^{ret}(t,t') = \int\limits_{-\infty}^{\infty}dt'F(t')\chi_{AB}(t,t'). \tag{1.45}$$

It should be noted that since the time-evolution in the Dirac picture is governed by $\hat{H}_0$, the operators $\hat{A}_D(t)$ and $\hat{B}_D(t')$ are equivalent to the corresponding Heisenberg-operators related to the unperturbed system, as most commonly used in the definition of the Green function, Eq. (1.43). Supposing that the operators $\hat{A}$ and $\hat{B}$ do

not explicitly depend on time, $G_{AB}^{ret}(t, t')$ and $\chi_{AB}(t, t')$ will be functions of $(t - t')$. Consequently, the Fourier coefficients of $\delta A(t)$ can be written as

$$\delta A(\omega) = \frac{1}{\hbar} F(\omega) G_{AB}^{ret}(\omega) = F(\omega) \chi_{AB}(\omega) \tag{1.46}$$

where

$$X(\omega) = \int\limits_{-\infty}^{\infty} dt\, X(t) e^{i\omega t} \;,\; X(t) = \frac{1}{2\pi} \int\limits_{-\infty}^{\infty} d\omega\, X(\omega) e^{-i\omega t} \tag{1.47}$$

holds for any time-dependent quantity, $X(t)$. It is important to take care by calculating $G_{AB}^{ret}(\omega)$, since it is analytical only in the upper complex semi-plane (retarded sheet), therefore, for a real argument ω, the limit $\varpi \to \omega + i0$ has to be considered. The complex admittance, $\chi_{AB}(\omega)$ can be expressed in terms of the retarded Green function as

$$\chi_{AB}(\omega) = \frac{1}{\hbar} G_{AB}^{ret}(\omega + i0) = -\frac{i}{\hbar} \int\limits_{0}^{\infty} dt\, e^{i(\omega + i0)t} Tr\left(\hat{\varrho}_0 \left[\hat{A}(t), \hat{B}(0)\right]\right) \;. \tag{1.48}$$

The appearance of the side-limit, $\omega + i0$, in $\chi_{AB}(\omega)$ is usually termed as the *adiabatic switching* of the perturbation as it corresponds to a time-dependent classical field,

$$F'(t) = \lim_{s \to 0} \left(F(t) e^{st}\right) \;. \tag{1.49}$$

The Kubo formula

Let us come back to Eq. (1.38),

$$\delta A(t) = -\frac{i}{\hbar} \int\limits_{-\infty}^{t} dt'\, Tr\left(\left[\hat{H}'_H(t'), \hat{\varrho}_0\right] \hat{A}_H(t)\right) \;, \tag{1.50}$$

where the operators are taken in the Heisenberg picture with respect to the unperturbed system. Employing *Kubo's identity*,

$$\frac{i}{\hbar} \left[\hat{X}_H(t), \hat{\varrho}\right] = \hat{\varrho} \int\limits_{0}^{\beta} d\lambda\, \dot{\hat{X}}_H(t - i\lambda\hbar) \tag{1.51}$$

with

$$\hat{\varrho} = \frac{e^{-\beta\hat{H}}}{Tr\left(e^{-\beta\hat{H}}\right)} \;,\quad \hat{X}_H(t) = e^{\frac{i}{\hbar}\hat{H}t}\hat{X}(t)e^{-\frac{i}{\hbar}\hat{H}t} \;,\ \text{and}\quad \dot{\hat{X}}_H(t) = -\frac{i}{\hbar}\left[\hat{X}_H(t),\hat{H}\right] \;,$$

Eq. (1.51) in Eq. (1.50) yields

$$\delta A(t) = -\int\limits_{-\infty}^{t} dt' \int\limits_{0}^{\beta} d\lambda\, Tr\left(\hat{\varrho}_0 \dot{\hat{H}}'_H(t' - i\lambda\hbar)\hat{A}_H(t)\right)$$

$$= -\int\limits_{-\infty}^{t} dt' \int\limits_{0}^{\beta} d\lambda\, Tr\left(\hat{\varrho}_0 \dot{\hat{H}}'(t')\hat{A}_H(t - t' + i\lambda\hbar)\right) \;, \qquad (1.52)$$

which is the *Kubo formula*. For proof of Eqs. (1.51) and (1.52), see Appendix B.

1.3.2 The electric conductivity tensor

The current-current correlation function

In case of electric transport a time dependent external electric field is applied to a solid. Obviously, this induces currents, which in turn creates internal electric fields. Let us assume that the total electric field, $\mathbf{E}(\mathbf{r},t)$ is related to the perturbation, $\hat{H}'(t)$ through a scalar potential, $\phi(\mathbf{r},t)$ as

$$\hat{H}'(t) = \int d^3r\, \hat{\rho}(\mathbf{r})\phi(\mathbf{r},t) \;,\quad \mathbf{E}(\mathbf{r},t) = -\boldsymbol{\nabla}\phi(\mathbf{r},t) \;, \qquad (1.53)$$

where $\hat{\rho}(\mathbf{r}) = e\psi(\mathbf{r})^{+}\psi(\mathbf{r})$ is the operator of the charge density, with $\psi(\mathbf{r})$ being the field operator and e the charge of the electron. It should be noted that a derivation of the conductivity tensor is possible also assuming a vectorpotential, $\mathbf{A}(\mathbf{r},t)$, related to the electric field by $\mathbf{E}(\mathbf{r},t) = -\frac{1}{c}\frac{d\mathbf{A}(\mathbf{r},t)}{dt}$, which in turn leads to an identical result as derived here. The time-derivative of $\hat{H}'_H(t)$ can be calculated as follows,

$$\dot{\hat{H}}'(t) = \int d^3r\, \underbrace{\frac{1}{i\hbar}\left[\hat{\mathcal{H}}_0,\hat{\rho}(\mathbf{r})\right]}_{\frac{\partial\hat{\rho}_H(\mathbf{r},t)}{\partial t}|_{t=0}}\phi(\mathbf{r},t) = -\int d^3r\, \boldsymbol{\nabla}\hat{\mathbf{J}}(\mathbf{r})\,\phi(\mathbf{r},t)$$

$$= \int d^3r\, \hat{\mathbf{J}}(\mathbf{r})\,\boldsymbol{\nabla}\phi(\mathbf{r},t) = -\int d^3r\, \hat{\mathbf{J}}(\mathbf{r})\,\mathbf{E}(\mathbf{r},t) \;, \qquad (1.54)$$

with the current-density operator,

$$\hat{\mathbf{J}}(\mathbf{r}) = \begin{cases} \frac{e\hbar}{2mi}\psi(\mathbf{r})^+ \left(\overrightarrow{\nabla} - \overleftarrow{\nabla}\right)\psi(\mathbf{r}) & \text{in non-relativistic case,} \\[2ex] ec\psi(\mathbf{r})^+ \,\hat{\boldsymbol{\alpha}}\,\psi(\mathbf{r}) & \text{in relativistic case,} \end{cases} \qquad (1.55)$$

and the Dirac matrices, $\hat{\boldsymbol{\alpha}}$. Note that in Eq. (1.54) the continuity equation was used and periodic boundary conditions were assumed at the surface of the solid, therefore, when using Gauss' integration theorem the corresponding surface term vanished. Making use of Eqs. (1.52) and (1.54), the μth component of the current density can be written as

$$J_\mu(\mathbf{r}, t) = \sum_\nu \int d^3r' \int\limits_{-\infty}^{\infty} dt' \sigma_{\mu\nu}(\mathbf{r}, \mathbf{r}'; t, t')\, E_\nu(\mathbf{r}', t')\,, \qquad (1.56)$$

where the occurring space-time correlation function is given by

$$\sigma_{\mu\nu}(\mathbf{r}, \mathbf{r}'; t, t') = \Theta(t - t') \int\limits_{0}^{\beta} d\lambda\, Tr\left(\hat{\varrho}_0\, \hat{J}_\nu(\mathbf{r}, 0)\hat{J}_\mu(\mathbf{r}', t - t' + i\lambda\hbar)\right)\,, \qquad (1.57)$$

expressing the linear response of the current density at $(\mathbf{r}, t)$ in direction μ to the local electric field at $(\mathbf{r}', t')$ applied in direction ν. Note that in the above equation the current-density operators are assumed to be Heisenberg operators.

As before, we look for the response of a Fourier component of the electric field,

$$\mathbf{E}(\mathbf{q}, \omega) = \int d^3r \int\limits_{-\infty}^{\infty} dt\, \mathbf{E}(\mathbf{r}, t)e^{-i\mathbf{qr}+i\varpi t}\,, \quad \mathbf{E}(\mathbf{r}, t) = \frac{1}{2\pi V}\int d^3q \int\limits_{-\infty}^{\infty} d\omega\, \mathbf{E}(\mathbf{q}, \omega)e^{i\mathbf{qr}-i\varpi t}\,,$$

$$(1.58)$$

where $\varpi = \omega + i0$ and V is the volume of the system. While $\sigma_{\mu\nu}(\mathbf{r}, \mathbf{r}'; t, t')$ trivially depends on $(t - t')$ according to Eq. (1.57), in general, it is a function of independent space variables, $\mathbf{r}$ and $\mathbf{r}'$. In cases, if the current density is an average of the local current density defined in (1.56) over a big region (many cells) of the solid, the assumption that $\sigma_{\mu\nu}(\mathbf{r}, \mathbf{r}'; t, t')$ is homogeneous in space, i.e.,

$\sigma_{\mu\nu}(\mathbf{r}, \mathbf{r}'; t - t') = \sigma_{\mu\nu}(\mathbf{r} - \mathbf{r}'; t - t')$ can be made, which facilitates a direct Fourier transformation of Eq. (1.56). Usually this happens if $|\mathbf{q}|$ is small, which means

that *long-wavelength excitations* are studied. The $(\mathbf{q}, \omega)$ component of the current density per unit volume,

$$J_\mu(\mathbf{q}, \omega) = \frac{1}{V} \int d^3r \int_{-\infty}^{\infty} dt\, J_\mu(\mathbf{r}, t) e^{-i\mathbf{q}\mathbf{r} + i\varpi t} \tag{1.59}$$

can then be determined from Eqs. (1.56) and (1.57),

$$J_\mu(\mathbf{q}, \omega) = \sum_\nu \sigma_{\mu\nu}(\mathbf{q}, \omega)\, E_\nu(\mathbf{q}, \omega)\,, \tag{1.60}$$

with the wave–vector and frequency dependent *conductivity tensor*,

$$\sigma_{\mu\nu}(\mathbf{q}, \omega) = \frac{1}{V} \int_0^\infty dt\, e^{i\varpi t} \int_0^\beta d\lambda\, Tr\left(\hat{\varrho}_0 \hat{J}_\nu(-\mathbf{q}, 0)\hat{J}_\mu(\mathbf{q}, t + i\lambda\hbar)\right)\,, \tag{1.61}$$

where

$$J_\mu(\mathbf{q}, t) = \int d^3r\, J_\mu(\mathbf{r}, t) e^{-i\mathbf{q}\mathbf{r}}\,. \tag{1.62}$$

After some algebra and contour integration tricks, see Appendix B, we arrive at

$$\sigma_{\mu\nu}(\mathbf{q}, \omega) = \frac{i}{\hbar V} \int_0^\infty dt\, e^{i\varpi t} \int_t^\infty dt'\, Tr\left(\hat{\varrho}_0 \left[\hat{J}_\mu(\mathbf{q}, t'), \hat{J}_\nu(-\mathbf{q}, 0)\right]\right)\,. \tag{1.63}$$

By introducing the current-current correlation function,

$$\Sigma_{\mu\nu}(\mathbf{q}, \varpi) = \frac{1}{\hbar V} \int_0^\infty dt\, e^{i\varpi t}\, Tr\left(\hat{\varrho}_0 \left[\hat{J}_\mu(\mathbf{q}, t), \hat{J}_\nu(-\mathbf{q}, 0)\right]\right)\,, \tag{1.64}$$

it is shown in Appendix B that the conductivity tensor can be expressed as

$$\sigma_{\mu\nu}(\mathbf{q}, \omega) = \frac{\Sigma_{\mu\nu}(\mathbf{q}, \varpi) - \Sigma_{\mu\nu}(\mathbf{q}, 0)}{\varpi}\,. \tag{1.65}$$

For a homogeneous system with carrier density, n and mass of the carriers, m,

$$-\frac{\Sigma_{\mu\nu}(\mathbf{q}, 0)}{\varpi} = i\frac{ne^2}{m\varpi}\delta_{\mu\nu}\,, \tag{1.66}$$

i.e., the phenomenological Drude term for non-interacting particles. It is furthermore clear, that the static, i.e., $\omega \to 0$ (and $|\mathbf{q}| \to 0$), limit has to be performed as

$$\sigma_{\mu\nu}(\mathbf{q} = 0, \omega = 0) = \lim_{s \to +0} \frac{\Sigma_{\mu\nu}(\mathbf{q} = 0, is) - \Sigma_{\mu\nu}(\mathbf{q} = 0, 0)}{is} = \frac{d\,\Sigma_{\mu\nu}(\mathbf{q} = 0, \varpi)}{d\varpi}\Bigg|_{\varpi=0}\,. \tag{1.67}$$

As what follows we shall derive more specific expressions for a system of non-interacting particles.

Kubo formula for independent particles

An important special case arises when the particles are treated to be independent. Skipping the quite straightforward but lengthy derivation, we can state that formulas (1.61) and (1.63)–(1.65) apply also for a system of independent particles, when the corresponding one-particle operators and the equilibrium distribution function, in case of electrons and all fermions, the Fermi-Dirac distribution function,

$$f(\varepsilon) = \frac{1}{e^{\beta(\varepsilon-\mu)} + 1} \tag{1.68}$$

are used. Working in the basis of eigenfuctions of $\hat{H}_0$ (spectral representation),

$$\hat{H}_0 \left| n \right\rangle = \varepsilon_n \left| n \right\rangle , \quad \left\langle m \mid n \right\rangle = \delta_{nm} , \quad \sum_n \left| n \right\rangle\left\langle n \right| = \hat{I} , \tag{1.69}$$

the equilibrium density operator and its matrixelements are

$$\hat{\varrho}_0 = \sum_n f(\varepsilon_n)|n\rangle\langle n| , \quad \langle n \left| \hat{\varrho}_0 \right| p \rangle = f(\varepsilon_n)\delta_{pn} \tag{1.70}$$

and the thermal average of the current–current commutator can be written as

$$Tr\left(\hat{\varrho}_0 \left[\hat{J}_\mu(\mathbf{q},t'), \hat{J}_\nu(-\mathbf{q},0) \right]\right) = \sum_{nm} \{f(\varepsilon_n) - f(\varepsilon_m)\} \, e^{\frac{i}{\hbar}(\varepsilon_n-\varepsilon_m)t'} J_\mu^{nm}(\mathbf{q})J_\nu^{mn}(-\mathbf{q}) , \tag{1.71}$$

with

$$J_\mu^{nm}(\mathbf{q}) \equiv \left\langle n \left| \hat{J}_\mu(\mathbf{q}) \right| m \right\rangle \text{ and } J_\nu^{mn}(-\mathbf{q}) \equiv \left\langle m \left| \hat{J}_\nu(-\mathbf{q}) \right| n \right\rangle . \tag{1.72}$$

The derivation of Eq. (1.71) can be found in Appendix B. Substituting Eq. (1.71) into Eq. (1.64) yields

$$\Sigma_{\mu\nu}(\mathbf{q},\omega) = \frac{1}{\hbar V} \sum_{nm} \{f(\varepsilon_n) - f(\varepsilon_m)\} \, J_\mu^{nm}(\mathbf{q})J_\nu^{mn}(-\mathbf{q}) \int_0^\infty dt \, e^{\frac{i}{\hbar}(\varepsilon_n-\varepsilon_m+\hbar\omega)t} . \tag{1.73}$$

The integral on the right–hand side with respect to t is just the Laplace transform of the identity,

$$\int_0^\infty dt \, e^{\left[\frac{i}{\hbar}(\varepsilon_n-\varepsilon_m+\hbar\omega)-s\right]t} \underset{(s>0)}{=} -\frac{e^{\left[\frac{i}{\hbar}(\varepsilon_n-\varepsilon_m+\hbar\omega)-s\right]t}}{\frac{i}{\hbar}(\varepsilon_n - \varepsilon_m + \hbar\omega) - s} , \tag{1.74}$$

therefore, Eq. (1.73) can be transformed to

$$\Sigma_{\mu\nu}(\mathbf{q},\omega) = \frac{i}{V} \sum_{nm} \frac{f(\varepsilon_n) - f(\varepsilon_m)}{\varepsilon_n - \varepsilon_m + \hbar\varpi} J_\mu^{nm}(\mathbf{q}) J_\nu^{mn}(-\mathbf{q}) , \tag{1.75}$$

which together with Eq. (1.63) provides a numerically tractable tool to calculate the conductivity tensor. It is worth to mention that since

$$\frac{1}{\varepsilon_n - \varepsilon_m + \hbar\varpi} - \frac{1}{\varepsilon_n - \varepsilon_m} = \frac{-\hbar\varpi}{(\varepsilon_n - \varepsilon_m)(\varepsilon_n - \varepsilon_m + \hbar\varpi)} ,$$

$\sigma_{\mu\nu}(\mathbf{q},\omega)$ can be written into the compact form,

$$\sigma_{\mu\nu}(\mathbf{q},\omega) = \frac{\hbar}{iV} \sum_{nm} \frac{f(\varepsilon_n) - f(\varepsilon_m)}{\varepsilon_n - \varepsilon_m} \frac{J_\mu^{nm}(\mathbf{q}) J_\nu^{mn}(-\mathbf{q})}{\varepsilon_n - \varepsilon_m + \hbar\varpi} . \tag{1.76}$$

It should also be noted that in calculations of optical spectra a finite, positive value of δ is considered in order to account for finite life-time effects. It is easy to show, that this is indeed equivalent by folding the spectrum with a Lorentzian of half-width δ. Therefore, we often speak about the *complex conductivity tensor*, $\sigma_{\mu\nu}(\mathbf{q},\varpi)$.
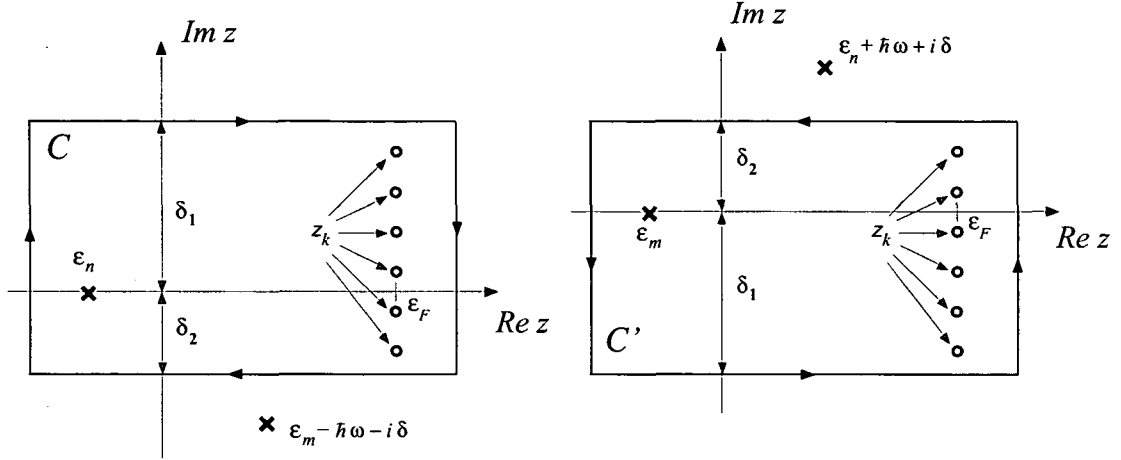
Contour integration technique

Let us now evaluate $\Sigma_{\mu\nu}(\mathbf{q},\varpi)$ by using a contour integration technique, keeping in mind that we have a finite imaginary part of the denominator in Eq. (1.75). Considering a pair of eigenvalues, ε_n and ε_m, for a suitable contour C in the complex energy plane (see Fig. 1.1) the residue theorem implies that

$$\oint_C dz \frac{f(z)}{(z - \varepsilon_n)(z - \varepsilon_m + \hbar\omega + i\delta)} = -2\pi i \frac{f(\varepsilon_n)}{\varepsilon_n - \varepsilon_m + \hbar\omega + i\delta} \tag{1.77}$$

$$+ 2i\delta_T \sum_{k=-N_2+1}^{N_1} \frac{1}{(z_k - \varepsilon_n)(z_k - \varepsilon_m + \hbar\omega + i\delta)} ,$$

where $z_k = E_F + i(2k - 1)\delta_T$ are the (fermionic) Matsubara-poles with E_F being the Fermi energy, $\delta_T \equiv \pi k_B T$ and T the temperature. In Eq. (1.77) it was supposed that N_1 and N_2 Matsubara-poles in the upper and lower semi-plane lie within the contour C, respectively. Eq. (1.77) can be rearranged as

$$i\frac{f(\varepsilon_n)}{\varepsilon_n - \varepsilon_m + \hbar\omega + i\delta} = -\frac{1}{2\pi} \oint_C dz \frac{f(z)}{(z - \varepsilon_n)(z - \varepsilon_m + \hbar\omega + i\delta)} \tag{1.78}$$

$$+ i\frac{\delta_T}{\pi} \sum_{k=-N_2+1}^{N_1} \frac{1}{(z_k - \varepsilon_n)(z_k - \varepsilon_m + \hbar\omega + i\delta)} .$$

Figure 1.1: Schematic view of contours C and C'.

Similarly, by choosing a contour C' (in fact, C mirrored to the real axis, see Fig. 1.1) the following expression,

$$-i\frac{f(\varepsilon_m)}{\varepsilon_n - \varepsilon_m + \hbar\omega + i\delta} = \frac{1}{2\pi}\oint_{C'} dz\, \frac{f(z)}{(z - \varepsilon_m)(z - \varepsilon_n - \hbar\omega - i\delta)} \qquad (1.79)$$

$$+i\frac{\delta_T}{\pi}\sum_{k=-N_1+1}^{N_2} \frac{1}{(z_k - \varepsilon_m)(z_k - \varepsilon_n - \hbar\omega - i\delta)}$$

can be derived. Inserting Eqs. (1.78) and (1.79) into Eq. (1.75) and by extending the contours to cross the real axis at ∞ and $-\infty$, $\Sigma_{\mu\nu}(\mathbf{q}, \varpi)$ can be expressed as

$$\Sigma_{\mu\nu}(\mathbf{q}, \varpi) = -\frac{1}{2\pi V}\left\{ \oint_C dz\, f(z) \sum_{mn} \frac{J_\mu^{nm}(\mathbf{q})J_\nu^{mn}(-\mathbf{q})}{(z - \varepsilon_n)(z - \varepsilon_m + \hbar\omega + i\delta)} - \right. \qquad (1.80)$$

$$\left. \oint_{C'} dz\, f(z) \sum_{mn} \frac{J_\mu^{nm}(\mathbf{q})J_\nu^{mn}(-\mathbf{q})}{(z - \varepsilon_m)(z - \varepsilon_n - \hbar\omega - i\delta)} \right\}$$

$$+i\frac{\delta_T}{\pi V}\left\{ \sum_{k=-N_2+1}^{N_1} \sum_{mn} \frac{J_\mu^{nm}(\mathbf{q})J_\nu^{mn}(-\mathbf{q})}{(z_k - \varepsilon_n)(z_k - \varepsilon_m + \hbar\omega + i\delta)} + \right.$$

$$\left. \sum_{k=-N_1+1}^{N_2} \sum_{mn} \frac{J_\mu^{nm}(\mathbf{q})J_\nu^{mn}(-\mathbf{q})}{(z_k - \varepsilon_m)(z_k - \varepsilon_n - \hbar\omega - i\delta)} \right\} .$$

Let us now define the resolvent operator,

$$\hat{G}(z) = (z\hat{I} - \hat{H})^{-1} \, , \tag{1.81}$$

and its adjoint,

$$\hat{G}(z)^{\dagger} = (z^*\hat{I} - \hat{H})^{-1} = \hat{G}(z^*) \, . \tag{1.82}$$

By using the spectral representation of the resolvent,

$$\hat{G}(z) = \sum_n \frac{|\, n \,\rangle\langle\, n \,|}{z - \varepsilon_n} \, , \tag{1.83}$$

it is straightforward to rewrite Eq. (1.80) as

$$\Sigma_{\mu\nu}(\mathbf{q}, \varpi) = -\frac{1}{2\pi V} \left\{ \oint_C dz \, f(z) \, Tr \left(\hat{J}_\mu(\mathbf{q}) \, \hat{G}(z + \hbar\omega + i\delta) \, \hat{J}_\nu(-\mathbf{q}) \, \hat{G}(z) \right) - \right.$$
$$\left. \oint_{C'} dz \, f(z) \, Tr \left(\hat{J}_\mu(\mathbf{q}) \, \hat{G}(z) \hat{J}_\nu(-\mathbf{q}) \, \hat{G}(z - \hbar\omega - i\delta) \right) \right\}$$
$$+ i\frac{\delta_T}{\pi V} \left\{ \sum_{k=-N_2+1}^{N_1} Tr \left(\hat{J}_\mu(\mathbf{q}) \, \hat{G}(z_k + \hbar\omega + i\delta) \, \hat{J}_\nu(-\mathbf{q}) \, \hat{G}(z_k) \right) + \right.$$
$$\left. \sum_{k=-N_1+1}^{N_2} Tr \left(\hat{J}_\mu(\mathbf{q}) \, \hat{G}(z_k) \, \hat{J}_\nu(-\mathbf{q}) \, \hat{G}(z_k - \hbar\omega - i\delta) \right) \right\} \, . \tag{1.84}$$

By using the quantity,

$$\widetilde{\Sigma}_{\mu\nu}(\mathbf{q}; z_1, z_2) = -\frac{1}{2\pi V} Tr \left(\hat{J}_\mu(\mathbf{q})\hat{G}(z_1)\hat{J}_\nu(-\mathbf{q})\hat{G}(z_2) \right) \, , \tag{1.85}$$

for which the following symmetry relations apply,

$$\widetilde{\Sigma}_{\nu\mu}(-\mathbf{q}; z_2, z_1) = \widetilde{\Sigma}_{\mu\nu}(\mathbf{q}; z_1, z_2) \, ; \, \widetilde{\Sigma}_{\mu\nu}(\mathbf{q}; z_1^*, z_2^*) = \widetilde{\Sigma}_{\nu\mu}(\mathbf{q}; z_1, z_2)^* = \widetilde{\Sigma}_{\mu\nu}(-\mathbf{q}; z_2, z_1)^* \, , \tag{1.86}$$

Eq. (1.84) can be written as

$$\Sigma_{\mu\nu}(\mathbf{q}, \varpi) = \oint_C dz \, f(z) \, \widetilde{\Sigma}_{\mu\nu}(\mathbf{q}; z + \hbar\omega + i\delta, z) - \oint_{C'} dz \, f(z) \, \widetilde{\Sigma}_{\mu\nu}(\mathbf{q}; z, z - \hbar\omega - i\delta)$$
$$-2i\delta_T \left\{ \sum_{k=-N_2+1}^{N_1} \widetilde{\Sigma}_{\mu\nu}(\mathbf{q}; z_k + \hbar\omega + i\delta, z_k) + \sum_{k=-N_1+1}^{N_2} \widetilde{\Sigma}_{\mu\nu}(\mathbf{q}; z_k, z_k - \hbar\omega - i\delta) \right\} \, , \tag{1.87}$$

which can be transformed to

$$\Sigma_{\mu\nu}(\mathbf{q}, \varpi) = \oint_C dz\, f(z)\, \widetilde{\Sigma}_{\mu\nu}(\mathbf{q}; z + \hbar\omega + i\delta, z) - \left(\oint_C dz\, f(z)\, \widetilde{\Sigma}_{\mu\nu}(-\mathbf{q}; z - \hbar\omega + i\delta, z) \right)^*$$

$$-2i\delta_T \sum_{k=-N_2+1}^{N_1} \left(\widetilde{\Sigma}_{\mu\nu}(\mathbf{q}; z_k + \hbar\omega + i\delta, z_k) + \widetilde{\Sigma}_{\mu\nu}(-\mathbf{q}; z_k - \hbar\omega + i\delta, z_k)^* \right) , \quad (1.88)$$

because of the reflection symmetry for the contours C and C' (see Fig. 1.1) and the relations in Eq. (1.86).

Integration along the real axis: the limit of zero life-time broadening

Deforming the contour C to the real axis such that the contributions from the Matsubara poles vanish and using relations in Eq. (1.86), Eq. (1.88) trivially reduces to

$$\Sigma_{\mu\nu}(\mathbf{q}, \varpi) = \int_{-\infty}^{\infty} d\varepsilon\, f(\varepsilon) \left\{ \widetilde{\Sigma}_{\mu\nu}(\mathbf{q}; \varepsilon + \hbar\omega + i\delta, \varepsilon + i0) - \widetilde{\Sigma}_{\mu\nu}(-\mathbf{q}; \varepsilon + \hbar\omega + i\delta, \varepsilon - i0) \right\}$$

$$- \int_{-\infty}^{\infty} d\varepsilon\, f(\varepsilon) \left\{ \widetilde{\Sigma}_{\mu\nu}(\mathbf{q}; \varepsilon - i0, \varepsilon - \hbar\omega - i\delta) - \widetilde{\Sigma}_{\mu\nu}(-\mathbf{q}; \varepsilon + i0, \varepsilon - \hbar\omega - i\delta) \right\} ,$$

$$(1.89)$$

or by inserting the definition of $\widetilde{\Sigma}_{\mu\nu}(\mathbf{q}; z_1, z_2)$,

$$\Sigma_{\mu\nu}(\mathbf{q}, \varpi) = -\frac{1}{2\pi V} \int_{-\infty}^{\infty} d\varepsilon\, f(\varepsilon) \left\{ Tr\left(\hat{J}_\mu(\mathbf{q}) \hat{G}(\varepsilon + \hbar\omega + i\delta) \hat{J}_\nu(-\mathbf{q}) \hat{G}^+(\varepsilon) \right) \right. \quad (1.90)$$

$$- Tr\left(\hat{J}_\mu(-\mathbf{q}) \hat{G}(\varepsilon + \hbar\omega + i\delta) \hat{J}_\nu(\mathbf{q}) \hat{G}^-(\varepsilon) \right)$$

$$- Tr\left(\hat{J}_\mu(\mathbf{q}) \hat{G}^-(\varepsilon) \hat{J}_\nu(-\mathbf{q}) \hat{G}(\varepsilon - \hbar\omega - i\delta) \right)$$

$$\left. + Tr\left(\hat{J}_\mu(-\mathbf{q}) \hat{G}^+(\varepsilon) \hat{J}_\nu(\mathbf{q}) \hat{G}(\varepsilon - \hbar\omega - i\delta) \right) \right\}$$

with the up- and down-side limits of the resolvent, called advanced and retarded Green operators, $\hat{G}^+(\varepsilon)$ and $\hat{G}^-(\varepsilon)$, respectively, defined as

$$\hat{G}^\pm(\varepsilon) = \lim_{\theta \to +0} \hat{G}(\varepsilon \pm i\theta) \quad \text{and obviously} \quad \hat{G}^\pm(\varepsilon)^\dagger = \hat{G}^\mp(\varepsilon) . \quad (1.91)$$

It is important to mention that in spectral representation,

$$\hat{G}^{\pm}(\varepsilon) = \lim_{\theta \to +0} \sum_n \frac{|n\rangle\langle n|}{\varepsilon - \varepsilon_n \pm i\theta} = \sum_n \left[\mathbb{P}\left(\frac{1}{\varepsilon - \varepsilon_n}\right) \mp i\pi\delta(\varepsilon - \varepsilon_n) \right] |n\rangle\langle n| , \quad (1.92)$$

where $\mathbb{P}$ denotes the principal part distribution.

By taking the limit $\delta \to 0$ in Eq. (1.90), it transforms to

$$\Sigma_{\mu\nu}(\mathbf{q}, \omega) = -\frac{1}{2\pi V} \int_{-\infty}^{\infty} d\varepsilon \, f(\varepsilon) \left\{ Tr\left(\hat{J}_\mu(\mathbf{q})\hat{G}^+(\varepsilon + \hbar\omega)\hat{J}_\nu(-\mathbf{q})\hat{G}^+(\varepsilon) \right) \right. \quad (1.93)$$

$$- Tr\left(\hat{J}_\mu(-\mathbf{q})\hat{G}^+(\varepsilon + \hbar\omega)\hat{J}_\nu(\mathbf{q})\hat{G}^-(\varepsilon) \right)$$

$$- Tr\left(\hat{J}_\mu(\mathbf{q})\hat{G}^-(\varepsilon)\hat{J}_\nu(-\mathbf{q})\hat{G}^-(\varepsilon - \hbar\omega) \right)$$

$$\left. + Tr\left(\hat{J}_\mu(-\mathbf{q})\hat{G}^+(\varepsilon)\hat{J}_\nu(\mathbf{q})\hat{G}^-(\varepsilon - \hbar\omega) \right) \right\} .$$

In particular, for $\mathbf{q} = 0$, Eq. (1.93) reduces to

$$\Sigma_{\mu\nu}(\omega) = -\frac{1}{2\pi V} \int_{-\infty}^{\infty} d\varepsilon \, f(\varepsilon) \left\{ Tr\left(\hat{J}_\mu \hat{G}^+(\varepsilon + \hbar\omega)\hat{J}_\nu \left[\hat{G}^+(\varepsilon) - G^-(\varepsilon) \right] \right) \right. \quad (1.94)$$

$$\left. + Tr\left(\hat{J}_\mu \left[\hat{G}^+(\varepsilon) - G^-(\varepsilon) \right] \hat{J}_\nu \hat{G}^-(\varepsilon - \hbar\omega) \right) \right\} . \quad (1.95)$$

The hermitian part of $\Sigma_{\mu\nu}(\omega)$ is

$$\operatorname{Re}\Sigma_{\mu\nu}(\omega) \equiv \frac{1}{2}\left(\Sigma_{\mu\nu}(\omega) + \Sigma_{\mu\nu}(\omega)^*\right) , \quad (1.96)$$

which can be expressed as

$$\operatorname{Re}\Sigma_{\mu\nu}(\omega) = \frac{1}{\pi V} \int_{-\infty}^{\infty} d\varepsilon \, (f(\varepsilon) - f(\varepsilon + \hbar\omega)) \, Tr\left(\hat{J}_\mu \operatorname{Im}\hat{G}^+(\varepsilon + \hbar\omega)\hat{J}_\nu \operatorname{Im}\hat{G}^+(\varepsilon) \right) ,$$

$$(1.97)$$

see in Appendix B, with the imaginary part of the resolvent,

$$\operatorname{Im}\hat{G}^+(\varepsilon) = \frac{1}{2i}\left(\hat{G}^+(\varepsilon) - \hat{G}^-(\varepsilon) \right) , \quad (1.98)$$

which can be written using Eq. (1.92) as

$$\operatorname{Im}\hat{G}^+(\varepsilon) = -\pi \sum_n \delta(\varepsilon - \varepsilon_n)|n\rangle\langle n| . \quad (1.99)$$

Since, quite clearly, $\operatorname{Re}\Sigma_{\mu\nu}(0) = 0$,

$$\operatorname{Re}\sigma_{\mu\nu}(\omega) = \frac{\operatorname{Re}\Sigma_{\mu\nu}(\omega)}{\omega}, \qquad (1.100)$$

as used in practical calculations.

The static limit

In order to obtain the correct zero-frequency conductivity tensor, Eq. (1.90) has to be used in formula (1.67). Making use of the analyticity of the Green functions in the upper and lower complex semi-planes this leads to the Kubo-Luttinger formula [20, 42],

$$\sigma_{\mu\nu} = -\frac{\hbar}{2\pi V}\int\limits_{-\infty}^{\infty}d\varepsilon\, f(\varepsilon) \qquad (1.101)$$

$$\times Tr\left(\hat{J}_\mu\frac{\partial\hat{G}^+(\varepsilon)}{\partial\varepsilon}\hat{J}_\nu\left[\hat{G}^+(\varepsilon) - \hat{G}^-(\varepsilon)\right] - \hat{J}_\mu\left[\hat{G}^+(\varepsilon) - \hat{G}^-(\varepsilon)\right]\hat{J}_\nu\frac{\partial\hat{G}^-(\varepsilon)}{\partial\varepsilon}\right).$$

Integrating by parts yields

$$\sigma_{\mu\nu} = -\int\limits_{-\infty}^{\infty}d\varepsilon\,\frac{df(\varepsilon)}{d\varepsilon}S_{\mu\nu}(\varepsilon) \qquad (1.102)$$

with

$$S_{\mu\nu}(\varepsilon) = -\frac{\hbar}{2\pi V}\int\limits_{-\infty}^{\varepsilon}d\varepsilon' \qquad (1.103)$$

$$\times Tr\left(\hat{J}_\mu\frac{\partial\hat{G}^+(\varepsilon')}{\partial\varepsilon'}\hat{J}_\nu\left[\hat{G}^+(\varepsilon') - \hat{G}^-(\varepsilon')\right] - \hat{J}_\mu\left[\hat{G}^+(\varepsilon') - \hat{G}^-(\varepsilon')\right]\hat{J}_\nu\frac{\partial\hat{G}^-(\varepsilon')}{\partial\varepsilon'}\right),$$

which has the meaning of a zero-temperature, energy dependent conductivity. For $T = 0$, $\sigma_{\mu\nu}$ is obviously given by

$$\sigma_{\mu\nu} = S_{\mu\nu}(E_F). \qquad (1.104)$$

A numerically tractable formula can be obtained only for the *diagonal elements of the conductivity tensor*, see in Appendix B, resulting the widely used Kubo-Greenwood

formula [21, 22] of the dc-conductivity at finite temperatures,

$$\sigma_{\mu\mu} = -\frac{\hbar}{4\pi V} \int\limits_{-\infty}^{\infty} d\varepsilon \left(-\frac{df(\varepsilon)}{d\varepsilon}\right) Tr \left(\hat{J}_\mu \left[\hat{G}^+(\varepsilon) - \hat{G}^-(\varepsilon)\right] \hat{J}_\mu \left[\hat{G}^+(\varepsilon) - \hat{G}^-(\varepsilon)\right]\right) ,$$

(1.105)

which can obviously be written at $T = 0$ temperature as

$$\sigma_{\mu\mu} = -\frac{\hbar}{4\pi V} Tr \left(\hat{J}_\mu \left[\hat{G}^+(E_F) - \hat{G}^-(E_F)\right] \hat{J}_\mu \left[\hat{G}^+(E_F) - \hat{G}^-(E_F)\right]\right)$$

$$= \frac{\hbar}{\pi V} Tr \left(\hat{J}_\mu \operatorname{Im}\hat{G}^+(E_F) \hat{J}_\mu \operatorname{Im}\hat{G}^+(E_F)\right) .$$

(1.106)

It should be mentioned that by recalling the spectral resolution of the resolvents,

$$\operatorname{Im}\hat{G}^+(\varepsilon) = -\pi \sum_n |n\rangle\langle n| \,\delta(\varepsilon - \varepsilon_n) ,$$

(1.107)

Eq. (1.106) turns to be identical with the original Greenwood formula [21],

$$\sigma_{\mu\mu} = \frac{\pi\hbar}{V} \sum_{nm} J_\mu^{nm} J_\mu^{mn} \,\delta(E_F - \varepsilon_n) \,\delta(E_F - \varepsilon_m) .$$

(1.108)

On the other hand, Eq. (1.101) can be reformulated as follows,

$$\sigma_{\mu\nu} = \frac{\hbar}{2\pi V} \int\limits_{-\infty}^{\infty} d\varepsilon \, f(\varepsilon) \, Tr \left(\hat{J}_\mu \frac{d\hat{G}^+(\varepsilon)}{d\varepsilon} \hat{J}_\nu \hat{G}^-(\varepsilon) + \hat{J}_\mu \hat{G}^+(\varepsilon) \hat{J}_\nu \frac{d\hat{G}^-(\varepsilon)}{d\varepsilon}\right)$$

$$- \frac{\hbar}{2\pi V} \int\limits_{-\infty}^{\infty} d\varepsilon \, f(\varepsilon) \, Tr \left(\hat{J}_\mu \frac{d\hat{G}^+(\varepsilon)}{d\varepsilon} \hat{J}_\nu \hat{G}^+(\varepsilon) + \hat{J}_\mu \hat{G}^-(\varepsilon) \hat{J}_\nu \frac{d\hat{G}^-(\varepsilon)}{d\varepsilon}\right)$$

$$= \frac{\hbar}{2\pi V} \int\limits_{-\infty}^{\infty} d\varepsilon \left(-\frac{df(\varepsilon)}{d\varepsilon}\right) Tr \left(\hat{J}_\mu \hat{G}^+(\varepsilon) \hat{J}_\nu \hat{G}^-(\varepsilon)\right)$$

(1.109)

$$- \frac{\hbar}{2\pi V} \int\limits_{-\infty}^{\infty} d\varepsilon \, f(\varepsilon) \, Tr \left(\hat{J}_\mu \frac{d\hat{G}^+(\varepsilon)}{d\varepsilon} \hat{J}_\nu \hat{G}^+(\varepsilon) + \hat{J}_\mu \hat{G}^-(\varepsilon) \hat{J}_\nu \frac{d\hat{G}^-(\varepsilon)}{d\varepsilon}\right) ,$$

namely in terms of an equation which is similar to the formulation of Baranger and Stone [43] but clearly can be cast into a relativistic form. This expression is reasonable to write if conductance has to be calculated, see Section 4.2.3.

Chapter 2

Multiple scattering theory

In this Chapter, the multiple scattering theory or alternatively called the Korringa-Kohn-Rostoker (KKR) method [49, 50] for calculating band structure in solids is presented. This method is also called a Green's function method which makes the KKR method extremely recommended to combine with the Kubo formalism, see Section 1.3, in order to investigate electric transport in solids within a fully quantummechanical description.

2.1 Elements of the formal scattering theory

The resolvent operator and some of its properties were introduced in the last Chapter in Eqs. (1.81), (1.82), (1.83), (1.91), (1.92), (1.98), and (1.99). It should be mentioned that the coordinate representation of the resolvent operator is called *Green function* [51],

$$G(z; \mathbf{r}, \mathbf{r}') = \sum_n \frac{\psi_n(\mathbf{r}) \psi_n^*(\mathbf{r}')}{z - \varepsilon_n} , \qquad (2.1)$$

where $\psi_n(\mathbf{r}) = \langle \mathbf{r} | n \rangle$.

2.1.1 The Lippmann-Schwinger equation

Let us define the $\hat{H}$ operator of a physical system such as in Eq. (1.3) as a sum of the Hamiltonian of a reference (unperturbed) system, $\hat{H}_0$, and a real perturbation operator (potential), $\hat{V}$,

$$\hat{H} = \hat{H}_0 + \hat{V} . \qquad (2.2)$$

The resolvent of the reference system and its side limits are

$$\hat{G}_0(z) = (z\hat{I} - \hat{H}_0)^{-1}, \quad \hat{G}_0^{\pm}(\varepsilon) = \lim_{\delta \to +0} \hat{G}_0(\varepsilon \pm i\delta) , \quad (2.3)$$

respectively. From Eqs. (1.81), (2.2) and (2.3)

$$\hat{G}(z) = \left(\hat{G}_0^{-1}(z) - \hat{V}\right)^{-1} = \hat{G}_0(z)\left(\hat{I} + \hat{V}\hat{G}(z)\right) = \left(\hat{I} + \hat{G}(z)\hat{V}\right)\hat{G}_0(z) \quad (2.4)$$

is obtained, which is called the Dyson equation for the resolvent. The above equation can be rewritten by using successive iterations as

$$\hat{G}(z) = \hat{G}_0(z) + \hat{G}_0(z)\hat{V}\hat{G}_0(z) + \hat{G}_0(z)\hat{V}\hat{G}_0(z)\hat{V}\hat{G}_0(z) + \dots . \quad (2.5)$$

Let us introduce the so-called transition operators (T-operators),

$$\hat{T}(z) = \hat{V} + \hat{V}\hat{G}(z)\hat{V}, \qquad \hat{T}^{\pm}(\varepsilon) = \hat{V} + \hat{V}\hat{G}^{\pm}(\varepsilon)\hat{V} . \quad (2.6)$$

It is obvious from the definitions that the T-operators have the same analytic properties as the corresponding resolvents. Using Eqs. (2.5) and (2.6),

$$\hat{T}(z) = \hat{V} + \hat{V}\hat{G}_0(z)\hat{V} + \hat{V}\hat{G}_0(z)\hat{V}\hat{G}_0(z)\hat{V} + \dots = \hat{V} + \hat{V}\hat{G}_0(z)\hat{T}(z) \quad (2.7)$$

is obtained, thus the following can be derived,

$$\hat{G}_0(z)\hat{T}(z) = \hat{T}(z)\hat{G}_0(z) = \hat{V}\hat{G}(z) = \hat{G}(z)\hat{V} . \quad (2.8)$$

Therefore, the resolvents expressed with the corresponding T-operator are

$$\hat{G}(z) = \hat{G}_0(z) + \hat{G}_0(z)\hat{T}(z)\hat{G}_0(z), \quad \hat{G}^{\pm}(\varepsilon) = \hat{G}_0^{\pm}(\varepsilon) + \hat{G}_0^{\pm}(\varepsilon)\hat{T}^{\pm}(\varepsilon)\hat{G}_0^{\pm}(\varepsilon) . \quad (2.9)$$

We are searching for the scattering states of $\hat{H}$. They can be found by solving the following inhomogeneous problem,

$$(\varepsilon\hat{I} - \hat{H}_0)|\psi_\alpha(\varepsilon)\rangle = \hat{V}|\psi_\alpha(\varepsilon)\rangle , \quad (2.10)$$

where the solutions of the homogeneous problem obey

$$(\varepsilon\hat{I} - \hat{H}_0)|\phi_\alpha(\varepsilon)\rangle = 0 . \quad (2.11)$$

The solution will be the sum of the general solution of the homogeneous and a particular solution of the inhomogeneous differential equation, such as

$$|\psi_\alpha(\varepsilon)\rangle = |\phi_\alpha(\varepsilon)\rangle + (\varepsilon\hat{I} - \hat{H}_0)^{-1}\hat{V}|\psi_\alpha(\varepsilon)\rangle = |\phi_\alpha(\varepsilon)\rangle + \hat{G}_0(\varepsilon)\hat{V}|\psi_\alpha(\varepsilon)\rangle . \quad (2.12)$$

Iterating this equation successively we get the Born series,

$$|\psi_\alpha(\varepsilon)\rangle = \left(\hat{I} + \hat{G}_0(\varepsilon)\hat{V} + \hat{G}_0(\varepsilon)\hat{V}\hat{G}_0(\varepsilon)\hat{V} + \ldots \right)|\phi_\alpha(\varepsilon)\rangle . \quad (2.13)$$

This expression can be rewritten by using Eqs. (2.5) and (2.8) as

$$|\psi_\alpha(\varepsilon)\rangle = \left(\hat{I} + \hat{G}(\varepsilon)\hat{V}\right)|\phi_\alpha(\varepsilon)\rangle = \left(\hat{I} + \hat{G}_0(\varepsilon)\hat{T}(\varepsilon)\right)|\phi_\alpha(\varepsilon)\rangle , \quad (2.14)$$

which is commonly referred to as the Lippmann-Schwinger equation. Here, the solutions of the perturbed problem, $|\psi_\alpha(\varepsilon)\rangle$ are given in terms of the unperturbed eigenstates, $|\phi_\alpha(\varepsilon)\rangle$.

2.1.2 Expectation values and Lloyd's formula

Let us consider a hermitian one-particle operator $\hat{A}$ which is an observable physical quantity and its expectation value restricted to a given energy range $(\varepsilon_a, \varepsilon_b)$ can be written as

$$A_{ab} = \int_{\varepsilon_a}^{\varepsilon_b} d\varepsilon \, Tr\left(\hat{A}\sum_n \delta(\varepsilon - \varepsilon_n)|n\rangle\langle n|\right) , \quad (2.15)$$

which, in turn, can be reformulated using Eq. (1.99) as

$$A_{ab} = -\frac{1}{\pi}\int_{\varepsilon_a}^{\varepsilon_b} d\varepsilon \, Tr\left(\hat{A}\,\mathrm{Im}\,\hat{G}^+(\varepsilon)\right) = -\frac{1}{\pi}\mathrm{Im}\int_{\varepsilon_a}^{\varepsilon_b} d\varepsilon \, Tr\left(\hat{A}\hat{G}^+(\varepsilon)\right) . \quad (2.16)$$

Using complex contour-integral techniques and some theorems from the theory of complex functions, see e.g. [52], the expectation value A_{ab} can be expressed as

$$A_{ab} = -\frac{1}{\pi}\mathrm{Im}\int_\frown dz \, Tr\left(\hat{A}\hat{G}(z)\right) , \quad (2.17)$$

where $\frown$ means the integration over a semi-circle contour in the upper complex semi-plane with the lower and upper limits at ε_a and ε_b, respectively.

The charge density can be calculated in terms of the Green function, see Eq. (2.1), as

$$\rho(\mathbf{r}) = \mp \frac{e}{\pi} \int\limits_{\varepsilon_a}^{\varepsilon_b} d\varepsilon Im \left[G^{\pm}(\varepsilon, \mathbf{r}, \mathbf{r}) \right] , \qquad (2.18)$$

as well as the orbital and spin magnetization densities,

$$\mathbf{l}(\mathbf{r}) = \mp \frac{1}{\pi} \int\limits_{\varepsilon_a}^{\varepsilon_b} d\varepsilon Im \left[\beta \mathbf{L} G^{\pm}(\varepsilon, \mathbf{r}, \mathbf{r}) \right] , \qquad (2.19)$$

$$\mathbf{m}(\mathbf{r}) = \mp \frac{1}{\pi} \int\limits_{\varepsilon_a}^{\varepsilon_b} d\varepsilon Im \left[\beta \mathbf{S} G^{\pm}(\varepsilon, \mathbf{r}, \mathbf{r}) \right] , \qquad (2.20)$$

respectively, where $\mathbf{L}$ and $\mathbf{S}$ are the irreducible vector operators of orbital and spin moments.

The density of states (DOS) per unit volume can be expressed using Eqs. (1.92) and (1.99) in terms of the side limits of the resolvent as follows,

$$n(\varepsilon) = \sum_n Tr \left\{ \delta(\varepsilon - \varepsilon_n) |n\rangle\langle n| \right\} = \mp \frac{1}{\pi} Tr \left(Im \, \hat{G}^{\pm}(\varepsilon) \right) = \mp \frac{1}{\pi} Im \, Tr \hat{G}^{\pm}(\varepsilon) , \quad (2.21)$$

where Im is an operator and Im denotes the imaginary part of an expression. Substituting Eq. (2.9) into Eq. (2.21) and using the interesting property of the resolvent,

$$\frac{d\hat{G}(z)}{dz} = -\hat{G}(z)^2 , \qquad (2.22)$$

the following is obtained,

$$n(\varepsilon) = n_0(\varepsilon) + \frac{1}{\pi} Im \, Tr \left(\frac{d\hat{G}_0^+(\varepsilon)}{d\varepsilon} \hat{T}^+(\varepsilon) \right) , \qquad (2.23)$$

where $n_0(\varepsilon)$ is the free electron contribution to the DOS. The second term of the right part of the equation can be rewritten using the following identity [53],

$$\frac{d\hat{G}_0^+(\varepsilon)}{d\varepsilon} \hat{T}^+(\varepsilon) = \hat{T}^+(\varepsilon)^{-1} \frac{d\hat{T}^+(\varepsilon)}{d\varepsilon} = \frac{d}{d\varepsilon} \left(\ln \hat{T}^+(\varepsilon) \right) . \qquad (2.24)$$

With this, the integrated density of states can be written as

$$
N(\varepsilon) = \int_{-\infty}^{\varepsilon} d\varepsilon' n(\varepsilon') = \int_{-\infty}^{\varepsilon} d\varepsilon' \left\{ n_0(\varepsilon') + \frac{1}{\pi} Im \, Tr \left(\frac{d}{d\varepsilon'} \ln \hat{T}^+(\varepsilon') \right) \right\}
$$

$$
= N_0(\varepsilon) + \frac{1}{\pi} Im \, Tr \left(\ln \hat{T}^+(\varepsilon) \right) = N_0(\varepsilon) + \frac{1}{\pi} Im \, ln \, det \left(\hat{T}^+(\varepsilon) \right) , \qquad (2.25)
$$

which is Lloyd's formula [54], [55].

2.2 The muffin-tin approach

The formalism of scattering theory described above can be applied to a collection of individual scatterers. If we assume that these scatterers can be characterized by non-overlapping, spatially bounded, spherically symmetric potentials V_i, centered at the lattice position $\mathbf{R}_i$ (i=1 ... N) where N denotes the number of scatterers in the system, the following can be written,

$$
V(\mathbf{r}) = \sum_{i=1}^{N} V_i(\mathbf{r}_i) \qquad (\mathbf{r}_i = \mathbf{r} - \mathbf{R}_i) \qquad (2.26)
$$

$$
V_i(\mathbf{r}_i) = \left\{ \begin{array}{ll} V_i(r_i) & \text{if } |\mathbf{r}_i| < S_i \\ constant & \text{otherwise} \end{array} \right. \qquad (2.27)
$$

If the spheres do not overlap, we speak about the *muffin-tin* approach and S_i is called the muffin-tin radius of the ith sphere. In the so-called *atomic sphere approximation* (ASA) the spheres are chosen to have the same volume as the Wigner-Seitz cell, thus they overlap, but the effect of overlapping is neglected. In the region between the potential spheres $V(\mathbf{r}) = constant$ which is commonly set to zero. The restriction of the shape of the potentials to be spherically symmetric is a simplification which will be used in the following although the expression of the Green function we are going to derive is valid for arbitrary shape of the potential. The muffin-tin approach allows us to work with the well-known eigenfunctions of the angular momentum operator and the solution for the multi-site problem can be expressed in terms of potential dependent and independent parts.

2.3 Single-site scattering

The main purpose of this Section is to write down expressions for the matrix elements of the transition operator (denoted as t-operator) when the system contains only one spherically symmetric scatterer. In the absence of effective fields the Kohn-Sham-Dirac equation in Eq. (A.31), see Appendix A, takes the form [56, 57],

$$\hat{H}|\psi\rangle = \begin{pmatrix} (V(r) + mc^2)\hat{I}_2 & c\hat{\sigma}_r \left(\frac{\partial}{\partial r} + \frac{1}{r} - \frac{1}{r}\hat{\beta}\hat{K} \right) \\ c\hat{\sigma}_r \left(\frac{\partial}{\partial r} + \frac{1}{r} - \frac{1}{r}\hat{\beta}\hat{K} \right) & (V(r) - mc^2)\hat{I}_2 \end{pmatrix} |\psi\rangle = W|\psi\rangle , \quad (2.28)$$

where $\hat{\sigma}_r = \hat{\mathbf{r}} \cdot \hat{\boldsymbol{\sigma}}$ with $\hat{\mathbf{r}} = \mathbf{r}/|\mathbf{r}|)$, W is the total energy of the particle which satisfies $W^2 = p^2 c^2 + m^2 c^4$ with p being the momentum of the particle,

$$\hat{K} = \hat{\boldsymbol{\sigma}} \cdot \hat{\mathbf{L}} + \hbar \hat{I}_2 , \quad \text{and} \quad \hat{\beta} = \begin{pmatrix} \hat{I}_1 & 0 \\ 0 & -\hat{I}_1 \end{pmatrix} . \quad (2.29)$$

The wavefunction $|\psi\rangle$ can be decoupled into two bi-spinors: $|\psi\rangle = |\phi, \chi\rangle$. The total angular momentum operator is defined as $\hat{\mathbf{J}} = \hat{\mathbf{L}} + \hat{\mathbf{S}}$, where $\hat{\mathbf{L}}$ is the angular momentum operator and $\hat{\mathbf{S}} = \frac{1}{2}\hat{\boldsymbol{\sigma}}$ is the spin momentum operator.

We can recognize that $\hat{K}$ commutes with $\hat{J}$, in addition it can be easily checked that $\hat{H}$ commutes with $\hat{J}^2$, $\hat{J}_z$ and $\hat{K}$, therefore, the following eigenvalue equations are fulfilled,

$$\hat{J}^2|\phi\rangle = \hbar^2 j(j+1)|\phi\rangle, \quad \hat{J}^2|\chi\rangle = \hbar^2 j(j+1)|\chi\rangle, \quad j = l \pm \frac{1}{2} = \frac{1}{2}, \frac{3}{2}, \frac{5}{2}, \cdots$$

$$\hat{J}_z|\phi\rangle = \hbar\mu|\phi\rangle, \quad \hat{J}_z|\chi\rangle = \hbar\mu|\chi\rangle, \quad \mu = -j, \ldots, j$$

$$\hat{K}|\phi\rangle = -\hbar\kappa|\phi\rangle, \quad \hat{K}|\chi\rangle = \hbar\kappa|\chi\rangle, \quad \kappa = \mp \left(j + \frac{1}{2} \right) . \quad (2.30)$$

Let us introduce the spinor spherical harmonics as

$$|\kappa, \mu\rangle = |Q\rangle = \sum_{s=\pm 1/2} C(l, j, 1/2|\mu - s, s)|l, \mu - s\rangle \Phi_s , \text{ and } |-\kappa, \mu\rangle = |\bar{Q}\rangle , \quad (2.31)$$

where $C(l, j, 1/2|\mu - s, s)$ are the Clebsch-Gordan coefficients [58],
$\langle l, \mu - s|\hat{\mathbf{r}}\rangle = Y_l^{\mu - s}(\hat{r})$ and $\langle \hat{\mathbf{r}}|l, \mu - s\rangle = Y_l^{\mu - s}(\hat{r})^*$ denote the complex spherical harmonics and Φ_s are the bispinor basis functions [56],

$$\Phi_{1/2} = \begin{pmatrix} 1 \\ 0 \end{pmatrix} , \ \Phi_{-1/2} = \begin{pmatrix} 0 \\ 1 \end{pmatrix} . \quad (2.32)$$

In the following we shall use the weak-relativistic limit of the total energy,

$$W - mc^2 = \sqrt{p^2c^2 + m^2c^4} - mc^2 \approx \frac{p^2}{2m} = \varepsilon \ll mc^2 \qquad (2.33)$$

The non-relativistic Green function of the free electron in angular momentum representation can be written as, [51],

$$G_0^{nr,\pm}(\varepsilon, \mathbf{r}, \mathbf{r}') = \mp ip \sum_L j_l \left(\frac{pr_<}{\hbar}\right) h_l^\pm \left(\frac{pr_>}{\hbar}\right) Y_L(\hat{r}) Y_L^*(\hat{r}') \,, \qquad (2.34)$$

where $L = (l, m)$, $r_< = \min(r, r')$, $r_> = \max(r, r')$, and $h_l^\pm = j_l \pm in_l$ is the spherical Hankel function with j_l and n_l being the spherical Bessel and Neumann functions, respectively [52]. The regular solution is j_l and the irregular solution is n_l.

In relativistic case the Green function of the free electron in angular momentum representation takes the form [51],

$$G_0^r(W, \mathbf{r}, \mathbf{r}') = -ip\frac{W + mc^2}{2mc^2} \sum_Q [J_Q(W, \mathbf{r})H_Q^+(W, \mathbf{r}')^\dagger \theta(r' - r) + H_Q^+(W, \mathbf{r})J_Q^\dagger(W, \mathbf{r}')\theta(r - r')] \,,$$
$$(2.35)$$

where the solutions of the free Dirac-equation (V=0) in angular momentum representation [56] are

$$F_Q(W, \mathbf{r}) = \begin{bmatrix} f_l\left(\frac{pr}{\hbar}\right)\langle Q|\hat{\mathbf{r}}\rangle \\ \frac{iS_\kappa pc}{W+mc^2}f_{\bar{l}}\left(\frac{pr}{\hbar}\right)\langle \bar{Q}|\hat{\mathbf{r}}\rangle \end{bmatrix} \qquad (2.36)$$

and their adjoints are

$$F_Q^\dagger(W, \mathbf{r}) = \begin{bmatrix} f_l\left(\frac{pr}{\hbar}\right)\langle \hat{\mathbf{r}}|Q\rangle, & \frac{-iS_\kappa pc}{W+mc^2}f_{\bar{l}}\left(\frac{pr}{\hbar}\right)\langle \hat{\mathbf{r}}|\bar{Q}\rangle \end{bmatrix} \,, \qquad (2.37)$$

with $S_\kappa = \frac{\kappa}{|\kappa|}$, $\bar{l} = l - S_\kappa$, in addition $F_Q = J_Q$, N_Q and $H_Q^\pm$ with $f_l = j_l$, n_l and $h_l^\pm$, the spherical Bessel, Neumann and Hankel functions, respectively, which are the solutions of the radial Schrödinger-equation in the non-relativistic and zero potential case.

Now we are looking for the general solution of Eq. (2.28) using the following assumption for the radial wavefunction,

$$R(\varepsilon, \mathbf{r}) = \sum_Q R_Q(\varepsilon, \mathbf{r}) = \sum_Q \begin{bmatrix} g_\kappa(\varepsilon, r)\langle Q|\hat{\mathbf{r}}\rangle \\ if_\kappa(\varepsilon, r)\langle \bar{Q}|\hat{\mathbf{r}}\rangle \end{bmatrix} \,. \qquad (2.38)$$

Using the real-space representation of Eq. (2.14) with the free solution of the Dirac-equation, $J_Q(\varepsilon, \mathbf{r})$ and the form of the relativistic Green function in Eq. (2.35), we can write the solution outside the muffin-tin sphere as

$$R_Q(\varepsilon, \mathbf{r}) = J_Q(\varepsilon, \mathbf{r}) - ip \sum_{Q'} H_{Q'}^+(\varepsilon, \mathbf{r}) t_{Q'Q}(\varepsilon) , \qquad (2.39)$$

where $t_{Q'Q}(\varepsilon)$ denotes the matrix element of the $\hat{T}$ operator of the single-site problem, called usually the single-site t-matrix,

$$t_{Q'Q}(\varepsilon) = \int\limits_{r<S} d^3r \int\limits_{r'<S} d^3r' \, J_{Q'}^\dagger(\varepsilon, \mathbf{r}') t(\varepsilon, \mathbf{r}', \mathbf{r}) J_Q(\varepsilon, \mathbf{r}) . \qquad (2.40)$$

We can write the solutions for the radial wavefunctions outside the muffin-tin sphere (where V=0) as

$$g_\kappa(\varepsilon, r) = \cos\delta_\kappa(\varepsilon) j_l\left(\frac{pr}{\hbar}\right) - \sin\delta_\kappa(\varepsilon) n_l\left(\frac{pr}{\hbar}\right) \qquad (2.41)$$

$$cf_\kappa(\varepsilon, r) = pS_\kappa\left[\cos\delta_\kappa(\varepsilon) j_{\bar{l}}\left(\frac{pr}{\hbar}\right) - \sin\delta_\kappa(\varepsilon) n_{\bar{l}}\left(\frac{pr}{\hbar}\right)\right] , \qquad (2.42)$$

where $\delta_\kappa(\varepsilon)$ is called the κ-dependent phaseshift. If we require the continuity of both components at the muffin-tin radius S, we obtain the following for the phaseshift,

$$\tan\delta_\kappa(\varepsilon) = \frac{L_\kappa(\varepsilon, S) j_l\left(\frac{pS}{\hbar}\right) - pS_\kappa j_{\bar{l}}\left(\frac{pS}{\hbar}\right)}{L_\kappa(\varepsilon, r) n_l\left(\frac{pS}{\hbar}\right) - pS_\kappa' n_{\bar{l}}\left(\frac{pS}{\hbar}\right)} , \qquad (2.43)$$

where

$$L_\kappa(\varepsilon, S) = \frac{cf_\kappa(\varepsilon, S)}{g_\kappa(\varepsilon, S)} . \qquad (2.44)$$

Let us define the so-called scattering solutions as

$$Z(\varepsilon, \mathbf{r}) = \sum_Q Z_Q(\varepsilon, \mathbf{r}) = \sum_{Q'Q} R_{Q'}(\varepsilon, \mathbf{r}) t_{Q'Q}^{-1}(\varepsilon) . \qquad (2.45)$$

Using Eq. (2.39) and the form of the Hankel-function we can write $Z_Q(\varepsilon, \mathbf{r})$ as

$$Z_Q(\varepsilon, \mathbf{r}) = \sum_{Q'} J_{Q'}(\varepsilon, \mathbf{r}') K_{Q'Q}^{-1}(\varepsilon) + pN_Q(\varepsilon, \mathbf{r}) , \qquad (2.46)$$

where $K_{Q'Q}(z)$ is the so-called reactance-matrix defined by

$$K_{QQ'}^{-1}(\varepsilon) = t_{QQ'}^{-1}(\varepsilon) - ip\delta_{QQ'} . \qquad (2.47)$$

It is easy to check that the reactance-matrix is hermitian,

$$K(\varepsilon) = K^\dagger(\varepsilon) \,. \tag{2.48}$$

Moreover, in the spherically symmetric case, without external magnetic field, the single-site t-matrix and $K_{QQ'}(\varepsilon)$ become diagonal and independent of the quantum number μ,

$$t_{QQ'}(\varepsilon) = t_\kappa(\varepsilon)\delta_{QQ'} \quad , \quad t_\kappa(\varepsilon) = -p^{-1}\sin\delta_\kappa(\varepsilon)e^{i\delta_\kappa(\varepsilon)} \tag{2.49}$$

$$K_{QQ'}(\varepsilon) = K_\kappa(\varepsilon)\delta_{QQ'} \quad , \quad K_\kappa(\varepsilon) = -p^{-1}\tan\delta_\kappa(\varepsilon) \,. \tag{2.50}$$

2.4 Multiple scattering (KKR)

Let us now consider more than one spherically symmetric scatterers in the system. The total potential of these muffin-tin scatterers can be written as in Eq. (2.26). By inserting the shape of this potential into Eq. (2.7), we obtain

$$\hat{T}(\varepsilon) = \sum_i V_i + \sum_{i,j} V_i\hat{G}_0(\varepsilon)V_j + \sum_{i,j,k} V_i\hat{G}_0(\varepsilon)V_j\hat{G}_0(\varepsilon)V_k + \ldots \tag{2.51}$$

where $(i,j,k,\ldots)$ are site indices and $\varepsilon = p^2/2m$ in the weak-relativistic limit, see Eq. (2.33). Let us introduce the $\hat{Q}_i(\varepsilon)$-operators,

$$\hat{Q}_i(\varepsilon) = V_i + V_i\hat{G}_0(\varepsilon)\sum_j V_j + V_i\hat{G}_0(\varepsilon)\sum_{j,k} V_j\hat{G}_0(\varepsilon)V_k + \ldots = V_i + V_i\hat{G}_0(\varepsilon)\sum_j \hat{Q}_j(\varepsilon) \,,$$
$$\tag{2.52}$$

with this, $\hat{T}(\varepsilon)$ can be written as

$$\hat{T}(\varepsilon) = \sum_i \hat{Q}_i(\varepsilon) \,. \tag{2.53}$$

It is easy to check that $\hat{Q}_i(\varepsilon)$ can be expressed as

$$\hat{Q}_i(\varepsilon) = \hat{t}_i(\varepsilon) + \hat{t}_i(\varepsilon)\hat{G}_0(\varepsilon)\sum_{j\neq i} \hat{Q}_j(\varepsilon) \,, \tag{2.54}$$

where $\hat{t}_i(\varepsilon)$ denotes the single-site t-operator corresponding to a particular site i. By substituting the above expression of $\hat{Q}_i(\varepsilon)$ into Eq. (2.53), the following is obtained,

$$\hat{T}(\varepsilon) = \sum_i \hat{t}_i(\varepsilon) + \sum_{j\neq i} \hat{t}_i(\varepsilon)\hat{G}_0(\varepsilon)\hat{t}_j(\varepsilon) + \sum_{j\neq i,\, k\neq j} \hat{t}_i(\varepsilon)\hat{G}_0(\varepsilon)\hat{t}_j(\varepsilon)\hat{G}_0(\varepsilon)\hat{t}_k(\varepsilon) + \ldots \,.$$
$$\tag{2.55}$$

Let us now introduce the so-called scattering path operator (SPO), $\hat{\tau}_{ij}(\varepsilon)$ [59] as

$$\hat{\tau}_{ij}(\varepsilon) = \hat{t}_i(\varepsilon)\delta_{ij} + \hat{t}_i(\varepsilon)\hat{G}_0(\varepsilon)\sum_{k\neq i}\hat{\tau}_{kj}(\varepsilon) = \hat{t}_i(\varepsilon)\delta_{ij} + \sum_{k\neq j}\hat{\tau}_{ik}(\varepsilon)\hat{G}_0(\varepsilon)\hat{t}_j(\varepsilon) . \quad (2.56)$$

The SPO can be interpreted to give the scattered wave from site i resulting from an incident wave at site j. The matrix-elements of the scattering path operator in relativistic case are

$$\tau_{QQ'}^{ij}(\varepsilon) = \int\limits_{r_i<S_i} d^3r_i \int\limits_{r_j'<S_j} d^3r_j' \, J_Q^\dagger(\varepsilon,\mathbf{r}_i)\tau(\varepsilon,\mathbf{r}_i,\mathbf{r}_j')J_{Q'}(\varepsilon,\mathbf{r}_j') . \quad (2.57)$$

Using the SPO, $\hat{T}(\varepsilon)$ and $\hat{G}(\varepsilon)$ can be expressed as

$$\hat{T}(\varepsilon) = \sum_{i,j}\hat{\tau}_{ij}(\varepsilon) \quad (2.58)$$

$$\hat{G}(\varepsilon) = \hat{G}_0(\varepsilon) + \hat{G}_0(\varepsilon)\sum_{i,j}\hat{\tau}_{ij}(\varepsilon)\hat{G}_0(\varepsilon) . \quad (2.59)$$

Applying the addition theorem of the Bessel functions [60] in Eq. (2.34),

$$-iph_L^\times(\varepsilon,\mathbf{r}+\mathbf{r}') = \sum_{L'}G_{LL'}^0(\varepsilon,\mathbf{r}')j_{L'}^\times(\varepsilon,\mathbf{r}) \quad (2.60)$$

is obtained where

$$G_{LL'}^0(\varepsilon,\mathbf{r}) = -4\pi i^{(l-l'+1)}p\sum_{L''}C_{LL''}^{L'}i^{-l''}h_{L''}(\varepsilon,\mathbf{r}) , \quad (2.61)$$

$$C_{LL''}^{L'} = \int d\hat{\mathbf{r}}\,Y_L(\hat{r})Y_{L'}^*(\hat{r})Y_{L''}(\hat{r}) , \quad (2.62)$$

with the notations $j_L(\varepsilon,\mathbf{r}) \equiv j_l\left(\frac{pr}{\hbar}\right)Y_L(\hat{r})$ and $j_L^\times(\varepsilon,\mathbf{r}) \equiv j_l\left(\frac{pr}{\hbar}\right)Y_L^*(\hat{r})$, in addition $h_L(\varepsilon,\mathbf{r})$ and $h_L^\times(\varepsilon,\mathbf{r})$ are defined similarly. $C_{LL''}^{L'}$ are called the Gaunt coefficients and $G_{LL'}^0(\varepsilon,\mathbf{r})$ denote the so-called non-relativistic free structure constants.

Using this addition theorem, $G_0^{nr}(\varepsilon,\mathbf{r},\mathbf{r}')$ can be expanded in terms of the Bessel functions centered around the ith and jth site $(i \neq j)$ as follows,

$$G_0^{nr}(\varepsilon,\mathbf{r}_i+\mathbf{R}_i,\mathbf{r}_j'+\mathbf{R}_j) = \sum_{L,L'}j_L(\varepsilon,\mathbf{r}_i)G_{LL'}^{0,ij}(\varepsilon)j_{L'}^\times(\varepsilon,\mathbf{r}_j') , \quad (2.63)$$

where the notation $G_{LL'}^{0,ij}(\varepsilon) = G_{LL'}^0(\varepsilon, \mathbf{R}_j - \mathbf{R}_i)$ is applied.

The relativistic Green function can be expressed similarly as

$$G_0^r(\varepsilon, \mathbf{r}_i + \mathbf{R}_i, \mathbf{r}_j' + \mathbf{R}_j) = \sum_{QQ'} J_Q(\varepsilon, \mathbf{r}_i) G_{QQ'}^{0,ij}(\varepsilon) J_{Q'}^\dagger(\varepsilon, \mathbf{r}_j') , \qquad (2.64)$$

where the relativistic free structure constants are obtained from the non-relativistic ones as

$$G_{QQ'}^{0,ij}(\varepsilon) = \frac{W + mc^2}{2mc^2} \sum_s C(l, j, 1/2 | \mu - s, s) G_{LL'}^{0,ij}(\varepsilon) C(l', j', 1/2 | \mu' - s, s) . \quad (2.65)$$

Substituting Eq. (2.64) into Eq. (2.56) and applying Eq. (2.57) leads to [51]

$$\tau_{QQ'}^{ij}(\varepsilon) = t_{QQ'}^i(\varepsilon)\delta_{ij} + \sum_{k \neq i} \sum_{Q_1 Q_2} t_{QQ_1}^i(\varepsilon) G_{Q_1 Q_2}^{0,ik}(\varepsilon) \tau_{Q_2 Q'}^{kj}(\varepsilon) , \qquad (2.66)$$

which can be expressed in a supermatrix formalism [18] as

$$\underline{\underline{\tau}}(\varepsilon) = \left(\underline{\underline{t}}^{-1}(\varepsilon) - \underline{\underline{G}}_0(\varepsilon) \right)^{-1} , \qquad (2.67)$$

with the notations,

$$\underline{\underline{t}}(\varepsilon) = \left\{ \underline{t}^i(\varepsilon)\delta_{ij} \right\} , \quad \underline{\underline{\tau}}(\varepsilon) = \left\{ \underline{\tau}^{ij}(\varepsilon) \right\} , \quad \underline{\underline{G}}_0(\varepsilon) = \left\{ \underline{G}_0^{ij}(\varepsilon) \right\} , \qquad (2.68)$$

and the underlined quantities are matrices of momentum indices (Q, Q'). Eq. (2.67) is usually referred to as the fundamental equation of multiple scattering in supermatrix notation (or simply KKR-equation). The inverse of the τ-matrix is commonly called the KKR-matrix. It is important to mention that the geometrical information of the lattice contained by $\underline{\underline{G}}_0(\varepsilon)$ and the scattering properties of the individual scatterers described by $\underline{\underline{t}}(\varepsilon)$ are completely separated.

The Green function from Eq. (2.59) can reformulated as

$$
\begin{aligned}
G(\varepsilon, \mathbf{r}_i, \mathbf{r}_j') &= \sum_{Q,Q'} \left[Z_Q^i(\varepsilon, \mathbf{r}_i) \tau_{QQ'}^{ij}(\varepsilon) Z_{Q'}^j(\varepsilon, \mathbf{r}_j')^\dagger - \right. \qquad (2.69) \\
&\quad \left. - \delta_{ij}\delta_{QQ'} \left(\theta(r_i - r_i') Z_Q^i(\varepsilon, \mathbf{r}_i') I_{Q'}^i(\varepsilon, \mathbf{r}_i)^\dagger + \theta(r_i' - r_i) I_Q^i(\varepsilon, \mathbf{r}_i') Z_{Q'}^i(\varepsilon, \mathbf{r}_i)^\dagger \right) \right] ,
\end{aligned}
$$

where $Z_Q^i(\varepsilon, \mathbf{r})$ and $I_Q^i(\varepsilon, \mathbf{r})$ denote the regular and irregular solutions of the Dirac equation in cell i. At the muffin-tin radius of the ith cell (S_i) the following have to be satisfied,

$$Z_Q^i(\varepsilon, S_i) = \sum_{Q'} \left(t_{QQ'}^i \right)^{-1} J_{Q'}(\varepsilon, S_i) - ip H_Q^{+i}(\varepsilon, S_i) , \qquad (2.70)$$

$$I_Q^i(\varepsilon, S_i) = J_Q(\varepsilon, S_i) . \qquad (2.71)$$

2.4.1 Layered systems

Layered systems are systems with (at least) two-dimensional translational symmetry. In the case of a surface or an interface, the translational symmetry is broken along the direction perpendicular to the plane. Suppose such a layered system corresponds to a parent infinite (three-dimensional periodic) system consisting of a simple lattice with only one atom per unit cell, then any lattice site $\mathbf{R}_{pi}$ can be written as

$$\mathbf{R}_{pi} = \mathbf{C}_p + \mathbf{T}_i \quad ; \quad \mathbf{T}_i \in L_2 \quad , \tag{2.72}$$

where $\mathbf{C}_p$ is the "spanning vector" of a particular layer p and the two-dimensional (real) lattice is denoted by $L_2 = \{\mathbf{T}_i\}$ with in-plane lattice vectors, $\mathbf{T}_i$ and the corresponding set of indices $I(L_2)$. It should be noted that $\mathbf{C}_p$ points into the origin of layer p but it does not necessarily mean that it must be perpendicular to the plane, e.g. in a body centered cubic (BCC) lattice for the (001)-plane $\mathbf{C}_p = p \cdot a \cdot (\frac{1}{2}, \frac{1}{2}, \frac{1}{2})$ where a is the three-dimensional lattice constant.

The real-space structure constants can be written as

$$\begin{aligned}
\underline{G}_0^{ij}(\varepsilon) &= \underline{G}_0(\varepsilon, \mathbf{R}_{pi} - \mathbf{R}_{qj}) = \underline{G}_0(\varepsilon, \mathbf{C}_p + \mathbf{T}_i - \mathbf{C}_q - \mathbf{T}_j) = \underline{\widehat{G}}_0^{pq}(\varepsilon, \mathbf{T}_i - \mathbf{T}_j) = \\
&= \frac{1}{\Omega_{BZ}} \int\limits_{BZ} d^2 k_{\|} \underline{\widehat{G}}_0^{pq}(\varepsilon, \mathbf{k}_{\|}) e^{-i \mathbf{k}_{\|}(\mathbf{T}_i - \mathbf{T}_j)} \, ,
\end{aligned} \tag{2.73}$$

where Ω_{BZ} denotes the volume of the two dimensional Brillouin-zone, $\mathbf{k}_{\|}$ lies in the first 2D Brillouin-zone and 'hat' denotes a layer-indexed quantity (angular momentum representation of an operator) in order to distinguish from a site-indexed one. The 2D lattice Fourier transform of the structure constants is defined as

$$\underline{\widehat{G}}_0^{pq}(\varepsilon, \mathbf{k}_{\|}) = \sum_{\mathbf{T}_i} \underline{\widehat{G}}_0^{pq}(\varepsilon, \mathbf{T}_i) e^{i \mathbf{k}_{\|} \mathbf{T}_i} \, . \tag{2.74}$$

Introducing a new matrix notation in terms of layer indices where 'hat' denotes here matrices with layer indices,

$$\underline{\widehat{t}}(\varepsilon) = \{\underline{\widehat{t}}_p(\varepsilon) \delta_{pq}\}, \quad \underline{\widehat{G}}_0(\varepsilon, \mathbf{k}_{\|}) = \{\underline{\widehat{G}}_0^{pq}(\varepsilon, \mathbf{k}_{\|})\}, \quad \underline{\widehat{\tau}}(\varepsilon, \mathbf{k}_{\|}) = \{\underline{\widehat{\tau}}_{pq}(\varepsilon, \mathbf{k}_{\|})\} \, , \tag{2.75}$$

the KKR-equation can be written in the same form as in Eq. (2.67),

$$\underline{\widehat{\tau}}(\varepsilon, \mathbf{k}_{\|}) = \left(\underline{\widehat{t}}^{-1}(\varepsilon) - \underline{\widehat{G}}_0(\varepsilon, \mathbf{k}_{\|}) \right)^{-1} \, , \tag{2.76}$$

but the dimension of the matrices are different from the matrices in Eq. (2.68).

2.5 The screened KKR-method (SKKR)

For systems containing several atoms per unit cell as well as for layered structures severe difficulties arise from the long range of the structure constants. For such systems, tight-binding (TB) methods seem to be better suited. However, it can be shown that applying the so-called screening transformation, the KKR-method can be transformed into a TB form [17, 25, 61].

It is known that the free space structure constants decay exponentially for negative energies since no eigensolutions of the Schrödinger-equation exist in free space in that energy range. This fact implies that we should find a reference system which has the same properties as described above. In [25] the muffin-tin approach is used as a reference system with a repulsive potential, V^r which is about 1-2 Ry above the valence band within the non-overlapping muffin-tin spheres and zero otherwise. In the following, r-indexed quantities are of the reference system and quantities without index are of the physical system. The so-called structural Green's function matrices can be written as

$$\underline{\underline{G}}(\varepsilon) = \underline{\underline{G}}_0(\varepsilon) \left(\underline{\underline{I}} - \underline{\underline{t}}(\varepsilon)\underline{\underline{G}}_0(\varepsilon) \right)^{-1}, \quad \underline{\underline{G}}^r(\varepsilon) = \underline{\underline{G}}_0(\varepsilon) \left(\underline{\underline{I}} - \underline{\underline{t}}^r(\varepsilon)\underline{\underline{G}}_0(\varepsilon) \right)^{-1}, \quad (2.77)$$

and the reference Green function, $\underline{\underline{G}}^r(\varepsilon)$ is found spatially localized in real space. Defining the difference of the inverse of the t-matrices as

$$\underline{\underline{t}}_\Delta(\varepsilon) = \underline{\underline{t}}(\varepsilon) - \underline{\underline{t}}^r(\varepsilon) \qquad (2.78)$$

and the screened scattering path operator as

$$\underline{\underline{\tau}}_\Delta(\varepsilon) = \left(\underline{\underline{t}}_\Delta^{-1}(\varepsilon) - \underline{\underline{G}}^r(\varepsilon) \right)^{-1}, \qquad (2.79)$$

the unscreened (physical) scattering path operator can be calculated from the screened one using the invariance property [25],

$$\underline{\underline{G}}(\varepsilon) = \underline{\underline{t}}^{-1}(\varepsilon)\underline{\underline{\tau}}(\varepsilon)\underline{\underline{t}}^{-1}(\varepsilon) - \underline{\underline{t}}^{-1}(\varepsilon) = \underline{\underline{t}}_\Delta^{-1}(\varepsilon)\underline{\underline{\tau}}_\Delta(\varepsilon)\underline{\underline{t}}_\Delta^{-1}(\varepsilon) - \underline{\underline{t}}_\Delta^{-1}(\varepsilon) \qquad (2.80)$$

$$\underline{\underline{\tau}}(\varepsilon) = \left[\underline{\underline{I}} - \underline{\underline{t}}^r(\varepsilon)\underline{\underline{t}}^{-1}(\varepsilon) \right] \underline{\underline{\tau}}_\Delta(\varepsilon) \left[\underline{\underline{I}} - \underline{\underline{t}}^{-1}(\varepsilon)\underline{\underline{t}}^r(\varepsilon) \right] + \left[\underline{\underline{t}}^r(\varepsilon) - \underline{\underline{t}}^r(\varepsilon)\underline{\underline{t}}^{-1}(\varepsilon)\underline{\underline{t}}^r(\varepsilon) \right].$$
$$(2.81)$$

Thus in a layered system first the 2D lattice Fourier transform of the screened scattering path operator must be calculated as

$$\widehat{\underline{\tau}}_{\Delta,pq}(\varepsilon, \mathbf{k}_\parallel) = \left\{ \left((\widehat{\underline{t}}_\Delta)^{-1}(\varepsilon) - \widehat{\underline{\underline{G}}}^r(\varepsilon, \mathbf{k}_\parallel) \right)^{-1} \right\}_{pq} . \tag{2.82}$$

Because of the screening, $\widehat{G}^r$ can be truncated for $|p - q| > n$, $n \approx 3$ in bcc and fcc systems, so $\widehat{G}^r$ becomes block-tridiagonal,

$$\widehat{\underline{\underline{G}}}^r(\varepsilon, \mathbf{k}_\parallel) = \begin{pmatrix} m_{00}(\varepsilon, \mathbf{k}_\parallel) & m_{01}(\varepsilon, \mathbf{k}_\parallel) & & \\ m_{10}(\varepsilon, \mathbf{k}_\parallel) & m_{00}(\varepsilon, \mathbf{k}_\parallel) & m_{01}(\varepsilon, \mathbf{k}_\parallel) & \\ & m_{10}(\varepsilon, \mathbf{k}_\parallel) & m_{00}(\varepsilon, \mathbf{k}_\parallel) & m_{01}(\varepsilon, \mathbf{k}_\parallel) \\ & & \ddots & \ddots & \ddots \end{pmatrix} . \tag{2.83}$$

The blocks are related to the so-called *principal layers* containing n atomic layers. If the layers lie on the top of a semi-infinite bulk (substrate) or between two semi-infinite bulks the so-called surface Green function method [17] must be considered to ensure proper boundary conditions.

We get the real-space physical τ-matrix by performing the 2D BZ-integral,

$$\underline{\tau}_\Delta(\varepsilon, \mathbf{R}_{pi} - \mathbf{R}_{qj}) = \frac{1}{\Omega_{BZ}} \int\limits_{BZ} d^2 k_\parallel \widehat{\underline{\tau}}_{\Delta,pq}(\varepsilon, \mathbf{k}_\parallel) e^{-i\mathbf{k}_\parallel (\mathbf{T}_i - \mathbf{T}_j)} \tag{2.84}$$

and by transforming it using Eq. (2.81). For a 2D translational invariant medium, the physical real space τ-matrix can now be written as

$$\underline{\tau}^{pi,qj}(\varepsilon) = \frac{1}{\Omega_{BZ}} \int\limits_{BZ} d^2 k_\parallel \widehat{\underline{\tau}}^{pq}(\varepsilon, \mathbf{k}_\parallel) e^{-i\mathbf{k}_\parallel (\mathbf{T}_i - \mathbf{T}_j)} . \tag{2.85}$$

We obtain the Green function of the layered system by substituting the physical τ-matrix into Eq. (2.69). This allows us to calculate one-particle observables as in Eq. (2.17) or even the non-local conductivity tensor at $T = 0$ temperature as in Eq. (4.4). The non-local conductivity can be expressed also in terms of the real-space τ-matrix, see Section 4.1.

For surface and interface problems, the computational complexity of the SKKR-method scales linearly with the number of layers, N taken into account. Compared to other methods which usually have an N^3 scaling this method provides us considerable savings in computer time especially in large systems.

For a more detailed description of the SKKR method, see [27].

2.6 The embedding technique

The embedding technique was developed by Podloucky et al. [62] and Weinberger et al. [63]. Considering a layered system serving as unperturbed host, arbitrary positions can be prescribed in the lattice where impurity atoms substitute the original .ones. In this Section a description of the scattering properties of this perturbed system is presented. In our calculations three types of embedding were performed: 1. The so-called "self-embedding", see Chapter 6, where arbitrary atoms in the host are substituted by themselves, which, in turn, means simply a real space calculation. 2. Magnetic impurities are embedded into the surface layer of a non-magnetic metal surface forming finite chains, see Chapter 8. 3. Noble metal atoms are embedded into the vacuum region between two semi-infinite leads of the same metal, thus, forming a nanocontact between them, see Chapter 9. The conductance for different atomic arrangements of the contact was studied as well as the effect of transition metal impurities on the conductance by embedding them into diverse positions of the contact.

It should be mentioned that the vacuum region consists of empty spheres. Combining the embedding technique with the SKKR method, the unperturbed host is chosen to be the reference system. It is also important that the host system and the perturbed one have the same lattice geometry which means that no lattice relaxation effects were taken into account in our calculations. Moreover, as described in details within the Coherent Potential Approximation (CPA) in Chapter 3, the calculation of restricted ensemble average of the real space τ-matrix can be obtained by performing an embedding of a single impurity (site-diagonal τ) or two impurities (site-offdiagonal τ) into the coherent medium.

2.6.1 The τ-matrix of a finite cluster

A finite *cluster* is defined as a geometrical arrangement of a set of scatterers. Let $\mathcal{C}$ denote the set of position vectors pointing to sites in the cluster,

$$\mathcal{C} \equiv \{\mathbf{R}_i\}, \quad i = 1, \ldots, N, \tag{2.86}$$

where N is the number of atoms in the cluster taken into account and i labels these sites. A set which contains the site-indices is defined as

$$C_N \equiv \{i \mid \mathbf{R}_i \in \mathcal{C}, \quad i = 1, \ldots, N\} \ . \tag{2.87}$$

For the host system the potential can be written as

$$V^{host}(\mathbf{r}) = \sum_i V_i^{host}(\mathbf{r}_i) \ , \tag{2.88}$$

while for a system with an embedded cluster as

$$V^{clus}(\mathbf{r}) = \sum_i V_i^{clus}(\mathbf{r}_i) \quad , \quad V_i^{clus}(\mathbf{r}_i) = \begin{cases} V_i^{host}(\mathbf{r}_i) & \text{if } i \notin C_N \\[2ex] V_i^{imp}(\mathbf{r}_i) & \text{if } i \in C_N \end{cases} \ . \tag{2.89}$$

Consequently, the t-matrices of the perturbed system have the form,

$$\underline{t}_{clus}^i(\varepsilon) = \begin{cases} \underline{t}_{host}^i(\varepsilon) & \text{if } i \notin C_N \\[2ex] \underline{t}_{imp}^i(\varepsilon) & \text{if } i \in C_N \end{cases} \ . \tag{2.90}$$

It is important to emphasize that by performing real embedding, a cluster usually contains the investigated impurity atoms, some sites from the host material, for which the changes caused by the impurities can be studied and even empty spheres (vacuum in the case of a surface or nanocontact) which can contain also some electron density, thus V_i^{imp}, $\underline{t}_{imp}^i$ are different for each cluster-site corresponding to the above classification. By performing real space calculation ("self-embedding"), $V_i^{clus}(\mathbf{r}_i) = V_i^{host}(\mathbf{r}_i)$, $\underline{t}_{clus}^i = \underline{t}_{host}^i$ for the whole system, there is no need of a self-consistent calculation of the cluster. Moreover, it should be noted that V_i^{host}, $\underline{t}_{host}^i$ could be different for different sites. In the present calculations V_i^{host}, $\underline{t}_{host}^i$ are different for different layers due to the choice of layered systems serving as host.

Let us write the KKR-equation for the unperturbed and perturbed systems,

$$\underline{\tau}_{host}^{-1}(\varepsilon) = \underline{t}_{host}^{-1}(\varepsilon) - \underline{G}_0(\varepsilon) \ , \quad \underline{\tau}_{clus}^{-1}(\varepsilon) = \underline{t}_{clus}^{-1}(\varepsilon) - \underline{G}_0(\varepsilon) \ , \tag{2.91}$$

respectively, with

$$\underline{\tau}(\varepsilon) = \left\{\underline{\tau}^{ij}(\varepsilon)\right\} \ , \ \underline{\tau}^{ij}(\varepsilon) = \left\{\tau_{QQ'}^{ij}(\varepsilon)\right\} \ , \ \underline{t}(\varepsilon) = \left\{\underline{t}^i(\varepsilon)\delta_{ij}\right\} \ , \ \underline{t}^i(\varepsilon) = \left\{t_{QQ'}^i(\varepsilon)\right\} \ . \tag{2.92}$$

Defining

$$\Delta\underline{t}^{-1}(\varepsilon) = \underline{t}^{-1}_{host}(\varepsilon) - \underline{t}^{-1}_{clus}(\varepsilon) = \left\{\Delta\underline{t}^{i}(\varepsilon)^{-1}\delta_{ij}\right\} ,$$

$$\Delta\underline{t}^{i}(\varepsilon)^{-1} = \begin{cases} 0 & \text{if } i \notin C_N \\ \underline{t}^{i}_{host}(\varepsilon)^{-1} - \underline{t}^{i}_{imp}(\varepsilon)^{-1} & \text{if } i \in C_N \end{cases} \tag{2.93}$$

and manipulating Eq. (2.91) results

$$\begin{aligned} \underline{\tau}^{-1}_{clus}(\varepsilon) &= \underline{\tau}^{-1}_{host}(\varepsilon) - \Delta\underline{t}^{-1}(\varepsilon) \tag{2.94} \\ &= \left[\underline{I} - \Delta\underline{t}^{-1}(\varepsilon)\underline{\tau}_{host}(\varepsilon)\right]\underline{\tau}^{-1}_{host}(\varepsilon) \\ &= \underline{\tau}^{-1}_{host}(\varepsilon)\left[\underline{I} - \underline{\tau}_{host}(\varepsilon)\Delta\underline{t}^{-1}(\varepsilon)\right] . \end{aligned}$$

Inverting this leads to the embedding equation,

$$\underline{\tau}_{clus}(\varepsilon) = \underline{\tau}_{host}(\varepsilon)\left[\underline{I} - \Delta\underline{t}^{-1}(\varepsilon)\underline{\tau}_{host}(\varepsilon)\right]^{-1} = \left[\underline{I} - \underline{\tau}_{host}(\varepsilon)\Delta\underline{t}^{-1}(\varepsilon)\right]^{-1}\underline{\tau}_{host}(\varepsilon) . \tag{2.95}$$

It should be noted that this equation is a generalization of the KKR method where a non-free space reference system is considered (here: host), which has some theoretical applications (SKKR, CPA, embedding). For studying local physical properties of impurities embedded into a host material, the diagonal blocks of $\underline{\tau}_{clus}$ matrix have to be calculated, while for non-local conductivities the full $\underline{\tau}_{clus}$ matrix is needed, see Section 4.1. Moreover, by performing real space calculation ("self-embedding"), $\Delta\underline{t}^{-1} \equiv 0$ which results that $\underline{\tau}_{clus} \equiv \underline{\tau}_{host}$, a cluster means here only a region under consideration in a specific material, there is no real embedding.

At this point it is important to write down the expression of the real space $\underline{\tau}_{host}$ once more. For a 2D translational invariant host medium, it has the form,

$$\underline{\tau}^{pi,qj}_{host}(\varepsilon) = \frac{1}{\Omega_{BZ}}\int_{BZ} d^2k_{\|}e^{-i\mathbf{k}_{\|}(\mathbf{T}_i-\mathbf{T}_j)}\widehat{\underline{\tau}}^{pq}_{host}(\varepsilon,\mathbf{k}_{\|}) . \tag{2.96}$$

It should be mentioned that specifically, for a single impurity at site i_0 the embedding equation reduces to

$$\underline{\tau}^{i_0,i_0}(\varepsilon) = \underline{\tau}^{i_0,i_0}_{host}(\varepsilon)\left[\underline{I} - \Delta\underline{t}^{i_0}(\varepsilon)^{-1}\underline{\tau}^{i_0,i_0}_{host}(\varepsilon)\right]^{-1} . \tag{2.97}$$

2.6.2   Self-consistent calculation for a cluster

An iterative method is carried out in order to find the solution of the non-linear Kohn-Sham-Dirac equation (A.31) which usually follows the scheme,

$$V^{(0)} \to \tau^{(0)} \to V^{(1)} \to \tau^{(1)} \to \ldots \to V^{(n)} \to \tau^{(n)} \to V^{(n+1)} \to \ldots \qquad (2.98)$$

where $\tau^{(i)}$ $(V^{(i)})$ is the SPO matrix (potential) after the ith iterative step. In the LSDA approach, see Appendix A, the potential is determined by the charge- and magnetization densities, see Eqs. (2.18) and (2.20). A self-consistent potential or charge density in a solid can be obtained as a fix-point of the iterative method,

$$\lim_{n\to\infty} V^{(n)}(\mathbf{r}) = V(\mathbf{r}) , \qquad (2.99)$$

$$\lim_{n\to\infty} \rho^{(n)}(\mathbf{r}) = \rho(\mathbf{r}) , \qquad (2.100)$$

which also implies for the τ-matrix,

$$\lim_{n\to\infty} \underline{\tau}^{(n)}(z) = \underline{\tau}(z) . \qquad (2.101)$$

Let us specify the scheme sketched in Eq. (2.98). The input potential for the next iteration $(n + 1)$ is obtained by the output from some of the previous iterations "mixed" with each other,

$$V_{in}^{(n+1)}(\mathbf{r}) = V_{out}^{(n)}(\mathbf{r}) + \sum_{j=1}^{m} \beta_j \left(V_{out}^{(n-j)}(\mathbf{r}) - V_{out}^{(n)}(\mathbf{r}) \right) . \qquad (2.102)$$

The following notations have been used, $V_{in}^{(i)}$ is the input potential of the ith step, $V_{out}^{(i)}$ is the corresponding output potential, m is an arbitrarily chosen integer and β_m is a weighting (mixing) factor for the previous output potentials. There are various *potential mixing* schemes the complexities of which can be different due to the different choice of m and the method of optimizing β_j (e.g. simple-mixing: $m = 1$ and β_1 arbitrary; Anderson mixing [64]: $m = 1$ and β_1 is determined by a least-square deviation process). In the present calculations the so-called *modified Broyden mixing* as proposed by Johnson [65] is used. It should be noted that the mixing procedure can be performed equivalently for the charge and spin densities. Moreover, the above described procedure have been used also for determining the self-consistent potentials of the layered systems serving as host. A more detailed description of the embedding technique can be found in Ref. [27].

Chapter 3

Disordered systems

The theoretical methods discussed in the previous chapters, with exception of the embedding procedure, are restricted to ordered matter, i.e. systems with well defined two- or three-dimensional translational symmetry. However, disordered systems are quite important in technological applications, thus the theoretical investigation of alloys is highly desirable. In this Chapter, the scattering properties of substitutional binary alloys are described within the Coherent Potential Approximation (CPA) [18, 66, 67] which can be combined with the SKKR electronic structure method, see Section 2.5. Electrical transport properties of substitutional binary alloys are described in Section 4.1.1 and 4.3.

3.1   Configurational averages

Suppose a binary bulk alloy is of composition A_cB_{1-c} with $c_A = c$ being the concentration of species A and $c_B = (1 - c)$ the concentration of species B. Supposing, moreover, the total number of atoms in the above system is N and the number of A atoms and B atoms is N_A and N_B, respectively, the following can be written,

$$N = N_A + N_B \ , \ N_A = cN \ , \ N_B = (1 - c)N \ . \tag{3.1}$$

A substitutional binary alloy means that there is no positional disorder, all atoms are in a position of an underlying ideal simple lattice $\mathcal{L}$ which is characterized by the set of indices, $I(\mathcal{L})$. Such alloys can be identified experimentally because the diffraction pattern of them have a specific feature, namely sharp Bragg maxima.

51

Assuming substitutional binary alloys, the potential can be written as

$$V\left(\mathbf{r}\right) = \sum_{i \in I(\mathcal{L})} V_i\left(\mathbf{r}_i - \mathbf{R}_i\right) , \tag{3.2}$$

$$V_i\left(\mathbf{r}_i - \mathbf{R}_i\right) = \xi_i V_A\left(\mathbf{r}_i - \mathbf{R}_i\right) + \left(1 - \xi_i\right) V_B\left(\mathbf{r}_i - \mathbf{R}_i\right) , \tag{3.3}$$

where ξ_i is an occupational variable such that $\xi_i = 1$ if site $\mathbf{R}_i$ is occupied by species A and $\xi_i = 0$ if this site is occupied by species B. For a completely random alloy the probability for $\xi_i = 1$ is c_A and correspondingly for $\xi_i = 0$ the probability is c_B. In Eq. (3.3) $V_A(\mathbf{r}_i - \mathbf{R}_i)$ and $V_B(\mathbf{r}_i - \mathbf{R}_i)$ are the individual (effective) potentials of species A and B at the site $\mathbf{R}_i$, respectively. Then $\{\xi_i \mid i \in I\left(\mathcal{L}\right)\}$ is one particular arrangement of atoms A and B on the positions of $\mathcal{L}$. Such an arrangement is called a *configuration*. Quite clearly for one particular configuration the Kohn-Sham equation can be solved, see Appendix A,

$$\hat{H}\left\{\xi_i\right\} \psi_n\left(\mathbf{r}, \left\{\xi_i\right\}\right) = \varepsilon_n\left\{\xi_i\right\} \psi_n\left(\mathbf{r}, \left\{\xi_i\right\}\right) , \tag{3.4}$$

where $\hat{H}$ is the Hamiltonian of the system and n labels the eigenstates. Observables, however, in general do not map a particular configuration but an average over all configurations. Let $\langle A_{nn'} \rangle$ be the configurationally averaged matrix element of a Hermitian operator $\hat{A}$. Then

$$\langle A_{nn'} \rangle = \sum_{\{\xi_i\}} P\left(\{\xi_i\}\right) \left\langle \psi_n\left\{\xi_i\right\} \middle| \hat{A} \middle| \psi_{n'}\left\{\xi_i\right\} \right\rangle , \tag{3.5}$$

where $P\left(\{\xi_i\}\right)$ is the microcanonical probability for a particular configuration $\{\xi_i\}$. It is assumed that the occupational probabilities for different sites are independent from each other, i.e., that

$$P\left(\{\xi_i\}\right) = \prod_i P_i\left(\xi_i\right) , \quad \sum_{\xi_i = 0,1} P_i\left(\xi_i\right) = P_i\left(0\right) + P_i\left(1\right) = 1 , \tag{3.6}$$

$$\langle \xi_i \rangle \equiv P_i\left(1\right) = c , \quad \langle 1 - \xi_i \rangle \equiv P_i\left(0\right) = 1 - c .$$

Obviously the calculation of averages such in Eq. (3.5) is greatly simplified by directly calculating the configurationally averaged Green function $\langle G^+(\varepsilon, \mathbf{r}, \mathbf{r}') \rangle$ from which typical one-particle physical properties can immediately be obtained, similarly as presented in Section 2.1.2. The expression of configurationally averaged conductivity is more complicated which will be given in Section 4.3. First, the *restricted*

ensemble averages denoted by $\langle \ldots \rangle_{(i=\alpha)}$ have to be introduced. It has the following meaning: in cell i the occupation is fixed to atom α ($\alpha \in \{A, B\}$) and the averaging is restricted to all configurations for the remaining $N-1$ sites. Without any details, by using restricted ensemble averages the configurational average is partitioned into two subsets, whereas the following condition has to be satisfied,

$$\left\langle G^+(\varepsilon, \mathbf{r}_i, \mathbf{r}_i) \right\rangle = \sum_{\alpha \in \{A,B\}} c_\alpha \left\langle G^+(\varepsilon, \mathbf{r}_i, \mathbf{r}_i) \right\rangle_{(i=\alpha)} . \tag{3.7}$$

3.2 The electron self-energy operator

The aim of this Section is to find a translationally invariant effective system with a resolvent being identical with the configurationally averaged resolvent of a disordered system. The averaged resolvent $\left\langle \hat{G}(z) \right\rangle$ of the Hamiltonian $\hat{H}$ in Eq. (3.4) can formally be written as

$$\left\langle \hat{G}(z) \right\rangle = \left\langle \left(z\hat{I} - \hat{H} \right)^{-1} \right\rangle = \left[z\hat{I} - \hat{H}_0 - \hat{\Sigma}(z) \right]^{-1} \tag{3.8}$$

with $\hat{\Sigma}(z)$ being the so-called *electron self-energy operator*. Assuming that in the system under consideration no positional disorder is present, $\hat{H}$ can formally be rewritten as

$$\hat{H} = \hat{H}_0 + \hat{V} - \hat{W}(z) + \hat{W}(z) = \tilde{\hat{H}}(z) + \tilde{\hat{V}}(z) ,$$
$$\tilde{\hat{H}}(z) = \hat{H}_0 + \hat{W}(z) , \quad \tilde{\hat{V}}(z) = \hat{V} - \hat{W}(z) . \tag{3.9}$$

where $\hat{V}$ is given by a superposition of (real) individual site potentials V_i, see Eq. (3.2), and $\hat{W}(z)$ as a superposition of energy-dependent translationally invariant site quantities $\hat{W}_i(z)$ as

$$\hat{W}(z) = \sum_i \hat{W}_i(z) , \quad [E \mid \mathbf{R}_i] W_i(\mathbf{r}, z) = W_i(\mathbf{r}, z) ; \ \forall \, [E \mid \mathbf{R}_i] \in T . \tag{3.10}$$

$$\tilde{\hat{V}}(z) = \sum_i \tilde{V}_i(z) = \sum_i (V_i - W_i(z)) . \tag{3.11}$$

Using the above expressions, the resolvent $\hat{G}(z)$ can be written as

$$\hat{G}(z) = \left[z\hat{I} - \tilde{\hat{H}}(z) - \tilde{\hat{V}}(z) \right]^{-1} . \tag{3.12}$$

Let $\tilde{\hat{G}}(z)$ be the resolvent of $\tilde{\hat{H}}(z)$,

$$\tilde{\hat{G}}(z) = \left[z\hat{I} - \tilde{\hat{H}}(z) \right]^{-1} , \tag{3.13}$$

the resolvent $\hat{G}(z)$ and the corresponding T-operator $\hat{T}(z)$ are then given by the Dyson equations, similarly as in Section 2.1.1,

$$\hat{G}(z) = \tilde{\hat{G}}(z) \left[\hat{I} + \tilde{\hat{V}}(z)\hat{G}(z) \right] = \tilde{\hat{G}}(z) \left[\hat{I} + \hat{T}(z)\tilde{\hat{G}}(z) \right] , \tag{3.14}$$

$$\hat{T}(z) = \tilde{\hat{V}}(z) \left[\hat{I} + \hat{G}(z)\tilde{\hat{V}}(z) \right] = \tilde{\hat{V}}(z) \left[\hat{I} + \tilde{\hat{G}}(z)\hat{T}(z) \right] . \tag{3.15}$$

It should be noted that the scattering processes are now much more complicated because the scattering from the individual site terms $\tilde{V}_i(z)$ is in relation to a generally non-hermitian reference medium. Moreover, $\tilde{\hat{G}}(z)$ is translationally invariant because of Eq. (3.10). Averaging Eq. (3.14) over all configurations therefore gives

$$\left\langle \hat{G}(z) \right\rangle = \tilde{\hat{G}}(z) + \tilde{\hat{G}}(z) \left\langle \hat{T}(z) \right\rangle \tilde{\hat{G}}(z) = \left[\hat{I} + \tilde{\hat{G}}(z) \left\langle \hat{T}(z) \right\rangle \right] \tilde{\hat{G}}(z) . \tag{3.16}$$

3.3 The coherent potential approximation (CPA)

Let $\left\langle \hat{T}\left(z; \hat{W}(z) \right) \right\rangle$ denote the averaged T-operator for a particularly chosen medium $\hat{W}(z)$, and let $\tilde{\hat{G}}\left(z; \hat{W}(z) \right)$ be the corresponding resolvent of $\tilde{\hat{H}}(z) = \hat{H}_0 + \hat{W}(z)$. Then from Eq. (3.16) it is obviously seen that

$$\left\langle \hat{G}(z) \right\rangle = \tilde{\hat{G}}\left(z; \hat{W}(z) \right) \tag{3.17}$$

if and only if

$$\left\langle \hat{T}\left(z; \hat{W}(z) \right) \right\rangle = 0 , \tag{3.18}$$

and consequently, the self-energy operator $\hat{\Sigma}(z)$ is simply given by

$$\hat{\Sigma}(z) = \hat{W}(z) . \tag{3.19}$$

Equations (3.17) and (3.18) serve both as definitions and as practical tools: if on average there is no additional scattering because of $\hat{W}(z)$, i.e., the condition in Eq. (3.18) is met, then the averaged resolvent $\left\langle \hat{G}(z) \right\rangle$ is indeed the translationally

invariant resolvent $\tilde{\hat{G}}(z)$ of an (in general non-hermitian) operator $\tilde{\hat{H}}(z) = \hat{H}_0 + \hat{W}(z)$ corresponding to the *complex potential operator* $\hat{W}(z)$. Therefore, in order to fulfil Eq. (3.17), Eq. (3.18) has to be solved self-consistently. The condition in Eq. (3.18) is usually called the *Coherent Potential Approximation* (CPA).

3.4 The CPA single-site approximation

The total T-operator can be written in terms of $\hat{Q}_i(z)$, see also Section 2.4,

$$\hat{T}(z) = \sum_i \hat{Q}_i(z) , \tag{3.20}$$

$$\hat{Q}_i(z) = \hat{t}_i(z) + \hat{t}_i(z)\tilde{\hat{G}}(z) \sum_{j \neq i} \hat{Q}_j(z) , \tag{3.21}$$

where

$$\hat{t}_i(z) = \tilde{\hat{V}}_i(z) + \tilde{\hat{V}}_i(z)\tilde{\hat{G}}(z)\hat{t}_i(z) \tag{3.22}$$

according to Eq. (3.15). The average of the T matrix, $\left\langle \hat{T}(z) \right\rangle$, is therefore given by

$$\left\langle \hat{T}(z) \right\rangle = \sum_i \left\langle \hat{Q}_i(z) \right\rangle . \tag{3.23}$$

Averaging $\hat{Q}_i(z)$, the following is obtained,

$$\begin{aligned}
\left\langle \hat{Q}_i(z) \right\rangle &= \left\langle \hat{t}_i(z) \right\rangle + \left\langle \hat{t}_i(z)\tilde{\hat{G}}(z) \sum_{j \neq i} \hat{Q}_j(z) \right\rangle \\
&= \left\langle \hat{t}_i(z) \right\rangle \left[\hat{I} + \tilde{\hat{G}}(z) \sum_{j \neq i} \left\langle \hat{Q}_j(z) \right\rangle \right] + \left\langle \left[\hat{t}_i(z) - \left\langle \hat{t}_i(z) \right\rangle \right] \tilde{\hat{G}}(z) \sum_{j \neq i} \hat{Q}_j(z) \right\rangle .
\end{aligned} \tag{3.24}$$

The first term on the right-hand side consists only of single-site quantities, whereas the second term is a kind of fluctuation or correlation term. The omission of the second term is called the *single-site approximation* for the configurational average. Within this approximation $\left\langle \hat{Q}_i(z) \right\rangle$ is given by

$$\left\langle \hat{Q}_i(z) \right\rangle = \left\langle \hat{t}_i(z) \right\rangle \left[\hat{I} + \tilde{\hat{G}}(z) \sum_{j \neq i} \left\langle \hat{Q}_j(z) \right\rangle \right] . \tag{3.25}$$

Let $\hat{T}\left(z;\hat{W}(z)\right)$ be the T-operator for a given periodic complex function $\hat{W}(z)$. Then the CPA equation in Eq. (3.18),

$$\left\langle \hat{T}\left(z;\hat{W}(z)\right)\right\rangle = \sum_{i}\left\langle \hat{Q}_{i}\left(z;\hat{W}(z)\right)\right\rangle = 0 \ , \qquad (3.26)$$

in the single-site approximation requires that

$$\left\langle \hat{Q}_{i}\left(z;\hat{W}(z)\right)\right\rangle = 0 \quad ; \qquad \forall i \in I(\mathcal{L}) \ . \qquad (3.27)$$

From Eq. (3.25), however, it is obviosly seen that within the single-site approximation the CPA condition is simply reduced to

$$\left\langle \hat{t}_{i}\left(z;\hat{W}(z)\right)\right\rangle = 0 \quad ; \qquad \forall i \in I(\mathcal{L}) \ . \qquad (3.28)$$

It should be noted that by applying the single-site approximation *short-range-order effects* are explicitly excluded. Multiple scattering effects, however, are implicitly included since the single-site approximation is based on the idea of a single scatterer immersed in an average medium, i.e., on the very concept of a 'mean field theory'. It is also worthwhile to mention that by satisfying Eq. (3.28) the lowest order correlation in terms of the t-matrices neglected with respect to the condition Eq. (3.26) is of fourth order [68].

From the definition of the SPO in Eq. (2.66) it is immediately seen that the condition in Eq. (3.28) can be rewritten for the site-diagonal SPO matrix *with the effective medium as reference* as

$$\left\langle \underline{\tau}^{ii}\left(\varepsilon;W(\varepsilon)\right)\right\rangle = 0 \quad ; \quad \forall i \in I(\mathcal{L}) \ . \qquad (3.29)$$

From Eq. (3.7) and the relation of the site-diagonal SPO to the Green function $G(\varepsilon,\mathbf{r},\mathbf{r}')$, it is clear that for a binary system $A_{c}B_{1-c}$ (simple lattice, one atom per unit cell) the restricted averages $\left\langle \underline{\tau}^{ii}(\varepsilon)\right\rangle_{(i=\alpha)}$, $\alpha \in \{A,B\}$, have to meet the condition,

$$c\left\langle \underline{\tau}^{ii}(\varepsilon)\right\rangle_{(i=A)} + (1-c)\left\langle \underline{\tau}^{ii}(\varepsilon)\right\rangle_{(i=B)} = \left\langle \underline{\tau}^{ii}(\varepsilon)\right\rangle \ . \qquad (3.30)$$

Since Eqs. (3.29) and (3.30) are valid for all site indices $i \in I(\mathcal{L})$, it is sufficient to restrict Eq. (3.30) according to the symmetries of the system, for example, to $i = 0$ (0=origin of the underlying lattice) for a bulk or to $i = p0$ ($\forall p$, $p0$=origin of the pth layer) for layered systems. The question arises how to calculate the restricted averages. This will be given in the next Section.

3.5   CPA condition for layered systems

Layered systems were introduced in Section 2.4.1. For a given interface region of n layers, containing also disordered layers, the coherent scattering path operator $\tau_c(\varepsilon)$ is given by the following 2D BZ-integral,

$$\underline{\tau}_c^{pi,qj}(\varepsilon) = \frac{1}{\Omega_{BZ}} \int_{BZ} e^{-i\mathbf{k}_{\parallel}(\mathbf{T}_i - \mathbf{T}_j)} \, \widehat{\underline{\tau}}_c^{pq}(\varepsilon, \mathbf{k}_{\parallel}) \, d^2 k_{\parallel} \,, \tag{3.31}$$

where pi and qj denote site i in layer p and site j in layer q, respectively. Moreover, $\widehat{\underline{\tau}}_c^{pq}(\varepsilon, \mathbf{k}_{\parallel})$ is the (pq)th block of the supermatrix,

$$\widehat{\underline{\underline{\tau}}}_c(\varepsilon, \mathbf{k}_{\parallel}) = \left[\widehat{\underline{\underline{t}}}_c(\varepsilon)^{-1} - \widehat{\underline{\underline{G}}}(\varepsilon, \mathbf{k}_{\parallel}) \right]^{-1} \,. \tag{3.32}$$

Here, the notation 'hat' is used as it was introduced in Section 2.4.1 and $\widehat{\underline{\underline{G}}}$ is a layer-angular momentum representation of the resolvent in Eq. (3.13) in Fourier space, similarly calculated as in Eqs. (2.73) and (2.74). Moreover, Eq. (3.31) implies two–dimensional translational invariance of the coherent medium for all layers of the interface region, i.e., that in each layer p for the coherent single–site t–matrices the following translational invariance applies,

$$\underline{t}_c^{pi}(\varepsilon) = \underline{t}_c^{p0}(\varepsilon) = \widehat{\underline{t}}_c^{p}(\varepsilon) \,; \quad \forall i \in I(L_2) \,. \tag{3.33}$$

It should be noted that numerical recipes to evaluate $\widehat{\underline{\tau}}_c^{pq}(\varepsilon, \mathbf{k}_{\parallel})$ in Eq. (3.31) for layered structures are provided by different variants of multiple scattering theory, see Chapter 2. Let us now write the supermatrices for better understanding,

$$\widehat{\underline{\underline{t}}}_c(\varepsilon) = \begin{pmatrix} \widehat{\underline{t}}_c^{1}(\varepsilon) & 0 & \cdots & \cdots & 0 \\ 0 & \ddots & & & \vdots \\ \vdots & & \widehat{\underline{t}}_c^{p}(\varepsilon) & & \vdots \\ \vdots & & & \ddots & 0 \\ 0 & \cdots & \cdots & 0 & \widehat{\underline{t}}_c^{n}(\varepsilon) \end{pmatrix} \,, \tag{3.34}$$

and

$$\widehat{\underline{\tau}}_c(\varepsilon) = \begin{pmatrix} & \vdots & & \vdots & \\ \cdots & \widehat{\underline{\tau}}_c^{pp}(\varepsilon) & \cdots & \widehat{\underline{\tau}}_c^{pq}(\varepsilon) & \cdots \\ & \vdots & & \vdots & \\ \cdots & \widehat{\underline{\tau}}_c^{qp}(\varepsilon) & \cdots & \widehat{\underline{\tau}}_c^{qq}(\varepsilon) & \cdots \\ & \vdots & & \vdots & \end{pmatrix} , \qquad (3.35)$$

$$p, q = 1, \ldots, n .$$

Quite clearly, a particular element of $\widehat{\underline{\tau}}_c(\varepsilon)$,

$$\widehat{\underline{\tau}}_c^{pq}(\varepsilon) = \underline{\tau}_c^{pi,qi}(\varepsilon) = \underline{\tau}_c^{p0,q0}(\varepsilon) = \frac{1}{\Omega_{BZ}} \int\limits_{BZ} \widehat{\underline{\tau}}_c^{pq}(\varepsilon, \mathbf{k}_\parallel) \, d^2 k_\parallel \qquad (3.36)$$

refers to the unit cells at the origin of L_2 in layers p and q. Suppose now, in general, the concentration for constituents A and B in layer p is denoted by c_p^α ($p = 1, \ldots, n$; $\alpha \in \{A, B\}$). By defining the so-called *impurity matrices* (see Eqs. (51),(52) of Ref. [22]), that specify a single impurity of type α in the translational invariant coherent host formed by layer p, as

$$\widehat{\underline{D}}_\alpha^p(\varepsilon) \equiv \underline{D}_\alpha^{p0}(\varepsilon) = \left[\underline{I} - \underline{\tau}_c^{p0,p0}(\varepsilon) \underline{m}_\alpha^{p0}(\varepsilon) \right]^{-1} , \qquad (3.37)$$

$$\widehat{\underline{\widetilde{D}}}_\alpha^p(\varepsilon) \equiv \widetilde{\underline{D}}_\alpha^{p0}(\varepsilon) = \left[\underline{I} - \underline{m}_\alpha^{p0}(\varepsilon) \underline{\tau}_c^{p0,p0}(\varepsilon) \right]^{-1} , \qquad (3.38)$$

with

$$\underline{m}_\alpha^{p0}(\varepsilon) = \underline{m}_\alpha^{pi}(\varepsilon) = \widehat{\underline{m}}_\alpha^p(\varepsilon) = \underline{\widehat{t}}_c^p(\varepsilon)^{-1} - \underline{\widehat{t}}_\alpha^p(\varepsilon)^{-1}, \quad \alpha \in \{A, B\} , \qquad (3.39)$$

where $\widehat{\underline{t}}_\alpha^p(\varepsilon)$ is the single–site t–matrix for constituent α in layer p, the coherent scattering path operator for the interface region, $\widehat{\underline{\tau}}_c(\varepsilon)$ is obtained from the following inhomogeneous CPA condition,

$$\widehat{\underline{\tau}}_c^{pp}(\varepsilon) = \sum_{\alpha \in \{A,B\}} c_p^\alpha \, \langle \widehat{\underline{\tau}}^{pp}(\varepsilon) \rangle_{p,\alpha} , \qquad (3.40)$$

$$\langle \widehat{\underline{\tau}}^{pp}(\varepsilon) \rangle_{p,\alpha} = \widehat{\underline{\tau}}_\alpha^p(\varepsilon) = \widehat{\underline{D}}_\alpha^p(\varepsilon) \widehat{\underline{\tau}}_c^{pp}(\varepsilon) = \widehat{\underline{\tau}}_c^{pp}(\varepsilon) \widehat{\underline{\widetilde{D}}}_\alpha^p(\varepsilon) , \qquad (3.41)$$

i.e., from a condition that implies solving *simultaneously* a layer-diagonal CPA condition for layers $p = 1, \ldots, n$. Once this condition is met then translational invariance

in each layer under consideration is achieved,

$$\left\langle \widehat{\underline{\tau}}^{pp}(\varepsilon)\right\rangle_{p,\alpha} \equiv \left\langle \underline{\tau}^{p0,p0}(\varepsilon)\right\rangle_{(p0=\alpha)} = \left\langle \underline{\tau}^{pi,pi}(\varepsilon)\right\rangle_{(pi=\alpha)} , \tag{3.42}$$

$$\forall i \in I(L_2) \quad , \quad p = 1,\ldots,n \quad .$$

It is obviosly seen that the restricted ensemble averages can be calculated by embedding an atom of type α into the 2D translationally invariant coherent medium,

$$\left\langle \underline{\tau}^{p0,p0}(\varepsilon)\right\rangle_{(p0=\alpha)} = \widehat{\underline{D}}_\alpha^p(\varepsilon)\underline{\tau}_c^{p0,p0}(\varepsilon) = \underline{\tau}_c^{p0,p0}(\varepsilon)\widehat{\widetilde{\underline{D}}}_\alpha^p(\varepsilon) . \tag{3.43}$$

Similarly, by specifying the occupation on two different sites the following restricted averages are obtained,

$$p \neq q : \quad \left\langle \underline{\tau}^{pi,qj}(\varepsilon)\right\rangle_{(pi=\alpha,qj=\beta)} = \widehat{\underline{D}}_\alpha^p(\varepsilon)\underline{\tau}_c^{pi,qj}(\varepsilon)\widehat{\widetilde{\underline{D}}}_\beta^q(\varepsilon) , \tag{3.44}$$

$$p = q, \; i \neq j : \quad = \left\langle \underline{\tau}^{pi,pj}(\varepsilon)\right\rangle_{(pi=\alpha,pj=\beta)} = \widehat{\underline{D}}_\alpha^p(\varepsilon)\underline{\tau}_c^{pi,pj}(\varepsilon)\widehat{\widetilde{\underline{D}}}_\beta^p(\varepsilon) , \tag{3.45}$$

where $\left\langle \underline{\tau}_c^{pi,qj}(\varepsilon)\right\rangle_{(pi=\alpha,qj=\beta)}$ has the meaning that site (subcell) pi is occupied by species α and site (subcell) qj by species β.

In a more general case, if no translational invariance is present at all, the restricted averages can be written as

$$\left\langle \underline{\tau}^{pi,pi}(\varepsilon)\right\rangle_{(pi=\alpha)} = \underline{D}_\alpha^{pi}(\varepsilon)\underline{\tau}_c^{pi,pi}(\varepsilon) = \underline{\tau}_c^{pi,pi}(\varepsilon)\widetilde{\underline{D}}_\alpha^{pi}(\varepsilon) , \tag{3.46}$$

$$\left\langle \underline{\tau}^{pi,qj}(\varepsilon)\right\rangle_{(pi=\alpha,qj=\beta)} = \underline{D}_\alpha^{pi}(\varepsilon)\underline{\tau}_c^{pi,qj}(\varepsilon)\widetilde{\underline{D}}_\beta^{qj}(\varepsilon) , \tag{3.47}$$

with the impurity matrices defined similarly as in Eqs. (3.37) and (3.38) with the exception that they are not equal to all sites in a given layer because of the absence of the 2D translational invariance.

3.6 Numerical solution of the CPA equations

In this Section, 3D translational invariance of the effective medium is assumed in order to get simpler formulas but the presented method is applicable also for other systems. It is worth to introduce the following quantity [22],

$$\underline{X}_\alpha(\varepsilon) = \left[\left(\underline{t}_\alpha^{-1}(\varepsilon) - \underline{t}_c^{-1}(\varepsilon)\right)^{-1} + \underline{\tau}_c^{00}(\varepsilon)\right]^{-1} , \tag{3.48}$$

which plays here the role of the single-site t-matrix of a tight-binding formalism. With this, the impurity matrices can be written as

$$\underline{D}_\alpha^{00}(\varepsilon) = \underline{1} - \underline{\tau}_c^{00}(\varepsilon)\underline{X}_\alpha(\varepsilon) \quad \text{and} \quad \underline{\tilde{D}}_\alpha^{00}(\varepsilon) = \underline{1} - \underline{X}_\alpha(\varepsilon)\underline{\tau}_c^{00}(\varepsilon) , \qquad (3.49)$$

and the single-site CPA condition in Eq. (3.30) can be reformulated as

$$c\underline{X}_A^{00}(\varepsilon) + (1-c)\underline{X}_B^{00}(\varepsilon) = \underline{0} , \qquad (3.50)$$

which is usually called the KKR-CPA equation. An efficient numerical solution of this expression of the CPA condition, generalized for m components,

$$\sum_{\alpha=1}^m c_\alpha \underline{X}_\alpha(\varepsilon) = \underline{0} \quad , \quad \sum_{\alpha=1}^m c_\alpha = 1 , \qquad (3.51)$$

was originally proposed by Mills et $al.$ [69] and then implemented first by Ginatempo and Staunton [70]. Suppose the condition in Eq. (3.51) is not satisfied in the n-th step of the iteration. Then the following matrix, $\underline{X}_c^{(n)}(\varepsilon)$ can be defined as

$$\underline{X}_c^{(n)}(\varepsilon) \equiv \sum_{\alpha=1}^m c_\alpha \underline{X}_\alpha^{(n)}(\varepsilon) \neq \underline{0} , \qquad (3.52)$$

where

$$\underline{X}_\alpha^{(n)}(\varepsilon) = \left[\left(\underline{t}_\alpha(\varepsilon)^{-1} - \underline{t}_c^{(n)}(\varepsilon)^{-1}\right)^{-1} + \underline{\tau}_c^{00(n)}(\varepsilon) \right]^{-1} . \qquad (3.53)$$

The subsequent guess for $\underline{t}_c(\varepsilon)$ can be estimated as follows,

$$\underline{X}_c^{(n)}(\varepsilon) = \left[\left(\underline{t}_c^{(n)}(\varepsilon)^{-1} - \underline{t}_c^{(n+1)}(\varepsilon)^{-1}\right)^{-1} + \underline{\tau}_c^{00(n)}(\varepsilon) \right]^{-1} , \qquad (3.54)$$

therefore,

$$\underline{t}_c^{(n+1)}(\varepsilon)^{-1} = \underline{t}_c^{(n)}(\varepsilon)^{-1} - \left[\underline{X}_c^{(n)}(\varepsilon)^{-1} - \underline{\tau}_c^{00(n)}(\varepsilon) \right]^{-1} , \qquad (3.55)$$

which can be used to calculate the next guess for $\underline{\tau}_c^{00}(\varepsilon)$. As was shown by Mills et $al.$ [69] the above iterative scheme guarantees a stable convergency for $\underline{t}_c(\varepsilon)$ when starting with the initial guess,

$$\underline{t}_c^{(0)}(\varepsilon) = \sum_{\alpha=1}^m c_\alpha \underline{t}_\alpha(\varepsilon) , \qquad (3.56)$$

the so-called average t-matrix approximation (ATA).

Chapter 4

Transport coefficients

In this Chapter, the applied methods for calculating transport properties in different structures are presented. In the first parts, the real space formulation is found, which have been implemented into a new computer code, while in the second part, conductivity for disordered layered systems is described.

4.1 Non-local conductivity

The definition of the non-local conductivity tensor can be obtained by rewriting the total conductivity in Eq. (1.106) as

$$
\sigma_{\mu\mu} = -\frac{\hbar}{4\pi V} Tr \left(\sum_{pi} \hat{P}_{pi}\hat{J}_{\mu} \left[\hat{G}^+(E_F) - \hat{G}^-(E_F) \right] \sum_{qj} \hat{P}_{qj}\hat{J}_{\mu} \left[\hat{G}^+(E_F) - \hat{G}^-(E_F) \right] \right)
$$

$$
= \frac{1}{N_0} \sum_{pi,qj} \sigma_{\mu\mu}^{pi,qj} , \tag{4.1}
$$

where $\mu \in \{x, y, z\}$, N_0 is the total number of sites in the system with total volume of $V = N_0 V_{at}$ (assuming no lattice relaxation, thus V_{at} is the same for all sites), and $\hat{P}_{pi}$ is a projection operator which projects to site i in the pth layer. It is obvious that

$$
\sum_{pi} \hat{P}_{pi} = \hat{I} . \tag{4.2}
$$

It can be shown that the non-local conductivity,

$$
\sigma_{\mu\mu}^{pi,qj} = -\frac{\hbar}{4\pi V_{at}} Tr \left(\hat{P}_{pi}\hat{J}_{\mu} \left[\hat{G}^+(E_F) - \hat{G}^-(E_F) \right] \hat{P}_{qj}\hat{J}_{\mu} \left[\hat{G}^+(E_F) - \hat{G}^-(E_F) \right] \right)
$$

$$
\tag{4.3}
$$

can be expressed as the following,

$$\sigma_{\mu\mu}^{pi,qj} = -\frac{\hbar}{4\pi V_{at}} \int\limits_{\Omega_{pi}} d^3 r_{pi} \int\limits_{\Omega_{qj}} d^3 r'_{qj} \qquad (4.4)$$

$$\times Tr\left(J_\mu \left[G^+(E_F; \mathbf{r}_{pi}, \mathbf{r}'_{qj}) - G^-(E_F; \mathbf{r}_{pi}, \mathbf{r}'_{qj}) \right] J_\mu \left[G^+(E_F; \mathbf{r}'_{qj}, \mathbf{r}_{pi}) - G^-(E_F; \mathbf{r}'_{qj}, \mathbf{r}_{pi}) \right] \right),$$

with up- and down-side limits of the Green's function in configurational space representation, see Eq. (2.69). Moreover, the integration is carried out over the ith unit cell in layer p, Ω_{pi}, and the jth unit cell in layer q, Ω_{qj}, while Tr denotes here a trace over four-component spinors (relativistic formulation). The non-local conductivity can be written in terms of the real space τ-matrix by substituting Eq. (2.69) into Eq. (4.4), thus, the diagonal elements between site i in layer p and site j in layer q can be partitioned into four parts, the so-called "up" and "down" side limits,

$$\sigma_{\mu\mu}^{pi,qj} = \frac{1}{4} \left[\widetilde{\sigma}_{\mu\mu}^{pi,qj}(\varepsilon^+, \varepsilon^+) + \widetilde{\sigma}_{\mu\mu}^{pi,qj}(\varepsilon^-, \varepsilon^-) - \widetilde{\sigma}_{\mu\mu}^{pi,qj}(\varepsilon^+, \varepsilon^-) - \widetilde{\sigma}_{\mu\mu}^{pi,qj}(\varepsilon^-, \varepsilon^+) \right] , \qquad (4.5)$$

where each term can be expressed using Eqs. (2.69) and (4.4) in terms of the cluster-SPO as

$$\widetilde{\sigma}_{\mu\mu}^{pi,qj}(\varepsilon_1, \varepsilon_2) = -\frac{\hbar}{\pi V_{at}} tr \left[\underline{J}_\mu^{pi}(\varepsilon_2, \varepsilon_1) \underline{\tau}_{clus}^{pi,qj}(\varepsilon_1) \underline{J}_\mu^{qj}(\varepsilon_1, \varepsilon_2) \underline{\tau}_{clus}^{qj,pi}(\varepsilon_2) \right] , \qquad (4.6)$$

where the underlined quantities are matrices in angular momentum space where *trace* is also performed and the τ-matrix of the cluster according to the embedding equation, Eq. (2.95) is used. Inherent to the SKKR method, a finite imaginary part, δ, of the Fermi energy has to be applied,

$$\varepsilon_{1,2} = \varepsilon^\pm = E_F \pm i\delta , \qquad (4.7)$$

which, however, has to be continued to zero ($\delta \to 0$) in order to ensure current conservation. Concomitantly, the number of $k_\|$ points for calculating the real space host τ-matrix in Eq. (2.96) has to be considerably increased.

The current matrices are given in a relativistic formulation by

$$\underline{J}_\mu^{pi}(\varepsilon_1, \varepsilon_2) = J_{\mu,QQ'}^{pi} = ec \int\limits_{\Omega_{pi}} Z_Q^{pi}(\mathbf{r}_{pi}, \varepsilon_1)^\dagger \alpha_\mu Z_{Q'}^{pi}(\mathbf{r}_{pi}, \varepsilon_2) d^3 r_{pi}, \quad Q = (\kappa, \mu) , \qquad (4.8)$$

where α_μ are the standard 4×4 Dirac matrices, while in the non-relativistic case,

$$\underline{J}_\mu^{pi}(\varepsilon_1, \varepsilon_2) = J_{\mu,\Lambda\Lambda'}^{pi} = \frac{e}{m}\frac{\hbar}{i}\int_{\Omega_{pi}} Z_\Lambda^{pi}(\mathbf{r}_{pi}, \varepsilon_1)^\dagger \frac{\partial}{\partial r_{pi,\mu}} Z_{\Lambda'}^{pi}(\mathbf{r}_{pi}, \varepsilon_2) d^3 r_{pi}, \quad \Lambda = (l, m) ,$$

(4.9)

where $Z^{pi}(\mathbf{r}_{pi}, \varepsilon)$'s are properly normalized regular scattering solutions of the Dirac equation, see Section 2.4. It is important to mention that in the calculations the relativistic current matrices have been used.

4.1.1 Non-local conductivity in disordered systems

In order to be able to perform real space calculations ("self-embedding" of coherent sites, $\underline{\tau}_{clus} = \underline{\tau}_{host} = \underline{\tau}_c$) in a 2D translational invariant substitutional binary alloy, configurational averages have to be performed in Eq. (4.6) [22, 23], e.g., for the site-diagonal terms in the following manner,

$$\left\langle \widetilde{\sigma}_{\mu\mu}^{pi,pi}(\varepsilon_1, \varepsilon_2) \right\rangle = \sum_\alpha c_\alpha \left\langle tr \left[\underline{J}_\mu^\alpha(\varepsilon_2, \varepsilon_1) \underline{\tau}^{pi,pi}(\varepsilon_1) \underline{J}_\mu^\alpha(\varepsilon_1, \varepsilon_2) \underline{\tau}^{pi,pi}(\varepsilon_2) \right] \right\rangle_{(pi=\alpha)} , \quad (4.10)$$

where c_α denotes the concentration of the α-th component, $\alpha \in \{A, B\}$, of a binary alloy and the current matrix $\underline{J}_\mu^\alpha$ can be similarly written as in Eqs. (4.8) and (4.9) with the only difference that the regular scattering solutions of type α must be taken. Omitting vertex corrections the above expression reduces to

$$\left\langle \widetilde{\sigma}_{\mu\mu}^{pi,pi}(\varepsilon_1, \varepsilon_2) \right\rangle = \sum_\alpha c_\alpha tr \left[\underline{J}_\mu^\alpha(\varepsilon_2, \varepsilon_1) \left\langle \underline{\tau}^{pi,pi}(\varepsilon_1) \right\rangle_{(pi=\alpha)} \underline{J}_\mu^\alpha(\varepsilon_1, \varepsilon_2) \left\langle \underline{\tau}^{pi,pi}(\varepsilon_2) \right\rangle_{(pi=\alpha)} \right] ,$$

(4.11)

and $\left\langle \underline{\tau}^{pi,pi}(\varepsilon) \right\rangle_{(pi=\alpha)}$ can be calculated as in Eq. (3.43). By using the property of a trace,

$$tr[\underline{ABC}] = tr[\underline{CAB}] , \quad (4.12)$$

for $(pi) = (qj)$ the following is obtained,

$$\left\langle \widetilde{\sigma}_{\mu\mu}^{pi,pi}(\varepsilon_1, \varepsilon_2) \right\rangle = \sum_\alpha c_\alpha tr \left[\widetilde{\underline{D}}_\alpha^{pi}(\varepsilon_2) \underline{J}_\mu^\alpha(\varepsilon_2, \varepsilon_1) \underline{D}_\alpha^{pi}(\varepsilon_1) \underline{\tau}_c^{pi,pi}(\varepsilon_1) \underline{J}_\mu^\alpha(\varepsilon_1, \varepsilon_2) \tau_c^{pi,pi}(\varepsilon_2) \right] .$$

(4.13)

By defining the following quantity,

$$\widetilde{\underline{J}}_{\mu}^{pi,\alpha}(\varepsilon_1,\varepsilon_2) = \widetilde{\underline{D}}_{\alpha}^{pi}(\varepsilon_1)\underline{J}_{\mu}^{\alpha}(\varepsilon_1,\varepsilon_2)\underline{D}_{\alpha}^{pi}(\varepsilon_2) \, , \tag{4.14}$$

it can be rewritten as

$$\left\langle \widetilde{\sigma}_{\mu\mu}^{pi,pi}(\varepsilon_1,\varepsilon_2) \right\rangle = \sum_{\alpha} c_{\alpha} tr \left[\widetilde{\underline{J}}_{\mu}^{pi,\alpha}(\varepsilon_2,\varepsilon_1)\underline{\tau}_c^{pi,pi}(\varepsilon_1)\underline{J}_{\mu}^{\alpha}(\varepsilon_1,\varepsilon_2)\tau_c^{pi,pi}(\varepsilon_2) \right] \, . \tag{4.15}$$

For the $(pi) \neq (qj)$ case,

$$\left\langle \widetilde{\sigma}_{\mu\mu}^{pi,qj}(\varepsilon_1,\varepsilon_2) \right\rangle = \sum_{\alpha,\beta} c_{\alpha}c_{\beta} \left\langle tr \left[\underline{J}_{\mu}^{\alpha}(\varepsilon_2,\varepsilon_1)\underline{\tau}^{pi,qj}(\varepsilon_1)\underline{J}_{\mu}^{\beta}(\varepsilon_1,\varepsilon_2)\underline{\tau}^{qj,pi}(\varepsilon_2) \right] \right\rangle_{(pi=\alpha,qj=\beta)} \, , \tag{4.16}$$

which by omitting vertex corrections reduces to

$$\left\langle \widetilde{\sigma}_{\mu\mu}^{pi,qj}(\varepsilon_1,\varepsilon_2) \right\rangle = \sum_{\alpha,\beta} c_{\alpha}c_{\beta} tr \left[\underline{J}_{\mu}^{\alpha}(\varepsilon_2,\varepsilon_1) \left\langle \underline{\tau}^{pi,qj}(\varepsilon_1) \right\rangle_{(pi=\alpha,qj=\beta)} \underline{J}_{\mu}^{\beta}(\varepsilon_1,\varepsilon_2) \left\langle \underline{\tau}^{qj,pi}(\varepsilon_2) \right\rangle_{(pi=\alpha,qj=\beta)} \right] \, . \tag{4.17}$$

Using the restricted averages by specifying the occupation on two different sites in Eq. (3.44) or (3.45) and the property of a trace, Eq. (4.12), the configurational averaged non-local conductivity tensor between different sites can be obtained,

$$\left\langle \widetilde{\sigma}_{\mu\mu}^{pi,qj}(\varepsilon_1,\varepsilon_2) \right\rangle = \sum_{\alpha,\beta} c_{\alpha}c_{\beta} \tag{4.18}$$

$$\times tr \left[\widetilde{\underline{D}}_{\alpha}^{pi}(\varepsilon_2)\underline{J}_{\mu}^{\alpha}(\varepsilon_2,\varepsilon_1)\underline{D}_{\alpha}^{pi}(\varepsilon_1)\underline{\tau}_c^{pi,qj}(\varepsilon_1)\widetilde{\underline{D}}_{\beta}^{qj}(\varepsilon_1)\underline{J}_{\mu}^{\beta}(\varepsilon_1,\varepsilon_2)\underline{D}_{\beta}^{qj}(\varepsilon_2)\underline{\tau}_c^{qj,pi}(\varepsilon_2) \right] \, ,$$

or using Eq. (4.14),

$$\left\langle \widetilde{\sigma}_{\mu\mu}^{pi,qj}(\varepsilon_1,\varepsilon_2) \right\rangle = \sum_{\alpha,\beta} c_{\alpha}c_{\beta} tr \left[\widetilde{\underline{J}}_{\mu}^{pi,\alpha}(\varepsilon_2,\varepsilon_1)\underline{\tau}_c^{pi,qj}(\varepsilon_1)\widetilde{\underline{J}}_{\mu}^{qj,\beta}(\varepsilon_1,\varepsilon_2)\underline{\tau}_c^{qj,pi}(\varepsilon_2) \right] \, . \tag{4.19}$$

4.2 Conductivities, resistivities, conductance

Transport properties characteristic to a specific physical system can be obtained by choosing different ways to sum up the non-local conductivities. The summation depends strongly on the system itself. In this Section real space summations are presented which have been used in the calculations. It should be noted that all the

studied systems are related to systems with 2D translational symmetry: either the system under investigation ("large cluster" limit in Chapter 6, AMR in Chapter 7) itself or the host for some embedding procedure (finite magnetic chains in surface layer in Chapter 8, nanocontacts in Chapter 9). In the calculations two current geometries have been taken into account, namely *current in plane* (CIP) and *current perpendicular to the planes* (CPP). The applied current direction is explicitly shown for each studied system.

4.2.1 "Large cluster" limit

If only unperturbed host atoms form the cluster, then by increasing the size of the cluster, the physical properties characteristic for the bulk or surface host can be expected. As a rigorous test for the proposed method, therefore, such a "self-embedding" procedure has been used, i.e., $\underline{\underline{\tau}}_{clus} = \underline{\underline{\tau}}_{host}$ (or $= \underline{\underline{\tau}}_c$ for a disordered system) has been taken and the quantities

$$\rho_{\mu\mu} = \lim_{\delta \to 0} \rho_{\mu\mu}(r_0; \delta) \,, \quad \rho_{\mu\mu}(r_0; \delta) = \lim_{r \to r_0} \rho_{\mu\mu}(r; \delta) \tag{4.20}$$

have been calculated, where r_0 is a sufficiently large radius of the cluster, while

$$\rho_{\mu\mu}(r; \delta) = \left[\sigma^0_{\mu\mu}(r; \delta)\right]^{-1} \,, \quad \sigma^0_{\mu\mu}(r; \delta) = \sum_j \sigma^{0j}_{\mu\mu}(\delta) \,, \tag{4.21}$$

where ρ is a resistivity, $\sigma^{0j}_{\mu\mu}$ denotes the μth component of the non-local conductivity tensor between the origin of the lattice (0) and site j and is defined by Eq. (4.5), and the summation over sites j is restricted to those, which are not further from the origin than r, with formula $|\mathbf{R}_0 - \mathbf{R}_j| \le r$. Moreover, δ refers to the imaginary part of the Fermi energy, see Eq. (4.7). Performing the $\delta \to 0$ limit at the stage of Eq. (4.20) actually means that the side limits in Eq. (4.5) are taken at the last possible step. Two kinds of summation are considered: It is possible to involve sites in the summation only from a specific layer p (e.g. surface layer), where in the $r \to \infty$ limit

$$\lim_{r \to \infty} \rho_{\mu\mu}(r, \delta) = \widehat{\rho}^{pp}_{\mu\mu}(\delta) \,, \quad \widehat{\rho}^{pp}_{\mu\mu}(\delta) = \left[\widehat{\sigma}^{pp}_{\mu\mu}(\delta)\right]^{-1} \tag{4.22}$$

must be satisfied where $\widehat{\sigma}^{pp}_{\mu\mu}$ is the layer-diagonal conductivity of layer p,

$$\widehat{\sigma}^{pp}_{\mu\mu}(\delta) = \frac{1}{4}\left[\widetilde{\sigma}^{pp}_{\mu\mu}(\varepsilon^+, \varepsilon^+) + \widetilde{\sigma}^{pp}_{\mu\mu}(\varepsilon^-, \varepsilon^-) - \widetilde{\sigma}^{pp}_{\mu\mu}(\varepsilon^+, \varepsilon^-) - \widetilde{\sigma}^{pp}_{\mu\mu}(\varepsilon^-, \varepsilon^+)\right] \,, \tag{4.23}$$

and each term can be calculated directly using a 2D lattice Fourier transformation,

$$\widetilde{\sigma}_{\mu\mu}^{pp}(\varepsilon_1, \varepsilon_2) = -\frac{\hbar}{\pi V_{at}} \frac{1}{\Omega_{BZ}} \int\limits_{BZ} d^2 k_{\parallel} \, tr \left[\underline{\widehat{J}}_{\mu}^{p}(\varepsilon_2, \varepsilon_1) \underline{\widehat{\tau}}^{pp}(\varepsilon_1, \mathbf{k}_{\parallel}) \underline{\widehat{J}}_{\mu}^{p}(\varepsilon_1, \varepsilon_2) \underline{\widehat{\tau}}^{pp}(\varepsilon_2, \mathbf{k}_{\parallel}) \right] \, .$$

$$(4.24)$$

For the calculated convergence of the real space summation in 2D, see Section 6.1. Another possibility is to sum up over sites within a sphere with r being its radius. In the $r \to \infty$ limit the summation must provide the total conductivity of the bulk system,

$$\lim_{r\to\infty} \sigma_{\mu\mu}^{0}(r, \delta) = \sigma_{\mu\mu}^{total}(\delta) \, . \tag{4.25}$$

Taking the $\delta \to 0$ limit of this expression, and inverting $\sigma_{\mu\mu}^{total}$, the resistivity of a bulk system is obtained, which is zero for pure metals. This behavior is shown in Section 6.2.1. Alloy bulk systems do not have zero resistivity due to disorder, and the so-called residual resistivity of them can be obtained performing real space summation in 3D, which is shown in Section 6.2.2. Moreover, this method has also been tested for determining the anisotropic magnetoresistance of permalloy, see Chapter 7.

Quite clearly there are more efficient methods to evaluate resistivities for bulk or layered systems by making use of three- or two-dimensional lattice Fourier transformations, respectively. For disordered layered systems, see, e.g., Section 4.3. However, once it comes to determine, e.g., the electric properties of magnetic islands on surfaces, these methods are no longer applicable, and one has to rely on real space approaches as presented in Sections 4.1 and 4.2. It should be noted that the calculations in "large cluster" limit are only illustrations of the reliability and applicability of the real space approach.

4.2.2 "Residual resistivity" for nanostructures

If no translational symmetry is present in the system, which holds if impurities are embedded into the 2D translational invariant host medium, then in principle one has to sum over all sites in the system including leads, contacts, etc., i.e.,

$$\widetilde{\sigma}_{\mu\mu}(\varepsilon_1, \varepsilon_2) = \frac{1}{N_0} \sum_{i=1}^{N_0} \sum_{j=1}^{N_0} \widetilde{\sigma}_{\mu\mu}^{ij}(\varepsilon_1, \varepsilon_2) \tag{4.26}$$

with $N_0 \approx 10^{23}$. Here, i and j denote sites without labelling layers explicitly. As such a procedure is numerically not accessible, the following quantity can be defined,

$$\widetilde{\sigma}_{\mu\mu}(\varepsilon_1, \varepsilon_2; n) = \frac{1}{n} \sum_{i=1}^{n} \sum_{j=1}^{n} \widetilde{\sigma}_{\mu\mu}^{ij}(\varepsilon_1, \varepsilon_2) \qquad (4.27)$$

with n being the number of sites in a chosen region ("cluster"). This implies, however, that the convergence properties of $\widetilde{\sigma}_{\mu\mu}(\varepsilon_1, \varepsilon_2; n)$ with respect to n have to be investigated. Clearly enough, the most useful test cases are pure (bulk) metals or binary bulk substitutional alloys, see Sections 4.2.1 and 6.2.

The embedding of impurities forming a finite chain into the surface layer of a substrate was investigated. Since clearly enough a summation over all sites including the semi-infinite substrate would yield only the resistivity of the substrate, namely zero in the case of a pure metal, a kind of "residual resistivity" for finite clusters has to be defined,

$$\rho_{\mu\mu}^{\alpha}(r) = \left[\frac{1}{n} \sum_{i \in chain} \sum_{j=1}^{N(r)} \sigma_{\mu\mu}^{ij} \right]^{-1} , \qquad (4.28)$$

where n denotes the number of atoms in the chain of type α and $N(r)$ is the number of atoms involved in the cluster (chain + environmental atoms up to the furthermost distance of r). Using this formula, in-plane resistivities depending on the orientation of the magnetization of magnetic finite chains in the surface layer of a non-magnetic substrate have been investigated, see Chapter 8.

4.2.3   Expression of the conductance

Linear response theory applies to an arbitrary choice for the perturbating electric field because the response function is obtained in the zero limit of perturbation. Let us assume, therefore, that a constant electric field, E_z^q, pointing along the z axis, i.e., normal to the planes, is applied in all cells of layer q. Denoting the z component of current density averaged over cell i in layer p by j_z^{pi}, the microscopic Ohm's law reads as

$$j_z^{pi} = \frac{1}{V_{at}} \sum_{j} \sigma_{zz}^{pi,qj} E_z^q , \qquad (4.29)$$

where V_{at} is the volume of the unit cell in layer p. Note, that in neglecting lattice relaxations, V_{at} is uniform in the whole system. According to the Kubo-Greenwood formula at zero temperature, Eq. (1.106), the zz component of the non-local conductivity tensor, $\sigma_{zz}^{pi,qj}$ can be written as

$$\sigma_{zz}^{pi,qj} = -\frac{\hbar}{4\pi} \int_{\Omega_{pi}} d^3 r_{pi} \int_{\Omega_{qj}} d^3 r'_{qj} \tag{4.30}$$

$$\times Tr \left(J_z \left[G^+(E_F; \mathbf{r}_{pi}, \mathbf{r}'_{qj}) - G^-(E_F; \mathbf{r}_{pi}, \mathbf{r}'_{qj}) \right] J_z \left[G^+(E_F; \mathbf{r}'_{qj}, \mathbf{r}_{pi}) - G^-(E_F; \mathbf{r}'_{qj}, \mathbf{r}_{pi}) \right] \right),$$

with the same quantities as in Eq. (4.4). The total current flowing through layer p can be written as

$$I_{tot} = A_{\parallel} \sum_i j_z^{pi} = gU , \tag{4.31}$$

where the summation has to be carried out for all sites in layer p. Here, the applied voltage U is

$$U = E_z^q d_\perp , \tag{4.32}$$

and $A_{\parallel}$ and $d_\perp$ denote the area of the 2D unit cell and the interlayer spacing, respectively $(V_{at} = A_{\parallel} d_\perp)$. Combining Eqs. (4.29), (4.31) and (4.32) results in an expression for the conductance,

$$g = \frac{1}{d_\perp^2} \sum_i \sum_j \sigma_{zz}^{pi,qj}, \tag{4.33}$$

where the summations should, in principle, be carried out over all the cells in layers p and q.

An alternative choice of the non-local conductivity tensor is suggested by Eq. (1.109). This type of non-local conductivity is more precise to use for calculating the conductance in the CPP geometry of a layered system than non-local conductivity in the Kubo-Greenwood approach because, as shown by Baranger and Stone [43] for free electron leads, the second term appearing in Eq. (1.109) becomes identically zero when integrated over the layers, $p \neq q$. This means also that the terms $\widetilde{\sigma}_{\mu\mu}^{pi,qj}(\varepsilon^+, \varepsilon^+)$ and $\widetilde{\sigma}_{\mu\mu}^{pi,qj}(\varepsilon^-, \varepsilon^-)$ should vanish after integration. It should be noted that very recently Mavropoulos et al. [71] rederived this result by assuming Bloch boundary

conditions for the leads. According to these theoretical results, at $T = 0$ temperature the diagonal elements of the non-local conductivity tensor between site i in layer p and site j in layer q can sufficiently be expressed as

$$\sigma_{zz}^{pi,qj} = -\frac{1}{2}\tilde{\sigma}_{zz}^{pi,qj}(\varepsilon^+,\varepsilon^-) = \frac{\hbar}{2\pi} \int\limits_{\Omega_{pi}} d^3r_{pi} \int\limits_{\Omega_{qj}} d^3r'_{qj} Tr\left[J_z G^+(E_F;\mathbf{r}_{pi},\mathbf{r}'_{qj})J_z G^-(E_F;\mathbf{r}'_{qj},\mathbf{r}_{pi})\right]$$

$$= \frac{\hbar}{2\pi} tr\left[\underline{J}_z^{pi}(\varepsilon^-,\varepsilon^+)\underline{\tau}_{clus}^{pi,qj}(\varepsilon^+)\underline{J}_z^{qj}(\varepsilon^+,\varepsilon^-)\underline{\tau}_{clus}^{qj,pi}(\varepsilon^-)\right] , \qquad (4.34)$$

in order to calculate the conductance in Eq. (4.33). Using this expression, the conductance can be written as

$$g = \frac{\hbar}{2\pi d_\perp^2} \sum_i \sum_j \int\limits_{\Omega_{pi}} d^3r_{pi} \int\limits_{\Omega_{qj}} d^3r'_{qj} Tr\left[J_z G^+(E_F;\mathbf{r}_{pi},\mathbf{r}'_{qj})J_z G^-(E_F;\mathbf{r}'_{qj},\mathbf{r}_{pi})\right] ,$$

$$(4.35)$$

or in terms of the SPO in Eq. (2.95),

$$g = \frac{\hbar}{2\pi d_\perp^2} \sum_i \sum_j tr\left[\underline{J}_z^{pi}(\varepsilon^-,\varepsilon^+)\,\underline{\tau}_{clus}^{pi,qj}(\varepsilon^+)\,\underline{J}_z^{qj}(\varepsilon^+,\varepsilon^-)\,\underline{\tau}_{clus}^{qj,pi}(\varepsilon^-)\right] , \qquad (4.36)$$

where *trace* have to be performed in angular momentum space and $\delta \to 0$ limit has also to be taken. It has to be emphasized that because of the use of linear response theory and current conservation, the choice of layers p and q is arbitrary in the above formula. The numerical test of the method will clearly demonstrate this feature. It can be established that the conductance is a suitable quantity to describe transport through nanocontacts. Moreover, the effects of impurities present in the contact can be easily studied with help of the above described tool, see Chapter 9. On the other hand, as shown in Ref. [71], when the layers p and q are asymptotically far from each other, the present formalism naturally recovers the Landauer-Büttiker approach [40, 41], see section 1.2.

4.3 Conductivity for disordered layered systems

First, it should be noted that the here described method was used for different orientations of magnetization supposed to be uniform in all layers of bulk permalloy systems in order to determine the anisotropic magnetoresistance of them, see Chapter 7.

Suppose the electrical conductivity of a disordered system, namely $\sigma_{\mu\mu}$, can be partitioned into four parts using the Kubo-Greenwood formula (Eq. (1.106)) similarly to Eq. (4.5) as

$$\sigma_{\mu\mu} = \frac{1}{4}\left[\tilde{\sigma}_{\mu\mu}(\varepsilon^+,\varepsilon^+) + \tilde{\sigma}_{\mu\mu}(\varepsilon^-,\varepsilon^-) - \tilde{\sigma}_{\mu\mu}(\varepsilon^+,\varepsilon^-) - \tilde{\sigma}_{\mu\mu}(\varepsilon^-,\varepsilon^+)\right] , \tag{4.37}$$

with the energy arguments defined by Eq. (4.7) and

$$\tilde{\sigma}_{\mu\mu}(\varepsilon_1,\varepsilon_2) = -\frac{\hbar}{\pi N_0 V_{at}}Tr\left\langle \hat{J}_\mu \hat{G}(\varepsilon_1)\hat{J}_\mu \hat{G}(\varepsilon_2)\right\rangle , \tag{4.38}$$

where N_0 is the number of atoms, V_{at} is the atomic volume, and $\langle \cdots \rangle$ denotes an average over configurations. Employing the expression of the Green function within the KKR method, a typical contribution to the conductivity can be expressed in terms of real space SPO,

$$\tilde{\sigma}_{\mu\mu}(\varepsilon_1,\varepsilon_2) = \tag{4.39}$$

$$= -\frac{\hbar}{\pi N_0 V_{at}}\sum_{p=1}^{n}\left\{\sum_{i\in I(L_2)}\sum_{q=1}^{n}\left\{\sum_{j\in I(L_2)} tr\left\langle \underline{J}_\mu^{pi}(\varepsilon_2,\varepsilon_1)\underline{\tau}^{pi,qj}(\varepsilon_1)\underline{J}_\mu^{qj}(\varepsilon_1,\varepsilon_2)\underline{\tau}^{qj,pi}(\varepsilon_2)\right\rangle\right\}\right\} ,$$

where the total number of sites in the interface region can be written as $N_0 = nN$, as given in terms of the number of layers in the interface region (n) and the order of the two-dimensional translational group N (number of atoms in one layer) and tr denotes now the trace in angular momentum space. Moreover, it should be noted that

$$\underline{J}_\mu^{pi}(\varepsilon_1,\varepsilon_2) = \underline{J}_\mu^{pi,\alpha}(\varepsilon_1,\varepsilon_2) = \underline{J}_\mu^{p0,\alpha}(\varepsilon_1,\varepsilon_2) = \widehat{\underline{J}}_\mu^{p\alpha}(\varepsilon_1,\varepsilon_2) , \quad \forall i \in I(L_2) \tag{4.40}$$

with $\alpha \in \{A,B\}$, being one component of the binary alloy. From the brackets in (4.39), it can be easily seen that for each layer p the first sum over L_2 yields N times the same contribution, provided two-dimensional invariance applies in all layers under consideration. Asumming this kind of symmetry, a typical contribution $\tilde{\sigma}_{\mu\mu}(\varepsilon_1,\varepsilon_2)$ to the conductivity is therefore given by

$$\tilde{\sigma}_{\mu\mu}(\varepsilon_1,\varepsilon_2) = -\frac{\hbar}{\pi n V_{at}}\sum_{p=1}^{n}\sum_{q=1}^{n}\left\{\sum_{j\in I(L_2)} tr\left\langle \underline{J}_\mu^{p0}(\varepsilon_2,\varepsilon_1)\underline{\tau}^{p0,qj}(\varepsilon_1)\underline{J}_\mu^{qj}(\varepsilon_1,\varepsilon_2)\underline{\tau}^{qj,p0}(\varepsilon_2)\right\rangle\right\} ,$$

$$\tag{4.41}$$

where $p0$ specifies the origin of L_2 for layer p. This kind of contribution can be split up into a (site-) diagonal and a (site-) off-diagonal part,

$$\widetilde{\sigma}_{\mu\mu}(\varepsilon_1, \varepsilon_2) = \widetilde{\sigma}_{\mu\mu}^0(\varepsilon_1, \varepsilon_2) + \widetilde{\sigma}_{\mu\mu}^1(\varepsilon_1, \varepsilon_2) \ . \tag{4.42}$$

4.3.1 Site-diagonal conductivity

By employing the CPA condition in (3.40) and omitting vertex corrections, for the diagonal part ($p0 = qj$) one simply gets in terms of the definitions given in (3.42) and (3.45),

$$\widetilde{\sigma}_{\mu\mu}^0(\varepsilon_1, \varepsilon_2) =$$

$$= -\frac{\hbar}{\pi n V_{at}} \sum_{p=1}^{n} \sum_{\alpha} c_p^\alpha tr \left[\widehat{\underline{J}}_\mu^{p\alpha}(\varepsilon_2, \varepsilon_1) \left\langle \widehat{\underline{\tau}}^{pp}(\varepsilon_1) \right\rangle_{(p=\alpha)} \widehat{\underline{J}}_\mu^{p\alpha}(\varepsilon_1, \varepsilon_2) \left\langle \widehat{\underline{\tau}}^{pp}(\varepsilon_2) \right\rangle_{(p=\alpha)} \right]$$

$$= -\frac{\hbar}{\pi n V_{at}} \sum_{p=1}^{n} \sum_{\alpha} c_p^\alpha tr \left[\widehat{\underline{J}}_\mu^{p\alpha}(\varepsilon_2, \varepsilon_1) \widehat{\underline{D}}_\alpha^p(\varepsilon_1) \widehat{\underline{\tau}}_c^{pp}(\varepsilon_1) \widehat{\underline{J}}_\mu^{p\alpha}(\varepsilon_1, \varepsilon_2) \widehat{\underline{\tau}}_c^{pp}(\varepsilon_2) \widehat{\underline{\widetilde{D}}}_\alpha^p(\varepsilon_2) \right]$$

$$= -\frac{\hbar}{\pi n V_{at}} \sum_{p=1}^{n} \sum_{\alpha} c_p^\alpha tr \left[\widehat{\underline{\widetilde{J}}}_\mu^{p\alpha}(\varepsilon_2, \varepsilon_1) \widehat{\underline{\tau}}_c^{pp}(\varepsilon_1) \widehat{\underline{J}}_\mu^{p\alpha}(\varepsilon_1, \varepsilon_2) \widehat{\underline{\tau}}_c^{pp}(\varepsilon_2) \right] \ , \tag{4.43}$$

where

$$\widehat{\underline{\widetilde{J}}}_\mu^{p\alpha}(\varepsilon_2, \varepsilon_1) = \widehat{\underline{\widetilde{D}}}_\alpha^p(\varepsilon_2) \widehat{\underline{J}}_\mu^{p\alpha}(\varepsilon_2, \varepsilon_1) \widehat{\underline{D}}_\alpha^p(\varepsilon_1) \tag{4.44}$$

is the same quantity as in Eq. (4.14) with the notation that here, 2D translational invariance is applied.

4.3.2 Site-off-diagonal conductivity

According to (3.44) and (3.45) the off-diagonal part can further be partitioned into two terms,

$$\widetilde{\sigma}_{\mu\mu}^1(\varepsilon_1, \varepsilon_2) = \widetilde{\sigma}_{\mu\mu}^2(\varepsilon_1, \varepsilon_2) + \widetilde{\sigma}_{\mu\mu}^3(\varepsilon_1, \varepsilon_2) \ , \tag{4.45}$$

with

$$\widetilde{\sigma}_{\mu\mu}^2(\varepsilon_1, \varepsilon_2) = \tag{4.46}$$

$$-\frac{\hbar}{\pi n V_{at}} \sum_{p=1}^{n} \sum_{q=1}^{n} (1 - \delta_{pq}) \left\{ \sum_{j \in I(L_2)} tr \left\langle \underline{J}_\mu^{p0}(\varepsilon_2, \varepsilon_1) \underline{\tau}^{p0,qj}(\varepsilon_1) \underline{J}_\mu^{qj}(\varepsilon_1, \varepsilon_2) \underline{\tau}^{qj,p0}(\varepsilon_2) \right\rangle \right\} \ ,$$

and

$$\widetilde{\sigma}_{\mu\mu}^3(\varepsilon_1, \varepsilon_2) = \tag{4.47}$$

$$-\frac{\hbar}{\pi n V_{at}} \sum_{p=1}^{n} \sum_{q=1}^{n} \delta_{pq} \left\{ \sum_{(j \neq 0) \in I(L_2)} tr \left\langle \underline{J}_{\mu}^{p0}(\varepsilon_2, \varepsilon_1) \underline{\tau}^{p0,qj}(\varepsilon_1) \underline{J}_{\mu}^{qj}(\varepsilon_1, \varepsilon_2) \underline{\tau}^{qj,p0}(\varepsilon_2) \right\rangle \right\} .$$

As it can be seen $\widetilde{\sigma}_{\mu\mu}^2(\varepsilon_1, \varepsilon_2)$ arises from pairs of sites located in *different* layers, whereas $\widetilde{\sigma}_{\mu\mu}^3(\varepsilon_1, \varepsilon_2)$ corresponds to pairs of sites in *one and the same* layer, excluding the site-diagonal pair already being accounted for in $\widetilde{\sigma}_{\mu\mu}^0(\varepsilon_1, \varepsilon_2)$. In general the averaging of $\widetilde{\sigma}_{\mu\mu}^2(\varepsilon_1, \varepsilon_2)$ is given by

$$\widetilde{\sigma}_{\mu\mu}^2(\varepsilon_1, \varepsilon_2) = -\frac{\hbar}{\pi n V_{at}} \sum_{p=1}^{n} \sum_{q=1}^{n} (1 - \delta_{pq}) \sum_{j \in I(L_2)} \sum_{\alpha,\beta} c_p^\alpha c_q^\beta$$

$$\times tr \left\{ \underline{\widehat{J}}_{\mu}^{p\alpha}(\varepsilon_2, \varepsilon_1) \left\langle \underline{\tau}^{p0,qj}(\varepsilon_1) J_{\mu}^{qj}(\varepsilon_1, \varepsilon_2) \underline{\tau}^{qj,p0}(\varepsilon_2) \right\rangle_{(p0=\alpha, qj=\beta)} \right\} . \tag{4.48}$$

By employing the CPA condition and omitting vertex corrections, $\widetilde{\sigma}_{\mu\mu}^2(\varepsilon_1, \varepsilon_2)$ is found to reduce to

$$\widetilde{\sigma}_{\mu\mu}^2(\varepsilon_1, \varepsilon_2) = -\frac{\hbar}{\pi n V_{at}} \sum_{p=1}^{n} \sum_{q=1}^{n} (1 - \delta_{pq}) \sum_{j \in I(L_2)} \sum_{\alpha,\beta} c_p^\alpha c_q^\beta$$

$$\times tr \left\{ \underline{\widehat{J}}_{\mu}^{p\alpha}(\varepsilon_2, \varepsilon_1) \left\langle \underline{\tau}^{p0,qj}(\varepsilon_1) \right\rangle_{)p0=\alpha, qj=\beta)} \underline{\widehat{J}}_{\mu}^{q\beta}(\varepsilon_1, \varepsilon_2) \left\langle \underline{\tau}^{qj,p0}(\varepsilon_2) \right\rangle_{(p0=\alpha, qj=\beta)} \right\} , \tag{4.49}$$

or, by using (3.44), to

$$\widetilde{\sigma}_{\mu\mu}^2(\varepsilon_1, \varepsilon_2) = -\frac{\hbar}{\pi n V_{at}} \sum_{p=1}^{n} \sum_{q=1}^{n} (1 - \delta_{pq}) \sum_{j \in I(L_2)} \sum_{\alpha,\beta} c_p^\alpha c_q^\beta$$

$$\times tr \left\{ \underline{\widetilde{J}}_{\mu}^{p\alpha}(\varepsilon_2, \varepsilon_1) \underline{\tau}_c^{p0,qj}(\varepsilon_1) \underline{\widetilde{J}}_{\mu}^{q\beta}(\varepsilon_1, \varepsilon_2) \underline{\tau}_c^{qj,p0}(\varepsilon_2) \right\} . \tag{4.50}$$

Since the site-off-diagonal scattering path operators $\tau_c^{p0,qj}(\varepsilon)$ are defined as

$$\underline{\tau}_c^{p0,qj}(\varepsilon) = \frac{1}{\Omega_{BZ}} \int_{BZ} e^{i \mathbf{k}_\| \mathbf{T}_j} \underline{\widehat{\tau}}_c^{pq}(\varepsilon, \mathbf{k}_\|) \, d^2 k_\| , \tag{4.51}$$

the orthogonality for irreducible representations of the two-dimensional translation group can be used,

$$\sum_{j \in I(L_2)} \underline{\tau}_c^{p0,qj}(\varepsilon_1) \underline{\tau}_c^{qj,p0}(\varepsilon_2) = \frac{1}{\Omega_{BZ}} \int_{BZ} \underline{\widehat{\tau}}_c^{pq}(\varepsilon_1, \mathbf{k}_\|) \underline{\widehat{\tau}}_c^{qp}(\varepsilon_2, \mathbf{k}_\|) d^2 k_\| . \tag{4.52}$$

For $\widetilde{\sigma}_{\mu\mu}^2(\varepsilon_1, \varepsilon_2)$, therefore, the following expression is obtained,

$$\widetilde{\sigma}_{\mu\mu}^2(\varepsilon_1, \varepsilon_2) = -\frac{\hbar}{\pi n(2\pi)^3} \sum_{p=1}^n \sum_{q=1}^n (1 - \delta_{pq}) \sum_{\alpha,\beta} c_p^\alpha c_q^\beta \tag{4.53}$$

$$\times \int_{BZ} tr \left\{ \widehat{\underline{J}}_\mu^{p\alpha}(\varepsilon_2, \varepsilon_1) \widehat{\underline{\tau}}_c^{pq}(\varepsilon_1, \mathbf{k}_\|) \widehat{\underline{J}}_\mu^{q\beta}(\varepsilon_1, \varepsilon_2) \widehat{\underline{\tau}}_c^{qp}(\varepsilon_2, \mathbf{k}_\|) \right\} d^2 k_\| .$$

From the above discussion of $\widetilde{\sigma}_{\mu\mu}^2(\varepsilon_1, \varepsilon_2)$ it is easy to see that $\widetilde{\sigma}_{\mu\mu}^3(\varepsilon_1, \varepsilon_2)$ is given by

$$\widetilde{\sigma}_{\mu\mu}^3(\varepsilon_1, \varepsilon_2) = -\frac{\hbar}{\pi n(2\pi)^3} \sum_{p=1}^n \sum_{\alpha,\beta} c_p^\alpha c_p^\beta \int_{BZ} tr \left\{ \widehat{\underline{J}}_\mu^{p\alpha}(\varepsilon_2, \varepsilon_1) \widehat{\underline{\tau}}_c^{pp}(\varepsilon_1, \mathbf{k}_\|) \widehat{\underline{J}}_\mu^{p\beta}(\varepsilon_1, \varepsilon_2) \widehat{\underline{\tau}}_c^{pp}(\varepsilon_2, \mathbf{k}_\|) \right\} d^2 k_\|$$

$$+ \widetilde{\sigma}_{\mu\mu}^{3,corr}(\varepsilon_1, \varepsilon_2) , \tag{4.54}$$

where $\widetilde{\sigma}_{\mu\mu}^{3,corr}(\varepsilon_1, \varepsilon_2)$ arises from extending the sum in (4.47) to $\forall j \in I(L_2)$ and subtracting a corresponding correction term of the form,

$$\widetilde{\sigma}_{\mu\mu}^{3,corr}(\varepsilon_1, \varepsilon_2) =$$

$$= \frac{\hbar}{\pi n V_{at}} \sum_{p=1}^n \sum_{\alpha,\beta} c_p^\alpha c_p^\beta \, tr \left\{ \widehat{\underline{J}}_\mu^{p\alpha}(\varepsilon_2, \varepsilon_1) \widehat{\underline{D}}_\alpha^p(\varepsilon_1) \widehat{\underline{\tau}}_c^{pp}(\varepsilon_1) \widehat{\underline{\widetilde{D}}}_\beta^p(\varepsilon_1) \widehat{\underline{J}}_\mu^{p\beta}(\varepsilon_1, \varepsilon_2) \widehat{\underline{D}}_\beta^p(\varepsilon_2) \widehat{\underline{\tau}}_c^{pp}(\varepsilon_2) \widehat{\underline{\widetilde{D}}}_\alpha^p(\varepsilon_2) \right\}$$

$$= \frac{\hbar}{\pi n V_{at}} \sum_{p=1}^n \sum_{\alpha,\beta} c_p^\alpha c_p^\beta \, tr \left\{ \widehat{\underline{J}}_\mu^{p\alpha}(\varepsilon_2, \varepsilon_1) \widehat{\underline{\tau}}_c^{pp}(\varepsilon_1) \widehat{\underline{J}}_\mu^{p\beta}(\varepsilon_1, \varepsilon_2) \widehat{\underline{\tau}}_c^{pp}(\varepsilon_2) \right\} . \tag{4.55}$$

4.3.3 Total conductivity for layered systems

Combining now all terms, a typical contribution $\widetilde{\sigma}_{\mu\mu}(\varepsilon_1, \varepsilon_2)$ to the conductivity is given by

$$\widetilde{\sigma}_{\mu\mu}(\varepsilon_1, \varepsilon_2) = \tag{4.56}$$

$$= -\frac{\hbar}{\pi n V_{at}} \sum_{p=1}^n \left(\sum_\alpha c_p^\alpha \, tr \left\{ \widehat{\underline{J}}_\mu^{p\alpha}(\varepsilon_2, \varepsilon_1) \widehat{\underline{\tau}}_c^{pp}(\varepsilon_1) \widehat{\underline{J}}_\mu^{p\alpha}(\varepsilon_1, \varepsilon_2) \widehat{\underline{\tau}}_c^{pp}(\varepsilon_2) \right\} \right.$$

$$- \sum_{\alpha,\beta} c_p^\alpha c_p^\beta \, tr \left\{ \widehat{\underline{J}}_\mu^{p\alpha}(\varepsilon_2, \varepsilon_1) \widehat{\underline{\tau}}_c^{pp}(\varepsilon_1) \widehat{\underline{J}}_\mu^{p\beta}(\varepsilon_1, \varepsilon_2) \widehat{\underline{\tau}}_c^{pp}(\varepsilon_2) \right\}$$

$$\left. + \frac{1}{\Omega_{BZ}} \sum_{q=1}^n \sum_{\alpha,\beta} c_p^\alpha c_q^\beta \int_{BZ} tr \left\{ \widehat{\underline{J}}_\mu^{p\alpha}(\varepsilon_2, \varepsilon_1) \widehat{\underline{\tau}}_c^{pq}(\varepsilon_1, \mathbf{k}_\|) \widehat{\underline{J}}_\mu^{q\beta}(\varepsilon_1, \varepsilon_2) \widehat{\underline{\tau}}_c^{qp}(\varepsilon_2, \mathbf{k}_\|) \right\} d^2 k_\| \right) ,$$

which, as far as the summations over layers are conserved, can be partitioned into 'single' and 'double' terms [23],

$$\widetilde{\sigma}_{\mu\mu}(\varepsilon_1, \varepsilon_2) = \sum_{p,q=1}^{n} \widetilde{\widehat{\sigma}}_{\mu\mu}^{pq}(\varepsilon_1, \varepsilon_2) = \sum_{p=1}^{n} \widetilde{\widehat{\sigma}}_{\mu\mu}^{pp}(\varepsilon_1, \varepsilon_2) + \sum_{\substack{p,q=1 \\ (p \neq q)}}^{n} \widetilde{\widehat{\sigma}}_{\mu\mu}^{pq}(\varepsilon_1, \varepsilon_2) \ . \qquad (4.57)$$

Quite clearly, the layer-diagonal contributions are defined as

$$\widetilde{\widehat{\sigma}}_{\mu\mu}^{pp}(\varepsilon_1, \varepsilon_2) = -\frac{\hbar}{\pi n V_{at}} \sum_{\alpha} c_p^{\alpha} \left(tr \left\{ \widetilde{\widehat{J}}_{\mu}^{p\alpha}(\varepsilon_2, \varepsilon_1) \widehat{\underline{\tau}}_c^{pp}(\varepsilon_1) \widetilde{\widehat{J}}_{\mu}^{p\alpha}(\varepsilon_1, \varepsilon_2) \widehat{\underline{\tau}}_c^{pp}(\varepsilon_2) \right\} \right.$$

$$\left. - \sum_{\beta} c_p^{\beta} \, tr \left\{ \widetilde{\widehat{J}}_{\mu}^{p\alpha}(\varepsilon_2, \varepsilon_1) \widehat{\underline{\tau}}_c^{pp}(\varepsilon_1) \widetilde{\widehat{J}}_{\mu}^{p\beta}(\varepsilon_1, \varepsilon_2) \widehat{\underline{\tau}}_c^{pp}(\varepsilon_2) \right\} \right) \qquad (4.58)$$

and the layer-offdiagonal $(p \neq q)$ terms as

$$\widetilde{\widehat{\sigma}}_{\mu\mu}^{pq}(\varepsilon_1, \varepsilon_2) = -\frac{\hbar}{\pi n (2\pi)^3} \sum_{\alpha,\beta} c_p^{\alpha} c_q^{\beta} \int tr \left\{ \widetilde{\widehat{J}}_{\mu}^{p\alpha}(\varepsilon_2, \varepsilon_1) \widehat{\underline{\tau}}_c^{pq}(\varepsilon_1, \mathbf{k}_{\parallel}) \widetilde{\widehat{J}}_{\mu}^{q\beta}(\varepsilon_1, \varepsilon_2) \widehat{\underline{\tau}}_c^{qp}(\varepsilon_2, \mathbf{k}_{\parallel}) \right\} d^2 k_{\parallel} \ .$$

$$(4.59)$$

It should be noted that the latter expression is computationally very expensive due to the integration over the 2D Brillouin zone.

Chapter 5

Computational details

Self-consistent calculations for both the 2D invariant host and the finite clusters were performed within the local spin-density approximation (LSDA) [72], see Section A.3, by using the atomic sphere approximation (ASA), see Section 2.2, applying the method described in Section 2.6.2. In both cases, for calculating Eq. (2.17), 16 complex energy points were taken on a semicircular contour in the complex energy plane which were sampled according to an asymmetric Gaussian quadrature, as illustrated in Fig. 5.1 with e.g. $\varepsilon_a = E_B$ and $\varepsilon_b = E_F$.
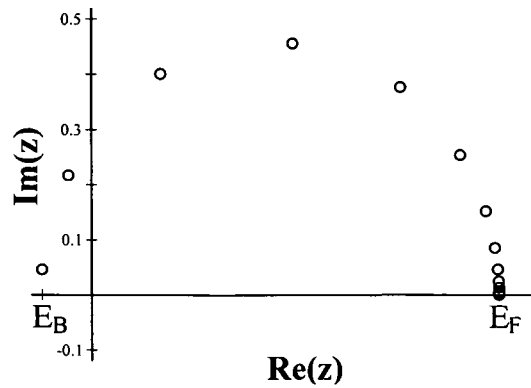
Figure 5.1: Semicircle contour sampled using an asymmetric Gaussian quadrature.

By performing real embedding (Chapter 8 and 9), for the self-consistent cluster calculations a sufficiently large number of atoms from the neighboring host (including sites in the vacuum) was taken into account in order to serve as a buffer for charge fluctuations.

It should be noted that the above described methods do not include lattice relaxation effects, the structure of the studied systems correspond to an underlying parent lattice. For the calculation of the real space SPO in a self-consistent method, see Eq. (2.96), 45 $k_\parallel$ points were taken from the irreducible wedge of the 2D Brillouin zone (IBZ), forming an equidistant sampling of the IBZ as shown in Fig. 5.2 for fcc(001) or bcc(001) planes. By determining the non-local conductivity in the cluster, more precise $k_\parallel$-integration should be performed. The number of $k_\parallel$ points, taken for calculating transport properties, are explicitly written for each studied system. Furthermore, it can be stated that they are strongly dependent on the imaginary part of the Fermi energy (δ) and on the size of the investigated cluster.
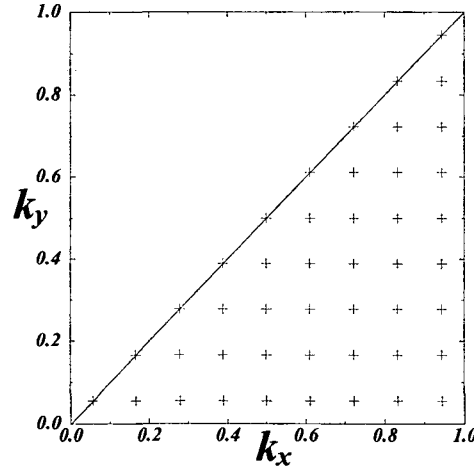
Figure 5.2: Irreducible Brillouin zone of a 2D square lattice with an equidistant mesh. k_x and k_y are in units of $2\pi/a_{2D}$. $\left(a_{2D}^{fcc(001)} = a_{3D}^{fcc}/\sqrt{2}\, ,\ a_{2D}^{bcc(001)} = a_{3D}^{bcc}\right)$

For the angular momentum expansion $l_{max} = 2$ was used, which means that all scattering channels up to and including a maximal angular moment quantum of two were taken into account. Furthermore, all matrices in angular momentum space in a relativistic formulation are of size $18{\times}18$ ($18 = 2(l_{max} + 1)^2$), while the supermatrices in site-angular momentum representation are of size $(18N){\times}(18N)$, where N denotes the number of sites taken in a specific cluster.

The orientation of magnetization ($\widehat{\mathbf{M}}$) was chosen to point to direction z (perpendicular to the layers), exceptions are the determination of AMR in permalloy (Chapter 7) and the surface magnetic chains (Chapter 8).

Chapter 6

"Large cluster" limit

In this Chapter calculations of transport properties in the so-called "large cluster" limit are presented. The results, as the first application of the newly developed computational code, are compared to former calculations and experiments in order to check the reliability of the presented method.

What does "large cluster" limit mean? A real space formalism allows to study the interesting transition of physical properties between nanoscaled and macroscopic (mesoscopic) systems, namely, the change of electrical transport properties from a nanostructure scale to thin films or even bulk systems can be investigated considering a set of clusters with increasing size. For the applied method, see Section 4.2.1.

6.1 Surface layer of Ag(001)

The studied system can be seen below, on Fig. 6.1. The fcc structure was taken with lattice constants $a_{3D} = 7.789\ a.u.$ and $a_{2D} = 5.508\ a.u.$
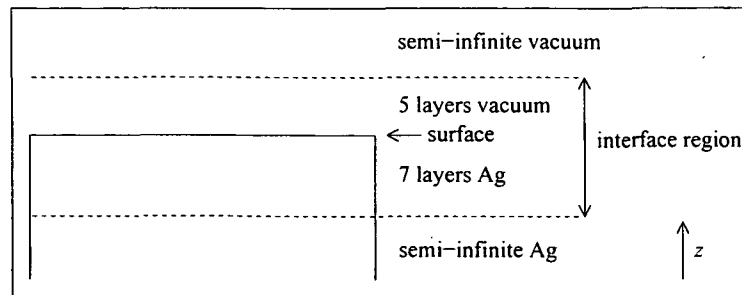
Figure 6.1: Geometrical setup of the studied semi-infinite Ag(001) system.

·It should be mentioned that Ag(001) surface can be prepared by homoepitaxial growth [73].

Let us first take a look at the non-local conductivities in the surface layer. They were calculated according to Eqs. (4.5) and (4.6) with real space SPOs obtained by taking 1830 $k_{\parallel}$ points in the 2D IBZ, see Eq. (2.96). In Fig. 6.2 the xx and zz components of the non-local conductivity tensor $\sigma_{\mu\nu}^{0j}(x_j, y_j)$ are shown, where site 0 is fixed to the origin $(0,0)$ of the surface layer, while the position of site j is varied in the (001)-oriented surface plane. As can be seen, for the out of plane conductivity (zz), only scatterers are important which are not too far away from the origin, while in the in-plane case (xx) also scatterers at farther distances do add non-negligible contributions to the corresponding component of the conductivity. Moreover, it should be noted that the yy component is not shown because it has similar form as xx: only the diagram of $\sigma_{xx}^{0j}(x_j, y_j)$ has to be rotated by 90°.
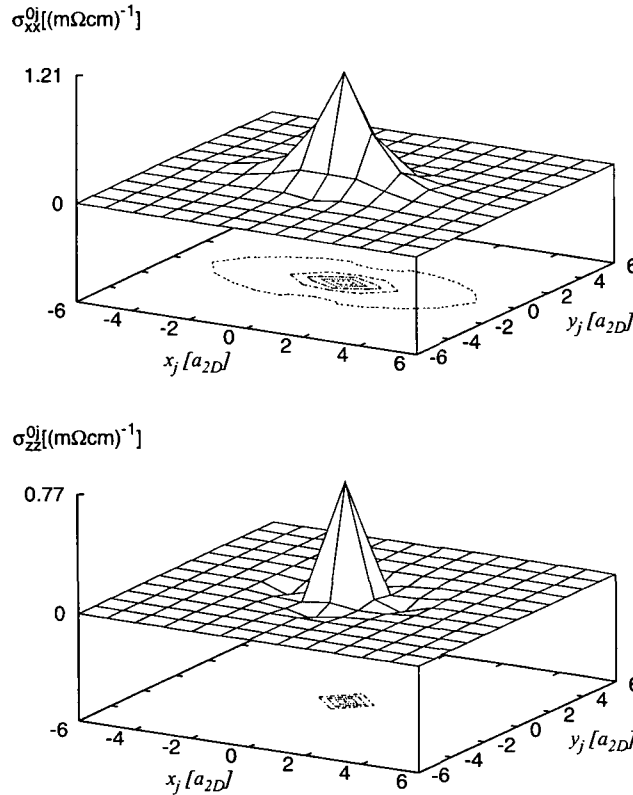
Figure 6.2: Non-local conductivities $\sigma_{\mu\mu}^{0j}(x_j, y_j)$ in the surface layer of Ag. $\delta = 1$ mRy.

The shape of the non-local conductivities suggest that by performing the summation according to Eq. (4.21) only for the layer sites, it should converge, namely Eq. (4.22) should hold true. In order to show that, two different square-shaped planar clusters were investigated, see Fig. 6.3, both having C_{4v} symmetry which implies that $\rho_{\mu\nu}(r; \delta)$ has two independent components, namely

$$\rho_{xx} = \rho_{yy} , \ \rho_{zz} , \text{ and } \rho_{\mu\nu} = 0 \text{ if } \mu \neq \nu. \tag{6.1}$$

The characteristic size (r) of the investigated clusters are given by the distance between the origin (0) and the farthermost atom from the origin, i.e. it can be written for the clusters with increasing size and fixed shape as a series, $r_n = n \cdot a_{2D}$ for type 1 (see Fig. 6.3) and $r_n = n\sqrt{2} \cdot a_{2D}$ for type 2 in the nth step of the cluster-building. The number of atoms involved in the cluster can be obtained by the formulas, $N(n) = (2n^2 + 2n + 1)$ for type 1 and $N(n) = (4n^2 + 4n + 1)$ for type 2. It is obviously seen that the clusters in Fig. 6.3 refer to $n = 3$.
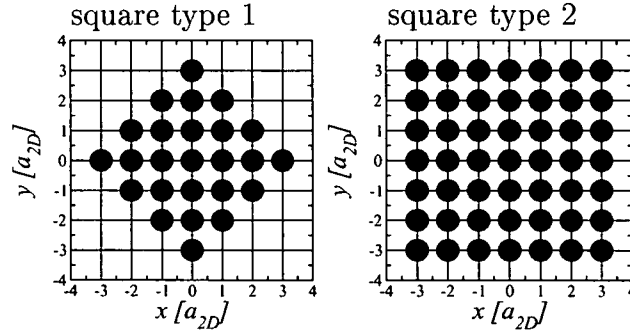
Figure 6.3: Different shapes of clusters in the surface plane of a fcc(001) substrate.

It should be emphasized that this procedure is performed in order to show the validity of Eq. (4.22), there is no real experimental setup which means that ρ_{zz} can not be measured, there is no current flowing from the substrate to the vacuum region. As can be seen from Fig. 6.4, a reliable convergence of the resistivity can be achieved for $r > 15 \ a_{2D}$. It should also be noted that, in particular, for the resistivity normal to the planes the visually faster convergence for clusters type 2 (also see Fig. 6.3) is due to the larger number of atoms forming these clusters than those of type 1.
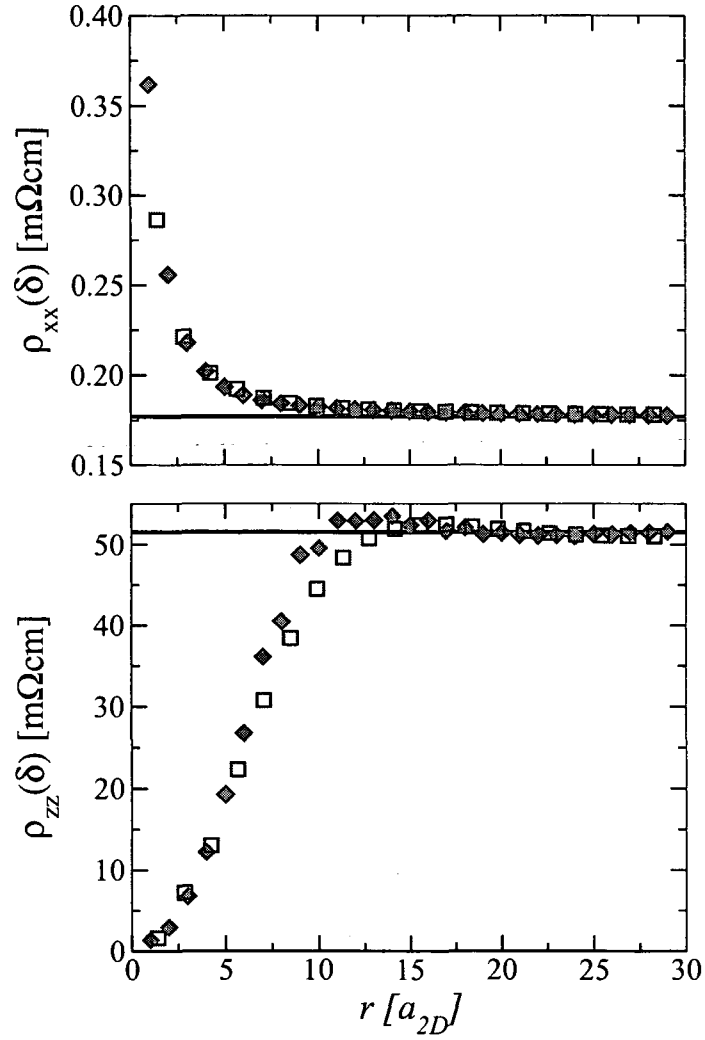
Figure 6.4: Real space study in the surface layer of an Ag(001) semi-infinite system is performed. The in-plane (xx) and perpendicular to the plane (zz) resistivity components for two different cluster shapes are shown versus the characteristic size of the cluster (r). The horizontal line refers to the layer-diagonal resistivity calculated by Eqs. (4.22)-(4.24). Diamonds correspond to type 1 in Fig. 6.3, squares to type 2. $\delta = 1$ mRy is applied.

6.2 Bulk resistivities

The studied systems can be seen below, on Fig. 6.5.
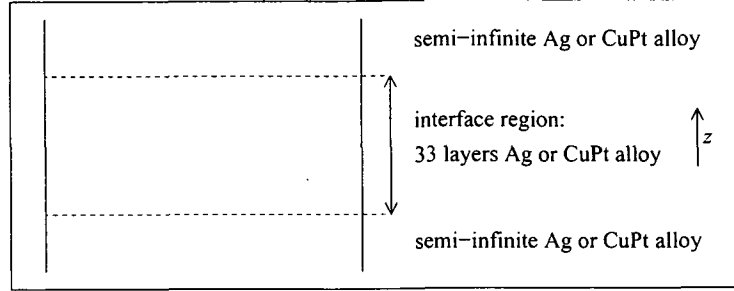
Figure 6.5: Geometrical setup of the studied Ag and CuPt bulk systems.

Non-local conductivities were calculated according to Eq. (4.5) with the side limits in Eq. (4.6) for Ag and in Eqs. (4.15), (4.19) for CuPt alloys with real space SPOs obtained by taking 630 $k_{\parallel}$ points in the 2D IBZ, see Eq. (2.96) for Ag and Eq. (3.31) for the alloys.

In the following, three-dimensional clusters were taken in the above bulk systems, and real space summation of the non-local conductivity tensor were performed according to Eq. (4.21). In addition by increasing the size of the clusters the convergence of Eq. (4.25) was studied, and our results were compared to known bulk resistivities (see Refs. [24, 28]). It is quite clear that for large clusters their resistivity has to approach to the corresponding bulk value, namely to zero for pure metals and to the residual resistivity for alloy systems. The clusters were chosen to be spheres with increasing radius, where the center of the spheres is the site denoted by 0 in Eq. (4.21) and sites j are within the sphere. Table 6.1 shows the number of atoms (N) involved in the sphere versus n which denotes a step of cluster-building. In the nth step, the sphere has a radius $r_n = \frac{n}{\sqrt{2}} \cdot a_{3D}$.

	Cluster											
n	0	1	2	3	4	5	6	7	8	9	10	11
N(n)	1	13	55	177	381	767	1289	2093	3055	4321	5979	7935

Table 6.1: The number of sites (N) in the considered spherical clusters.

If we assume the following behavior of the elements of the resistivity tensor with respect to the size of the cluster (r),

$$\rho_{\mu\mu}(r;\delta) = \rho_0(\delta) + \frac{\rho_1(\delta)}{r} , \tag{6.2}$$

(ρ_0 and ρ_1 are constants) it is obvious that

$$r\rho_{\mu\mu}(r;\delta) = r\rho_0(\delta) + \rho_1(\delta) , \tag{6.3}$$

which means that the residual resistivity, $\rho_0(\delta)$ can be obtained by a linear fit of $r\rho_{\mu\mu}(r;\delta)$ with respect to r. In the case of substitutional alloys, the slope ($\rho_0(\delta)$, $\delta \to 0$) corresponds then to the residual resistivity, while for pure bulk it should be zero.

It should be noted that Eq. (6.2) is more or less an empirical finding which was used also quite a bit in the experimental recording of resistivities. There all kinds of fits are proposed to extrapolate to infinite thickness.

6.2.1 Ag bulk

The fcc bulk Ag structure has the same lattice constants as mentioned in Section 6.1.

In principle it is sufficient to evaluate only one component of the resistivity because the system and also the clusters have cubic symmetry, which means that by choosing the coordinate system properly, the resistivity tensor has only one independent element, namely the diagonal components must be identical ($\rho_{xx} = \rho_{yy} = \rho_{zz}$) and all non-diagonal elements have to be zero. Deviations from this behavior can be used to estimate numerical errors inherent to the calculational scheme and the fitting procedure. The actual fitting, see Eq. (6.3), was performed for each calculated value of δ ($\delta = 1, 2, 3$ mRy) considering the last three points of $r\rho_{zz}(r;\delta)$, see top part of Fig. 6.6. These points have been chosen because they refer to the biggest clusters considered, see Table 6.1. In order to obtain the real physical residual resistivity an extrapolation to $\delta = 0$ is needed, see Eq. (4.20). This extrapolation for Ag bulk structure is illustrated in the top part of Fig. 6.7 and demonstrates that we made an absolute error of roughly 0.05 $\mu\Omega cm$ in our fitting procedure.
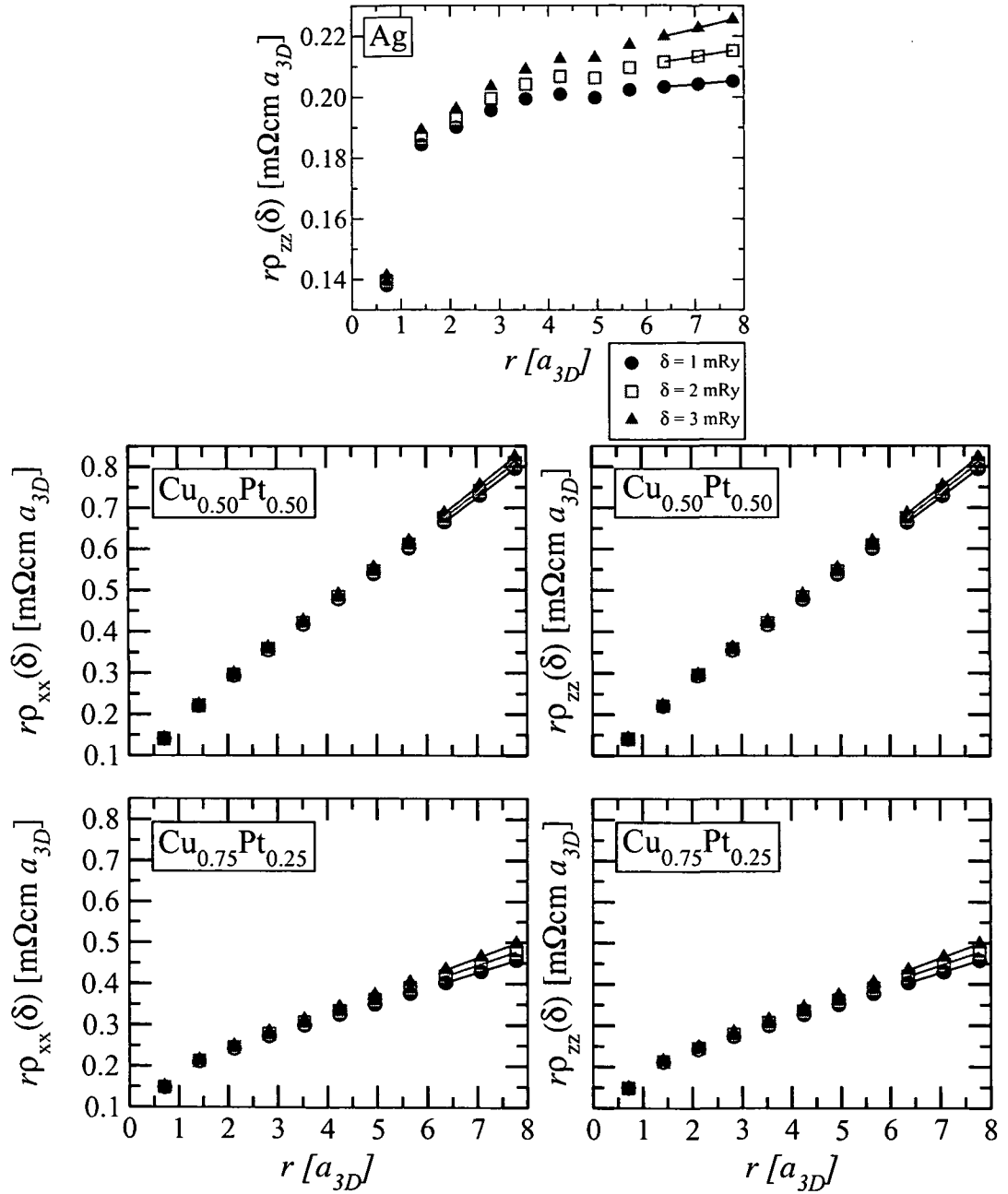
Figure 6.6: Real space study in bulk systems is performed. The characteristic size of the cluster (r) times the resistivity is shown versus the size of the cluster for three different imaginary parts (δ) of the Fermi energy in order to evaluate the slope (residual resistivity), see Eq. (6.3). The zz component of the resistivity is shown for fcc bulk Ag (top), while xx and zz components for fcc bulk CuPt alloys (bottom).
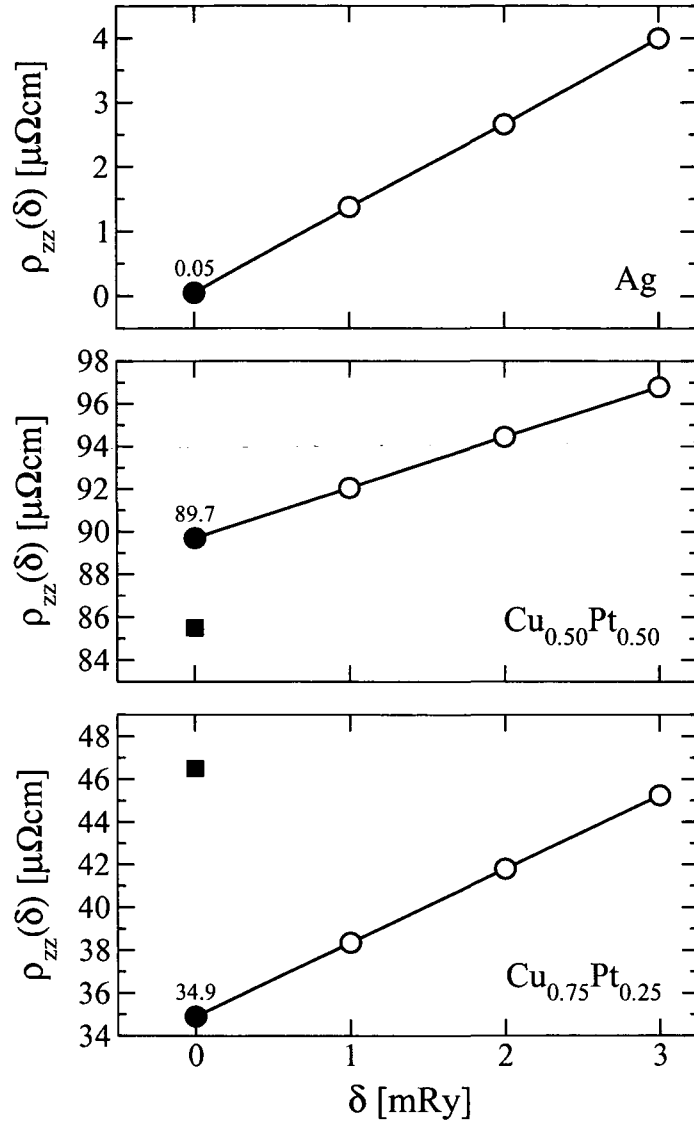
Figure 6.7: Extrapolation to $\delta = 0$ for the investigated bulk systems. Open circles are obtained from the fitting procedure in Eq. (6.3), while full circles refer to the extrapolated values and squares to experimental results measured at room temperature [24].

6.2.2 Cu_cPt_{1-c} bulk

More interesting than pure bulk metals are disordered bulk alloys because the accuracy of the present approach can be directly compared with experimental data and results of previous calculations. For this reason fcc $Cu_{0.50}Pt_{0.50}$ and $Cu_{0.75}Pt_{0.25}$ have been chosen with lattice constants $a_{3D}^{Cu_{0.50}Pt_{0.50}} = 7.140$ $a.u.$ and $a_{3D}^{Cu_{0.75}Pt_{0.25}} = 6.995$ $a.u.$ in order to test the reliability of the present approach. Again the fitting to a linear form has been applied {Eq. (6.3)} to the last three points of $r\rho_{\mu\mu}(r)$ function for each δ, in turn, see bottom part of Fig. 6.6.

Extrapolating to $\delta = 0$, we get the residual resistivity for the bulk systems shown in the lower parts of Fig. 6.7. As can be seen, the extrapolation can easily be performed because in the region $0 < \delta < 3$ mRy the resistivity depends linearly on δ. In comparing the present results with previous calculations and available experimental data, see in particular Ref. [24], we find that there is good quantitative agreement for both concentrations of CuPt. The results of Dulca et al. [28] are 80.2 and 31.5 $\mu\Omega cm$ for $Cu_{0.50}Pt_{0.50}$ and $Cu_{0.75}Pt_{0.25}$, respectively.

As already stated the numerical uncertainty of the present approach can be seen best by evaluating the difference between the in-plane and the perpendicular to the plane elements of the residual resistivity, since the residual resistivities, ρ_{xx} and ρ_{zz}, must be the same in cubic bulk systems. It can be seen from Fig. 6.8 that this difference is more or less independent of δ and is of order of a few tenth of a $\mu\Omega cm$.

It should be noted that in a recent paper Dulca et al. [28] applied real space scattering via the KKR method to the Kubo equation for bulk alloys. Although it might appear that formally their approach looks very similar to the one presented in here, fundamental conceptual differences have to be pointed out. The Embedded Cluster Method (ECM) used by them is restricted to infinite systems (three-dimensional translational invariance, see Eq. (10) in Ref. [28]), i.e., can only be used in the case of bulk systems, while in here only two-dimensional translational invariance for the substrate is assumed, which facilitates a correct embedding into semi-infinite systems (systems with surface or interfaces). Furthermore, as stated by Dulca et al. [28] their ECM necessarily is (charge) non-selfconsistent, whereas in the present case for substitutional alloys serving as substrate the embedding problem is solved (charge) selfconsistently. The results shown in here for bulk systems have to be

viewed entirely as an illustration of the accuracy of the present approach. The approach suggested by Dulca et al. [28] is perfectly suited to discuss short-range order effects in bulk binary substitutional alloys; it cannot be used for evaluating electric properties of nanostructures in or at surfaces of semi-infinite systems.
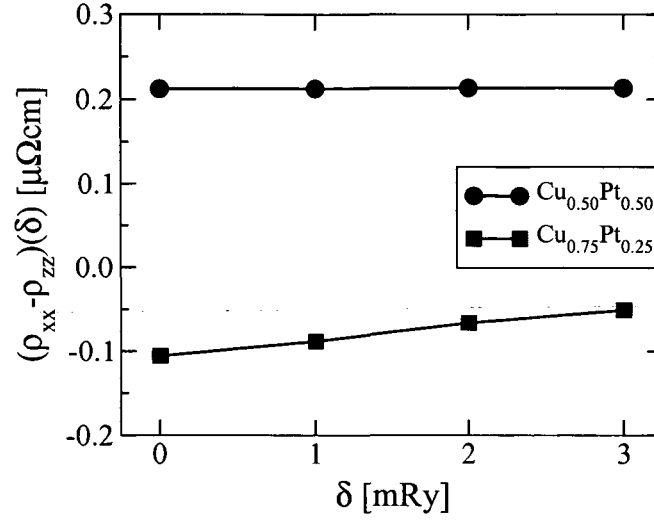

Figure 6.8: Difference between the residual resistivity for the in-plane (xx) and the perpendicular to the plane (zz) component are shown versus the imaginary part (δ) of the Fermi energy for $Cu_{0.50}Pt_{0.50}$ and $Cu_{0.75}Pt_{0.25}$.

Chapter 7

Anisotropic magnetoresistance in $Ni_{1-c}Fe_c$ bulk alloys

Among the compounds showing high AMR, because of their low coercivity and high magnetic moment, $Ni_{1-c}Fe_c$ alloys are perhaps most commonly used in technological applications. Due to this fact, for these systems a large amount of resistivity data from high quality measurements is available in the literature [2, 3, 4, 5, 6]. The aim of this Chapter is to determine the anisotropic magnetoresistance of $Ni_{1-c}Fe_c$ bulk alloys for diverse concentrations within framework of the presented theoretical approach. Besides to experiments, our results are compared with the earlier theoretical work of Banhart and Ebert on the same system [12]. These authors also pointed out [13, 14] the importance of spin-orbit coupling for the residual resistivities in magnetic binary substitutional alloys. In addition to AMR investigations, the dependence of the resistivity with respect to the angle between the magnetization and the current is also studied and the obtained results are successfully connected to the general formulation of Döring [74]. Two methods have been used to obtain the total conductivity of the systems with different orientations of magnetization, namely real space summation of non-local conductivities taking 3D clusters as described in Section 4.2.1,

$$\sigma_{\mu\mu}(N; c; \widehat{\mathbf{M}}) = \sum_{i,j=1}^{N} \sigma_{\mu\mu}^{ij}(c; \widehat{\mathbf{M}}) , \tag{7.1}$$

where N is the number of sites considered in the cluster, $\mu \in \{x, y, z\}$, and $\widehat{\mathbf{M}}$ is the direction of the magnetization, which is assumed to be uniform in all the layers of

the bulk alloy. Furthermore, the concentration of Fe, c is also fixed and identical in all layers.

The second method applies layer summation [23],

$$\sigma_{\mu\mu}(n; c; \widehat{\mathbf{M}}) = \sum_{p,q=1}^{n} \widehat{\sigma}_{\mu\mu}^{pq}(c; \widehat{\mathbf{M}}) , \qquad (7.2)$$

where n is the number of layers considered. For more details see Section 4.3. The corresponding resistivity is defined by

$$\rho_{\mu\mu}(\tilde{n}; c; \widehat{\mathbf{M}}) = 1/\sigma_{\mu\mu}(\tilde{n}; c; \widehat{\mathbf{M}}) , \qquad (7.3)$$

where $\tilde{n} = N$ or n depending on the type of summation, see Eqs. (7.1) and (7.2). Clearly, the calculated conductivity (and/or resistivity) of such layered systems converges to the bulk value in the limit of $N \rightarrow \infty$ or $n \rightarrow \infty$. Note, that the above formulation for layer summation is, in general, valid only for the current-in-plane (CIP) geometry (i.e., for $\mu \in \{x, y\}$). Since, however, in the present study bulk systems are represented by a sequence of identical layers,

$$Ni_{1-c}Fe_c(001)/(Ni_{1-c}Fe_c)_n/Ni_{1-c}Fe_c(001) , \qquad (7.4)$$

namely, n monolayers of permalloy capped from both sides by semi-infinite leads of the same material, see also Fig. 7.1, translational symmetry of the electric fields and currents is retained in the direction normal to the planes and, therefore, Eq. (7.2) and Eq. (7.3) with $\tilde{n} = n$ apply also in the case of $\mu = z$.
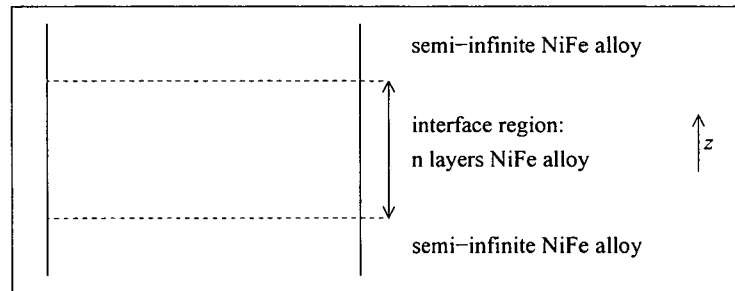
Figure 7.1: Geometrical setup of the studied NiFe bulk systems.

7.1 Real space summation

In order to perform real space summations in bcc $Ni_{0.15}Fe_{0.85}$, the system in Fig. 7.1 with $n = 33$ layers in the interface region was chosen. The bcc structure was taken with a lattice constant $a_{3D} = 5.442$ a.u.

Non-local conductivities were calculated according to Eq. (4.5) with the side limits in Eqs. (4.15), (4.19) with real space SPOs obtained by taking 1830 $k_\parallel$ points in the 2D IBZ, see Eq. (3.31).

The clusters were chosen to be spheres with increasing radius, where the center of the spheres is the site denoted by 0 in Eq. (4.21) and sites j are within the sphere. Table 7.1 shows the number of atoms (N) involved in the sphere versus k which denotes a step of cluster-building. In the kth step, the sphere has a radius $r_k = k \cdot a_{3D}$.

	Cluster								
k	0	1	2	3	4	5	6	7	8
N(k)	1	15	65	259	537	1067	1837	2891	4285

Table 7.1: The number of sites (N) in the considered spherical clusters.

Again the fitting to a linear form has been applied (Eq. 6.3) to the last three points of $r\rho_{\mu\mu}(r)$ function for each δ. The results with different orientations of magnetization ($\widehat{M} = \hat{z}$ and $\widehat{M} = \hat{x}$) are summarized in Table 7.2.

δ	Resistivity [$\mu\Omega cm$]				
[mRy]	$\rho_{xx}(\hat{z})$	$\rho_{zz}(\hat{z})$	$\rho_{xx}(\hat{x})$	$\rho_{yy}(\hat{x})$	$\rho_{zz}(\hat{x})$
0.0	15.9	15.7	20.7	20.3	20.7
0.5	18.6	18.4	23.0	22.6	22.9
1.0	21.3	21.0	25.3	24.9	25.1
2.0	26.7	26.3	29.8	29.5	29.5
3.0	32.2	31.8	34.2	34.1	33.9

Table 7.2: Calculated resistivities for $Ni_{0.15}Fe_{0.85}$ bulk system. The values for $\delta = 0$ are obtained by extrapolation of data from the calculations.

It can be stated that the resistivity $\rho_{zz}(\hat{z})$ is in good agreement with previous calculation, see Ref.[8], and the difference $\rho_{xx}(\hat{z}) - \rho_{zz}(\hat{z})$ agrees also with our finding

.in CuPt alloy system, see Fig. 6.8, while $\rho_{xx}(\hat{x})$ differs much from $\rho_{zz}(\hat{z})$. The reason can be the insufficient $k_{\|}$-integration in the 2D IBZ. Furthermore, it should be noted that the results obtained by real space summations are less accurate than the ones by layer summations with equal computing time, thus, it is better to use layer summations to determine the AMR in permalloy bulk systems.

7.2   Layer summation

In this Section $Ni_{1-c}Fe_c$ alloys in the Ni-rich regime ($0 < c < 0.5$) are investigated. Note that the experimental lattice constant of the structures were used. In addition, self-consistent potentials and effective fields were taken from Ref.[75].

The numerical procedure of performing the limit $n \to \infty$ for the resistivity in Eq. (7.3) and the overall stability of the method is discussed in length in Ref.[8]. As compared to the value of $n = 45$ taken in Ref.[8], in the present calculations a larger number of layers was used, namely, $n = 60$ that allowed us to perform a more stable fit for the resistivity of the bulk system.

When performing the configurational average within the CPA, no vertex corrections were taken into account [22, 23]. The electrical conductivity was calculated using 3160 $k_{\|}$ points in the 2D IBZ [23]. For some concentrations the stability of the obtained results was checked by increasing the number of $k_{\|}$ points up to 4950. In fact, we found that the 2D Brillouin zone summations converge faster for $\rho_{zz}(n; c; \widehat{M})$ than for $\rho_{xx}(n; c; \widehat{M})$, therefore, all the results presented in this Section refer to a current flowing normal to the planes (z), while we varied the orientation of the magnetization, $\widehat{M}$, with respect to this direction.

Because of computational reasons a finite imaginary part, δ, of the Fermi energy has to be used in the calculation of conductivity, see Section 4.1, Ref.[8]. The actual "bulk" resistivity is defined, therefore, as the following double limit,

$$\rho_{\mu\mu}(c; \widehat{M}) = \lim_{\delta \to 0} \lim_{n \to \infty} \rho_{\mu\mu}^{cal.}(n; c; \widehat{M}; \delta) . \qquad (7.5)$$

In Ref.[8] it was argued that for large enough n the slope of $n\rho_{\mu\mu}^{cal.}(n; c; \widehat{M}; \delta)$ behaves linear in δ. This observation greatly simplifies taking the $\delta \to 0$ limit in Eq. (7.5). In Ref.[8] the lowest value of $\delta = 2$ mRy produced a resistivity still 3-4 times larger than expected in the limit of $\delta \to 0$, leading, therefore, to some uncertaintity in

determining the bulk resistivity. In the present Section much smaller values of δ were used ($\delta_{min} = 0.1$ mRy), providing thus a more careful justification of the proposed numerical procedure. Fig. 7.2 shows the calculated resistivities, $\rho_{zz}^{cal.}(c;\widehat{M};\delta)$, of $Ni_{0.80}Fe_{0.20}$ for $\delta = 0.1$, 0.25, 0.5 and 1 mRy and for two different directions of the magnetization ($\widehat{M} = \hat{z}$ and $\widehat{M} = \hat{x}$), together with a linear least square fit to the data. The estimated relative error of the residual resistivity turned out to be about 1%. This accuracy of the fitting procedure applies in the entire concentration range, $0 < c < 0.5$.
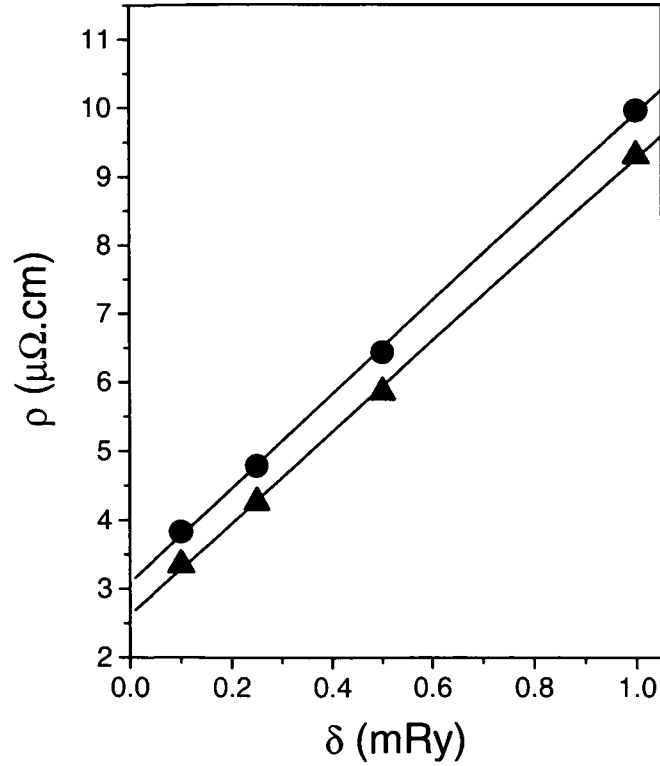
Figure 7.2: Calculated resistivities, $\rho_{zz}(\widehat{M};\delta)$, of the $Ni_{0.80}Fe_{0.20}$ alloy with various choices of the imaginary part of the Fermi energy, δ. Circles and triangles refer to the cases when the current is perpendicular or parallel to the direction of the magnetization, $\widehat{M} = \hat{x}$ and $\widehat{M} = \hat{z}$, respectively. The solid lines stand for a least square fit to the data. The residual resistivity is provided by the interception of the lines with the ordinate axis.

We adopted the commonly used definition [12, 76] for the AMR ratio of bulk alloys,

$$\frac{\Delta\rho(c)}{\rho_{av}(c)} = \frac{\rho_{\|}(c) - \rho_{\perp}(c)}{\rho_{av}(c)} , \tag{7.6}$$

with

$$\rho_{av}(c) = 1/3(\rho_{\|}(c) + 2\rho_{\perp}(c)) , \quad \rho_{\|}(c) = \rho_{zz}(c; \hat{z}) , \quad \rho_{\perp}(c) = \rho_{zz}(c; \hat{x}) . \tag{7.7}$$

Experimentally the above quantities are defined as an extrapolation of the measured results to zero applied magnetic field.
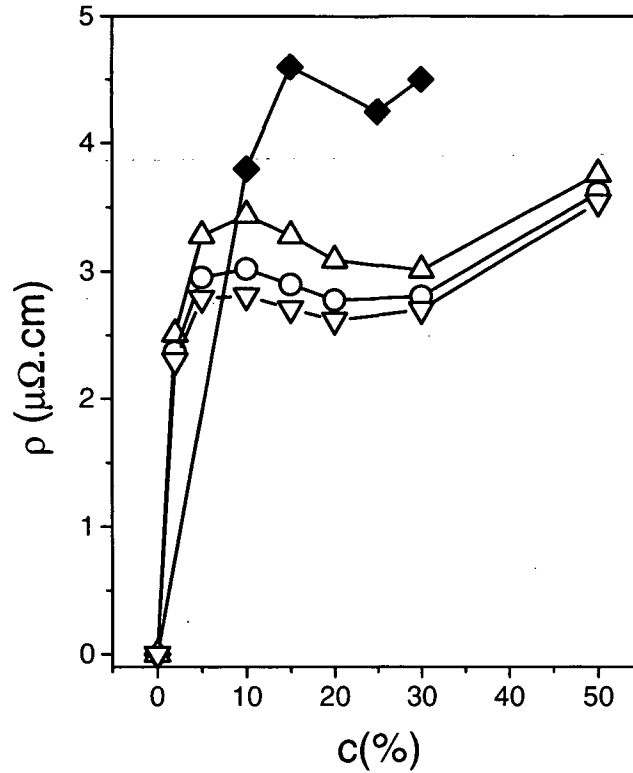
Figure 7.3: Calculated (open symbols) and experimental [2, 3] (diamonds) residual resistivities of $Ni_{1-c}Fe_c$ alloys with respect to the concentration, c. For the definitions of $\rho_{\|}$ (up-triangles) $\rho_{\perp}$ (down-triangles) and ρ_{av} (circles), see the expressions (7.7) in the text.

In Fig. 7.3 the calculated bulk resistivities, $\rho_{\|}$, $\rho_{\perp}$ and ρ_{av} of the $Ni_{1-c}Fe_c$ alloys are displayed in the concentration range, $0 < c < 0.5$. In full agreement with experiments, for all concentrations the resistivity for the current parallel to the field

is found to be larger than the perpendicular one, indicating that the AMR ratio defined by Eq. (7.6) is always positive. The shape of the curve $\rho_{av}(c)$ compares well to the experimental observations: for small concentrations it rapidly increases and reaches a flat minimum at about $c = 0.25$. The calculated magnitudes of the averaged residual resistivity, ρ_{av}, are significantly larger for $c < 0.1$ and by about 30-40% lower for $c > 0.1$ than the measured data. Similar observations were also made in the ab-initio calculations by Banhart and Ebert [12], with the exception that in the concentration range $0 < c < 0.1$ they found a rather moderate increase of the resistivity. This difference between the two theoretical results can be fairly well understood, as in Ref.[12] vertex corrections were taken into account, which, in particular, for small concentrations (weak disorder) should considerably lower the resistivity. The systematic error of about -30 to -40% of the calculated resistivities with respect to the experimental data can be *partially* attributed to additional scattering mechanisms, such as grain boundaries, short-range order, etc., not taken into account in the ab-initio calculations, giving rise, however, to an additional resistivity contribution. Clearly enough, missing correlations in the local density functional approximation (LDA) in particular for the Ni constituent may add to the discrepancy between the measured and the calculated averaged residual resistivity. As presently no ab-initio method is available that takes into account these correlations for calculating transport properties, it is very questionable to estimate its importance with respect to the above mentioned imperfections.

As can be seen from Fig. 7.4, both the functional shape and the magnitude of our calculated concentration dependent AMR ratios are in excellent agreement with the experimental data. In satisfactory agreement with experiments and the present calculations, the AMR ratio communicated in Ref.[12] shows a maximum at about $c = 0.1$ and a steady decrease for larger concentrations, however, in particular, for small concentrations its magnitude is largely overestimated. Supposing that excess scattering effects give rise to an isotropic resistivity contribution, in that work the AMR ratios were corrected by taking the measured ρ_{av}, keeping, however, the calculated $\Delta\rho$ in Eq. (7.6). Although, the overall agreement of the AMR curve improved as compared to experiments, for $c < 0.1$, the corrected AMR ratios were still too high by a factor of about two [12].
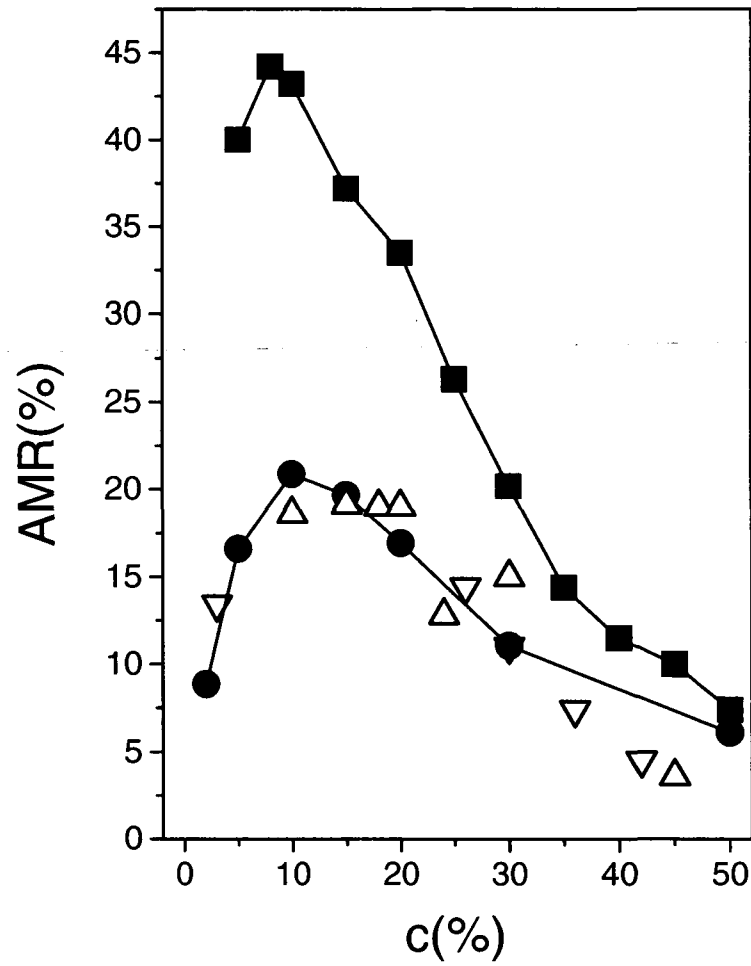
Figure 7.4: Calculated and experimental AMR ratios of $Ni_{1-c}Fe_c$ alloys. Full circles: present work, full squares: calculations of Ref.[12], up-triangles: experiment [2], down-triangles: experiment [4, 5]. The solid lines serve as a guide for eyes.

The good quantitative description of the AMR of the $Ni_{1-c}Fe_c$ alloys provided by our theoretical approach indicates that the effects not considered in the calculations do contribute to the average resistivity as well as to $\rho_{\parallel}$ and $\rho_{\perp}$ in equal terms and, therefore, the AMR ratio can safely be calculated by neglecting them. In fact, random structural imperfections (grain boundaries or clusters) are not expected to give an anisotropic contribution to the resistivity [12]. However, chemical fluctuations in the system (short–range order) and correlation effects alter the electronic structure whithout destroying the global cubic symmetry which, in combination with the spin-orbit coupling, is responsible for the observed anisotropic magnetoresistance. Of course, the AMR is only a particular transport property of the system that might be insufficient to rule out the dominance of the latter effects as compared to the structural imperfections.

By varying the direction of the magnetization, the dependence of the resistivity on the angle between the directions of the current and the magnetization can be studied. During the third decade of the last century Döring [74] put forward a general expression which describes the anisotropy of the resistivity in cubic crystals with respect to the direction of the magnetization and of the current relative to the crystallographic axes. In the special case, when the direction of the current is fixed along a certain crystallographic axis and the direction of the magnetization is varied between this and an other crystallographic axis, the Döring expression reduces to

$$\rho(\vartheta) = \rho_0 + B\cos^2\vartheta + C\cos^4\vartheta , \tag{7.8}$$

where ϑ is the angle between the magnetization and the current.

In Fig. 7.5 the results obtained for $Ni_{0.80}Fe_{0.20}$ and $Ni_{0.85}Fe_{0.15}$ alloys are presented. In these calculations the current is fixed along the (001) direction of the fcc crystal and the magnetization is rotated from the (001) to the (110) direction within the $(1\bar{1}0)$ plane. Note that the cases $\vartheta = 0$ and $\vartheta = \pi/2$ correspond to $\rho_{\parallel}$ and $\rho_{\perp}$, respectively. As inferred from Fig. 7.5, the calculated results almost perfectly fit the functional dependence given in Eq. (7.8). Looking at the fitting parameters listed in Table 7.3, it should be noted that even the $\cos^4\vartheta$ term has a non-negligible weight which cannot be omitted in the fitting procedure without a drastic loss in the overall quality of the fit.
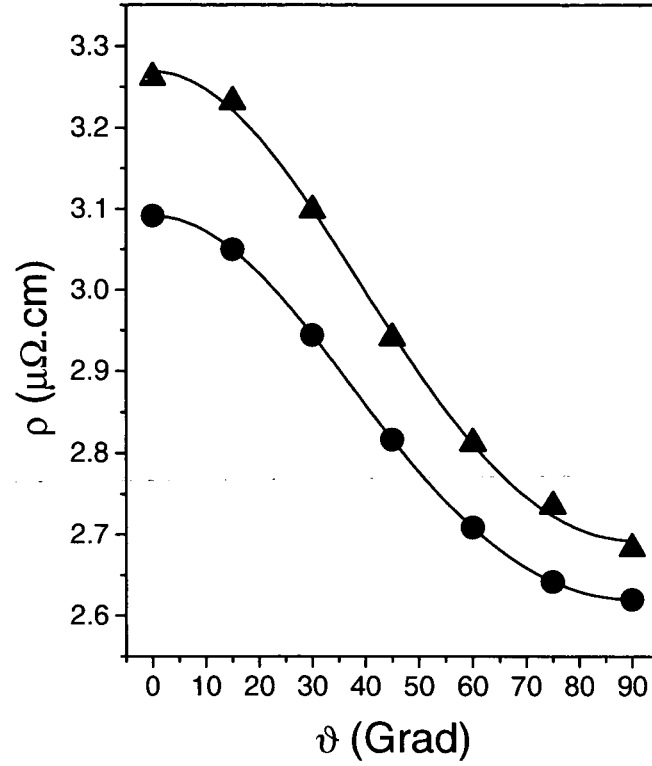
Figure 7.5: Calculated resistivities with respect to the the angle, ϑ, between the current and the magnetization for $Ni_{0.85}Fe_{0.15}$ (triangles) and $Ni_{0.80}Fe_{0.20}$ (circles) alloys. Solid lines visualize the results of least square fits according to Eq. (7.8), see text.

	ρ_0	B	C
$Ni_{0.85}Fe_{0.15}$	2.693	0.437	0.138
$Ni_{0.80}Fe_{0.20}$	2.620	0.315	0.156

Table 7.3: Parameters (in units of $\mu\Omega cm$) of the fit of the data presented in Fig. 7.5 to the function Eq. (7.8).

Chapter 8

Magnetic finite chains in the surface of Ag(001)

In Chapter 6 and Section 7.1 the reliability of the presented real space method for calculating transport properties was checked. It can be stated that the method works well in "large cluster" limit. As it is clear, real space methods have to be applied for investigating systems without any translational symmetry, such as nanostructures on top of a surface or nanocontacts between two leads. In this Chapter single impurities and finite chains (length of 2-10 atoms) of Fe and Co embedded along the (110) direction (x) in the surface layer of Ag(001) are investigated. The host system is the same as in Section 6.1, see Fig. 6.1. In this Chapter, the notation, e.g., Co_4 for a Co chain of four atoms is used. The $y = 0$ plane-section of the system with a chain of four atoms is shown in Fig. 8.1, while the arrangement of the atoms in the xy plane (in the surface layer) is found in Fig. 8.2.
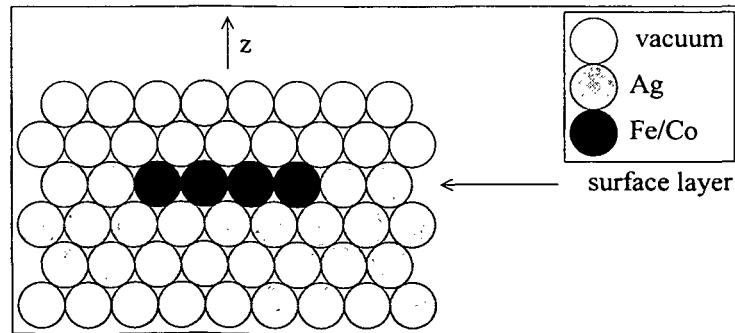
Figure 8.1: Chain of four atoms in the surface layer of Ag(001). $y = 0$ plane-section.

98
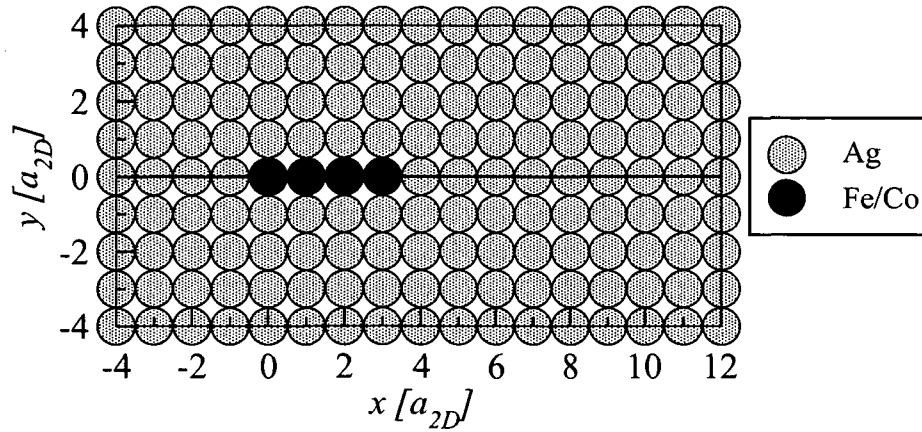
Figure 8.2: Chain of four atoms in the surface layer of Ag(001). xy plane-section in the surface layer.

The geometry of the self-consistently calculated clusters (chains+environment) is summarized in Table 8.1, while the applied method for calculating the self-consistent potentials of them can be found in Section 2.6.2.

Chain	Fe/Co	Ag		Vac.	No. of
length	S	S-1	S	S+1	atoms
1	1	4	4	4	13
2	2	6	6	6	20
3	3	8	8	8	27
4	4	10	10	10	34
5	5	12	12	12	41
6	6	14	14	14	48
7	7	16	16	16	55
8	8	18	18	18	62
9	9	20	20	20	69
10	10	22	22	22	76

Table 8.1: The setup of self-consistently calculated clusters "chain + 1 shell". The number of sites in the cluster are shown for each type (Fe/Co, Ag, vacuum) and each length of chains in the corresponding layer. Layer S denotes the surface layer, layers $S - i$ are located in the semi-infinite Ag, while layers $S + i$ in the vacuum region ($\forall i \in \mathbb{Z}^+$). The total number of atoms in each cluster is also explicitly shown.

8.1   Magnetic properties

The orbital (**L**) and spin moment (**S**) of site i can be calculated by integrating the orbital and spin magnetization densities defined by Eqs. (2.19) and (2.20) over the ith atomic cell (Ω_i), as

$$\mathbf{L}^i = \int\limits_{\Omega_i} d^3r\, \mathbf{l}(\mathbf{r}), \quad \mathbf{S}^i = \int\limits_{\Omega_i} d^3r\, \mathbf{m}(\mathbf{r}), \tag{8.1}$$

respectively.

Calculations showed that the magnitude of the spin moments is considerably insensitive to the direction of magnetization ($\widehat{\mathbf{M}}$), while for the orbital moments remarkably large anisotropy effects apply in full conformity with the findings of Ref.[26] where the magnetic clusters were located in the first vacuum layer. For a magnetization along the z axis ($\widehat{\mathbf{M}} = \hat{z}$), the calculated moments can be seen in Figs. 8.3 and 8.4 for Co and in Figs. 8.5 and 8.6 for Fe chains. As can be seen, the changes of the spin moment within the Co chains are smaller as compared to Fe chains where the atoms on the brink of the chain (with one Fe neighbor) have a spin moment systematically nearly 0.03 μ_B larger than the other Fe atoms (with two Fe neighbor) in the chain. Comparing the results to Ref.[26], it is found for chain lengths n=1,2,3 that both the orbital and spin moments are smaller than the moments of a corresponding structure located in the first vacuum layer. A detailed study [77] on magnetic properties of Fe chains at Cu(001) surface, with similar electronic structure as Ag(001), confirms this statement also for longer chains. It is remarkable to mention that both the spin and orbital moments are smaller in Fe chains embedded in the surface layer of Cu(001) than the moments of the corresponding chain located in the surface layer of Ag(001). One reason for this behavior can be that the lattice constant of fcc Cu structure is smaller than of fcc Ag.

A relatively weak magnetic polarization of the Ag atoms adjacent the magnetic chains were found. The calculated spin moments of these host atoms are about 0.01 μ_B adjacent Co and about 0.005 μ_B adjacent Fe, while the orbital moments are less than 10^{-3} μ_B.

It should be noted that the analyse of magnetic properties of nanostructures at the surface of a substrate is not subject of this work. For a detailed study, see Ref.[27].
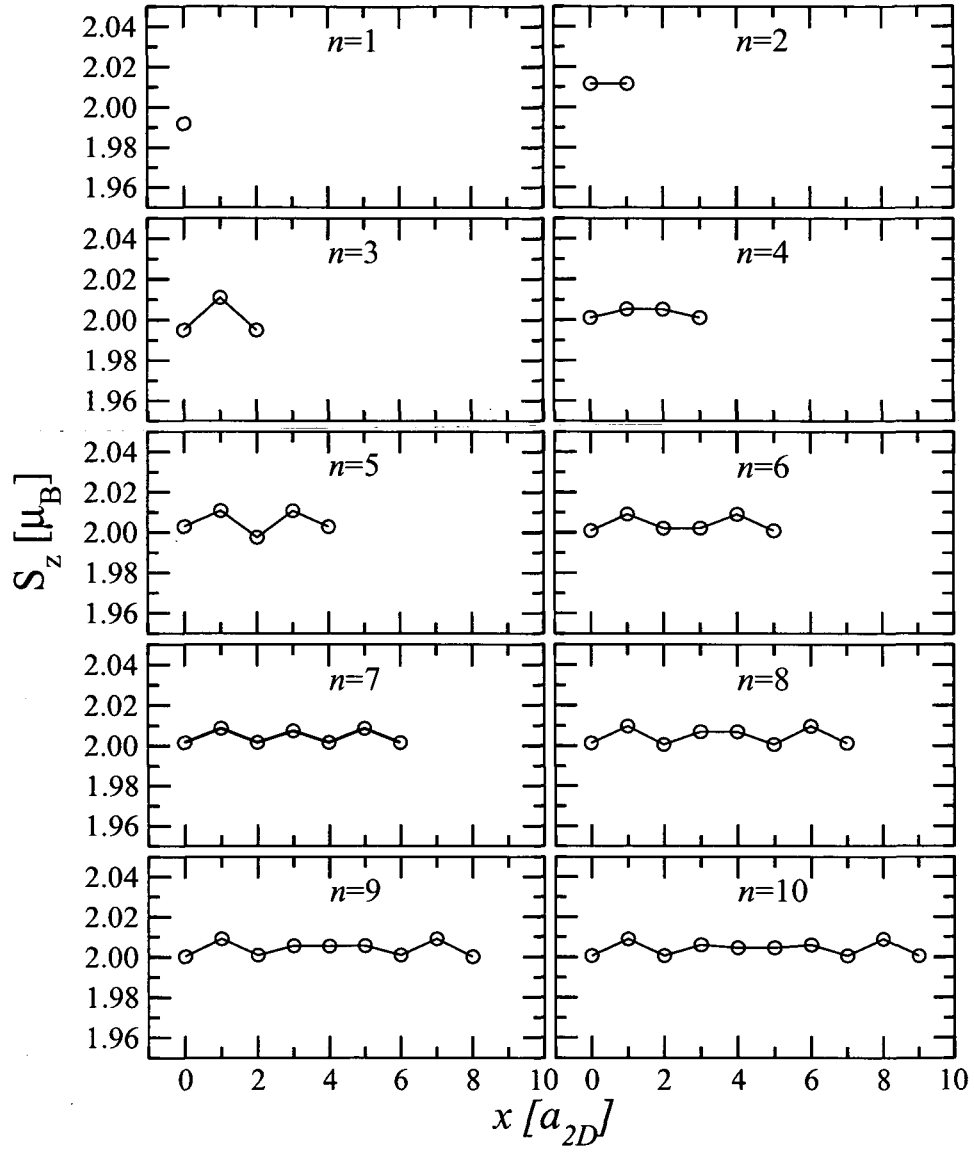
Figure 8.3: Calculated spin moments (S_z) of the Co atoms in Co_n $(n=1,...,10)$ chains in the surface layer of Ag(001) with $\widehat{M} = \hat{z}$.
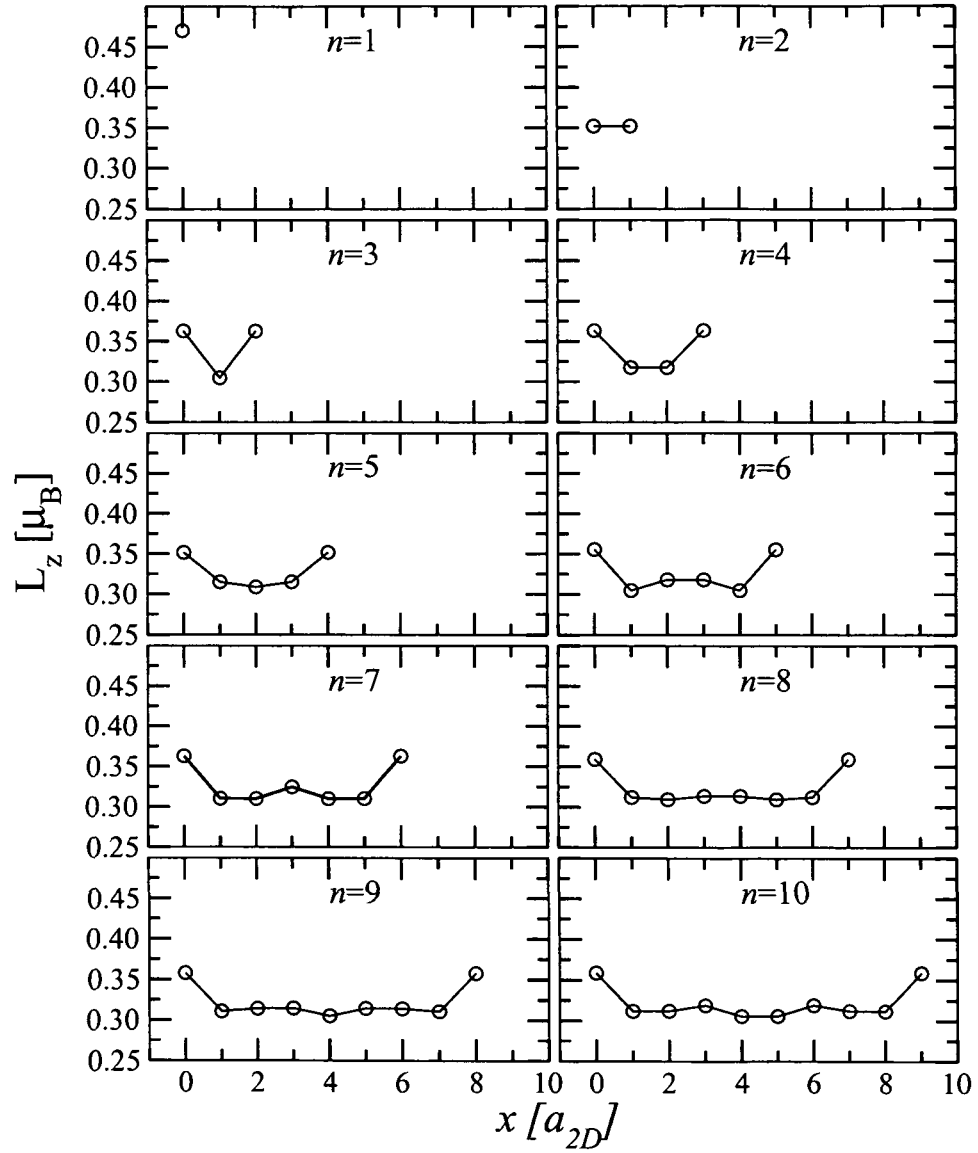
Figure 8.4: Calculated orbital moments (L_z) of the Co atoms in Co_n $(n=1,...,10)$ chains in the surface layer of Ag(001) with $\widehat{M} = \hat{z}$.
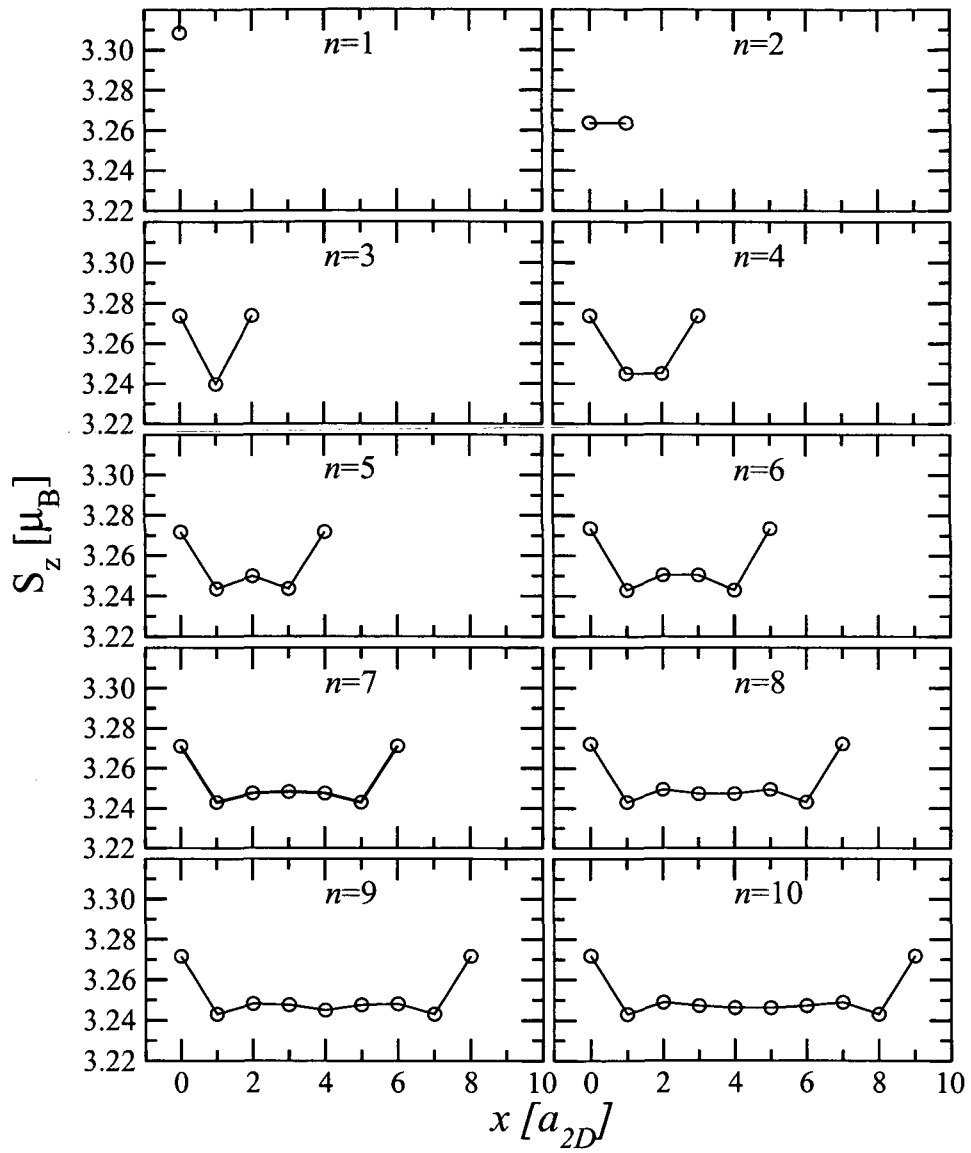
Figure 8.5: Calculated spin moments (S_z) of the Fe atoms in Fe$_n$ (n=1,...,10) chains in the surface layer of Ag(001) with $\widehat{\mathbf{M}} = \hat{z}$.
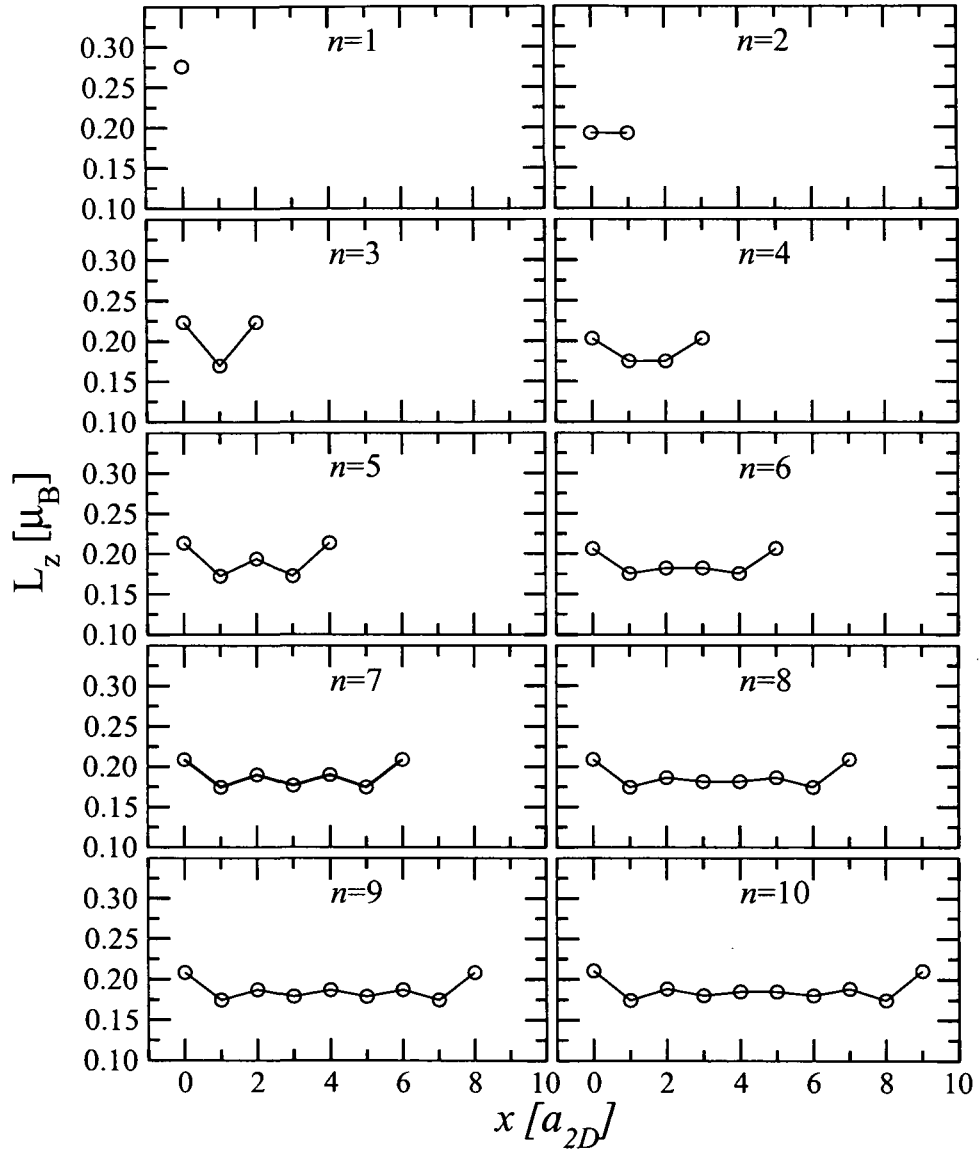
Figure 8.6: Calculated orbital moments (L_z) of the Fe atoms in Fe_n ($n=1,...,10$) chains in the surface layer of Ag(001) with $\widehat{M} = \hat{z}$.

8.2 Transport properties

8.2.1 Non-local conductivities

The influence of the chains to the in-plane transport in the surface layer was investigated, also CIP geometry is assumed. Non-local conductivities were calculated according to Eq. (4.5) with the side limits in Eq. (4.6), where the SPO of a specific cluster is obtained by the embedding equation, Eq. (2.95). The real space host SPOs were calculated by taking 210 $k_\parallel$ points in the 2D IBZ, see Eq. (2.96). The non-local conductivity was tested by increasing the number of self-consistently calculated atoms for Fe_1, Fe_2 and Co_1, Co_2. Since the relative difference between the conductivities by taking self-consistently calculated cluster "chain + 1 shell" and "chain + 2 shell" is below 0.2%, we decided to use the "chain + 1 shell" configurations to perform self-consistent calculations for longer chains, see Table 8.1, thus, saving computer time.

Let us fix a site and denote by 0 in the origin of the surface ($x = 0, y = 0$), see Fig. 8.2. In the impurity case the fixed site is the impurity. The xx-component of the non-local conductivity tensor between the impurity as fixed site (0) and all other atoms in the surface plane is shown in Fig. 8.7. The corresponding component of the non-local conductivity tensor of the pure Ag surface (Fig. 6.2) is also presented and rescaled in Fig. 8.7 in order to be able to compare the magnitudes of the site-diagonal conductivities. As it can be seen, the site-diagonal conductivity component of the fixed site at the origin (the peak) for Co is larger than for Fe, causing in turn of higher resistivity of Fe chains after performing summation in Eq. (8.2). Moreover, the height of the peaks are shown in decreasing order coming from Co to Ag. It can be stated that the studied magnetic impurities have 3-4 times more site-diagonal conductivity (Fe 3.2, Co 4.6) than an Ag atom in the pure Ag surface.

Let us have a look at the chains. Here, the atom on the brink of the chain is the fixed site (0), i.e. it is located in the origin of the surface. The xx-component of the non-local conductivity tensor between this fixed site and all other atoms in the surface plane is shown in Fig. 8.8 for Co and in Fig. 8.9 for Fe chains, including the results of the impurities (chain length=1), too. It can be seen that in the impurity case the shape of the conductivity is symmetric to the $x = 0$ plane, while in the chain cases the tensor-elements along the $+x$ direction (where the chain lies)

are much larger than in other directions, causing an asymmetry. This shape also means that by summing up the non-local conductivity σ_{xx}^{0j} over sites j in a three-dimensional cluster around the chain, a significant contribution is coming from the magnetic atoms, e.g. for a Co chain with length of six atoms the contribution from the magnetic atoms is 63%. This is not surprising because the contribution coming from site on the other brink of the chain {pos.(5,0)} is larger than from the second neighboring Ag atom in the other direction {pos.(-2,0)}. Furthermore, it can be seen that the magnitude of the site-diagonal conductivities decrease for the atoms forming a chain comparing to the single impurities embedded into the surface layer for both Co and Fe.
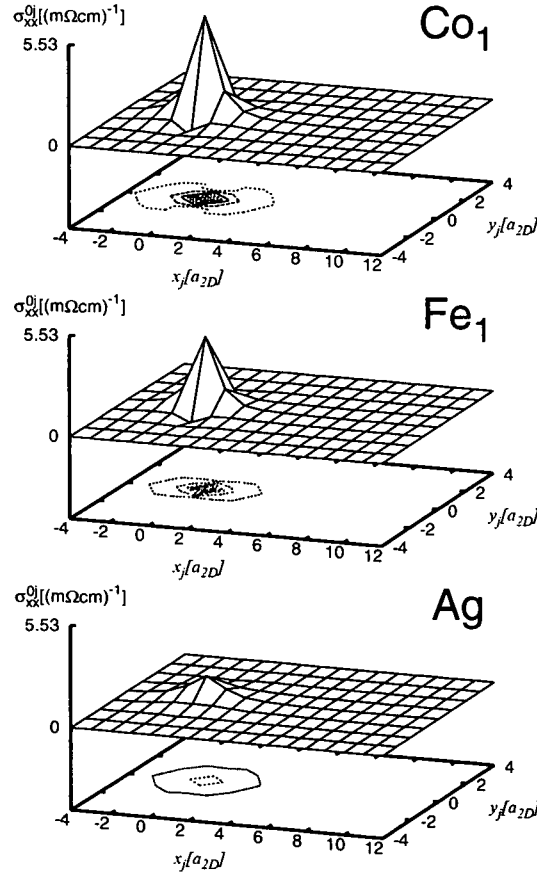
Figure 8.7: Non-local conductivities $\sigma_{xx}^{0j}(x_j, y_j)$ in the surface layer of Ag in presence of Co or Fe impurity being the fixed sites (0) or without any impurities (pure Ag surface). $\delta = 1$ mRy, $\widehat{M} = \hat{z}$.
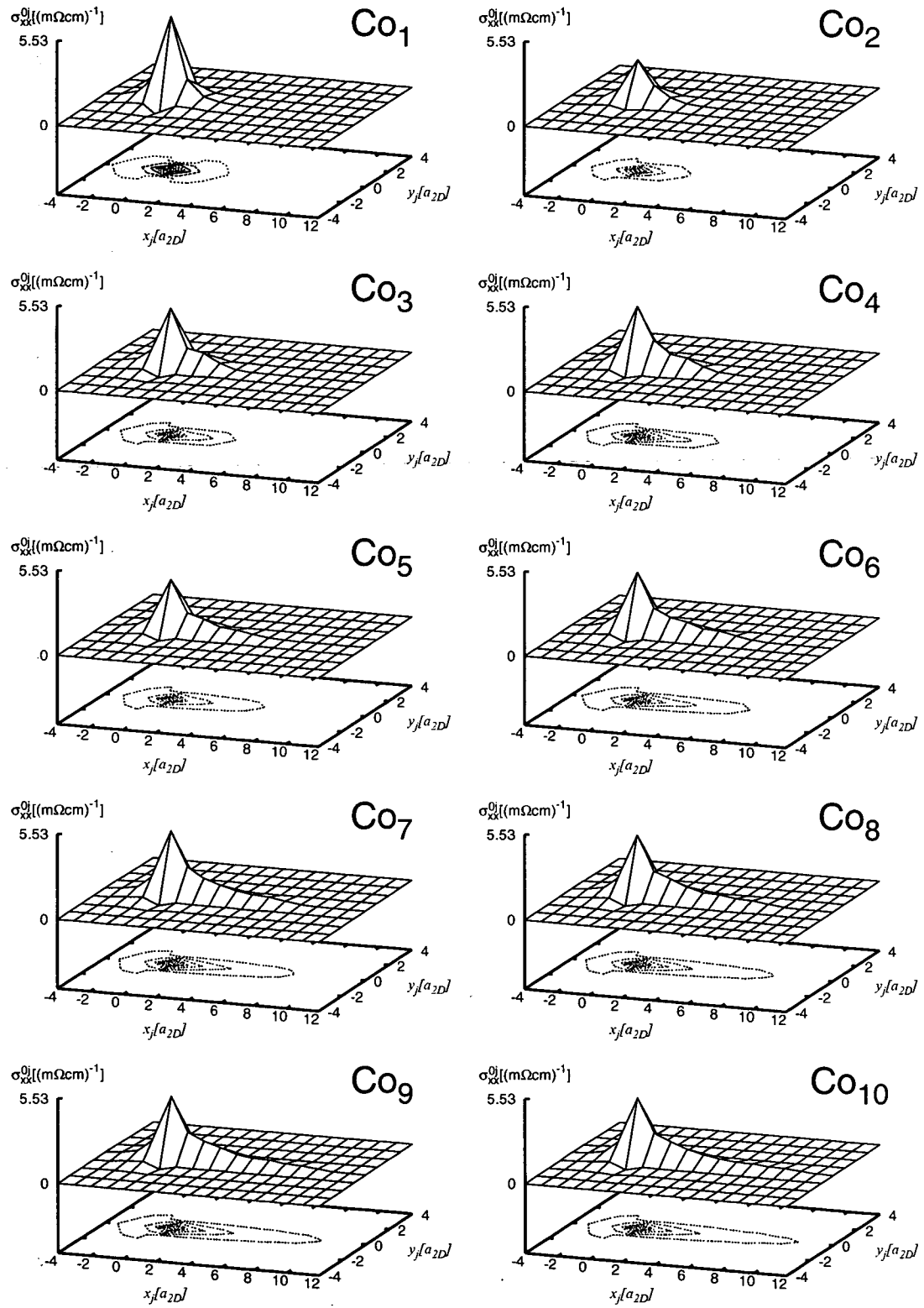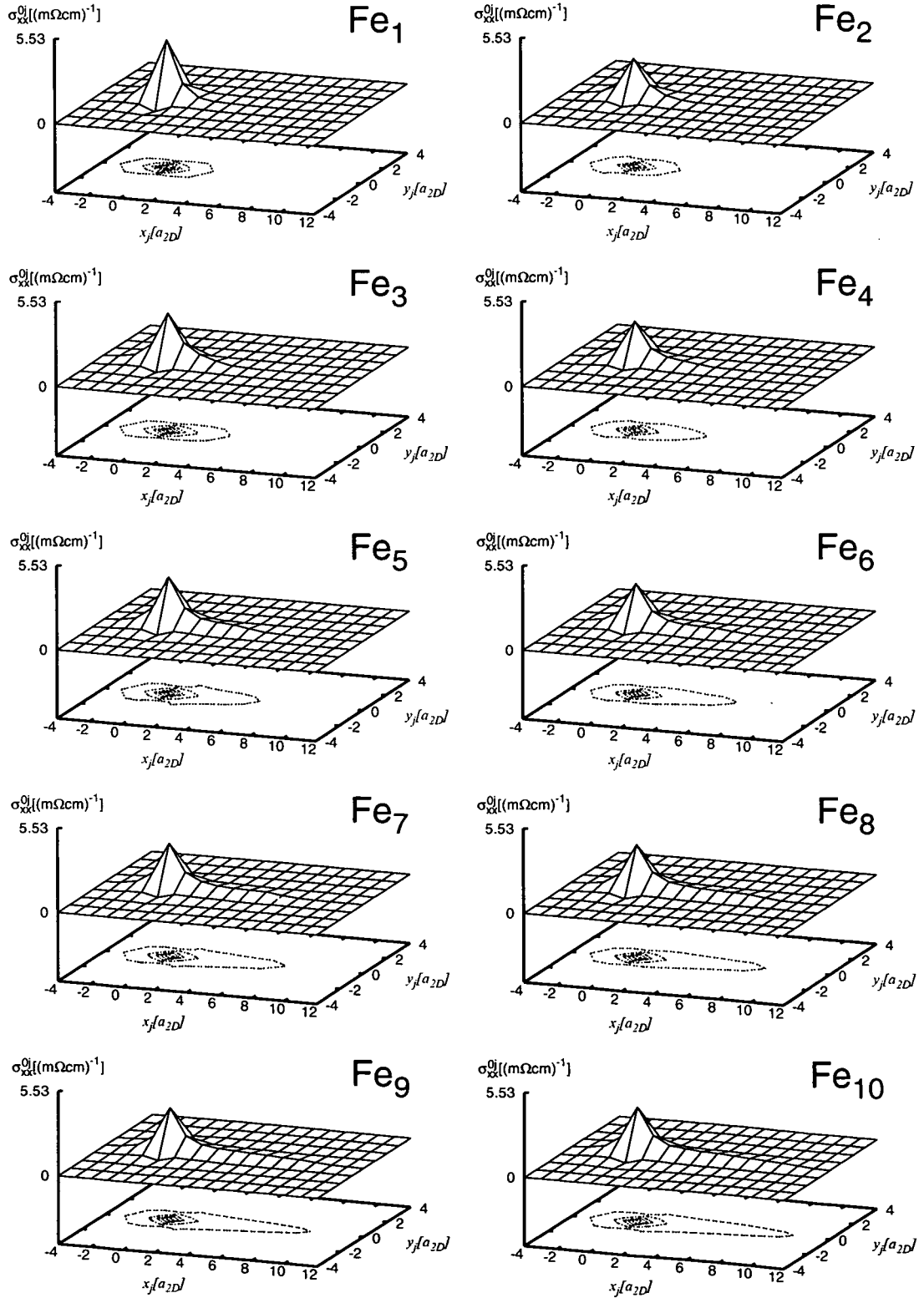
Figure 8.8: Non-local conductivities $\sigma_{xx}^{0j}(x_j, y_j)$ in the surface layer of Ag with Co atoms in a Co_n chain in positions $(0,0), ..., (n-1, 0)$. $\delta = 1$ mRy, $\widehat{\mathbf{M}} = \hat{z}$.

Figure 8.9: Non-local conductivities $\sigma^{0j}_{xx}(x_j, y_j)$ in the surface layer of Ag with Fe atoms in a Fe_n chain in positions $(0,0), ..., (n-1,0)$. $\delta = 1$ mRy, $\widehat{M} = \hat{z}$.

8.2.2 "Residual resistivities"

In Section 4.2.2 a "residual resistivity" for finite clusters was defined,

$$\rho^{\alpha}_{\mu\mu}(r) = \left[\frac{1}{n} \sum_{i \in chain} \sum_{j=1}^{N(r)} \sigma^{ij}_{\mu\mu}\right]^{-1}, \tag{8.2}$$

where n denotes the number of atoms in the chain of type α (Fe or Co) and $N(r)$ is the number of atoms involved in the cluster (chain + environmental atoms up to the furthermost distance of r). It should be noted that here, three-dimensional clusters were taken. Obviously, the convergence properties of $\rho^{\alpha}_{\mu\mu}(r)$ with respect to r can be investigated by taking clusters with increasing size. This is shown in Fig. 8.10 where all data refers to $\delta = 0$ which can be obtained by extrapolation of the calculated data in diverse δ values. In our calculations $\delta=1,2,3$ mRy were taken. As can be seen in Fig. 8.10, for all chain lengths (n) $\rho^{\alpha}_{xx}(r)$ decrease monotonously and can in principle be extrapolated to large values of N by considering them as products with the cluster size, see Eq. (6.3), while the difference, $\rho^{Fe}_{xx}(r) - \rho^{Co}_{xx}(r)$ is finite and varies slowly with respect to the cluster size. Furthermore, chains with length of three or five atoms differ distinctly from the rest, namely there is almost no difference wheter Fe or Co atoms form the chain, i.e., the difference, $\rho^{Fe}_{xx}(r) - \rho^{Co}_{xx}(r)$ is nearly vanishing for all cluster size considered.

The "residual resistivity" of finite clusters defined in Eq. (8.2) is a practical tool to study the influence on in-plane transport properties with respect to the orientation of magnetization $(\widehat{M})$ in the above described finite chain structures. The calculated results of the xx-component of the resistivity are listed in Table 8.2. As can be seen, $\widehat{M} = \hat{x}$, i.e., $\widehat{M}$ parallel to the orientation of the chains provides the smallest resistivity for all Fe chains and for the most Co chains. There are two exceptions where this is not true, namely Co_2 and Co_3 chains. In these chains the smallest resistivity is obtained with $\widehat{M} = \hat{y}$. This behavior is quite surprising if we watch the resistivities for the other chains. It can be stated that in most cases the direction of magnetization $\widehat{M} = \hat{y}$ provides the highest resistivity, however, the orientation of magnetization perpendicular to the chain $(\hat{y}$ and $\hat{z})$ results in minor differences in the resistivity. Moreover, in the impurity case, $\rho^{Fe}_{xx}(\hat{y})$ is by 13.6% larger than $\rho^{Fe}_{xx}(\hat{x})$, while $\rho^{Co}_{xx}(\hat{y})$ is only by 5.7% larger than $\rho^{Co}_{xx}(\hat{x})$ which means a higher sensitivity with respect to the orientation of the magnetization for the Fe impurity.
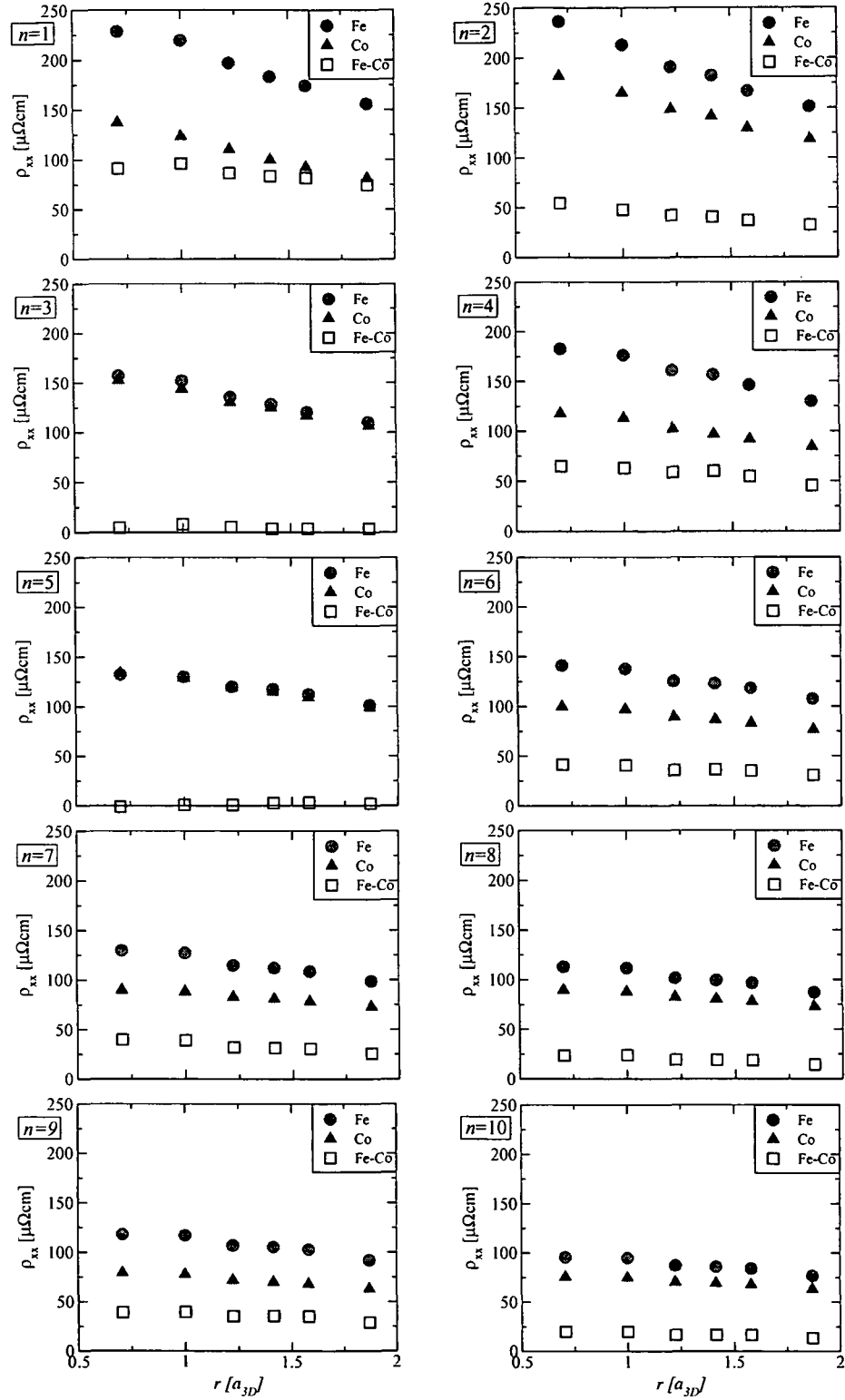
Figure 8.10: "Residual resistivities" of Fe (circles) and Co (triangles) chains. Open squares refer to $\rho_{xx}^{Fe}(r) - \rho_{xx}^{Co}(r)$. The length of the chains (n) is explicitly shown. $\delta = 0$ mRy (extrapolated), $\widehat{\mathbf{M}} = \hat{z}$.

length	Co			Fe		
	$\hat{x}$	$\hat{y}$	$\hat{z}$	$\hat{x}$	$\hat{y}$	$\hat{z}$
1	120.1	126.9	123.5	198.3	225.3	219.6
2	162.6	162.2	165.4	200.5	213.1	213.2
3	151.4	140.1	143.9	142.0	153.8	152.0
4	109.0	113.7	113.2	166.7	176.4	176.2
5	122.6	126.6	128.8	122.2	130.1	129.7
6	94.9	100.1	97.0	132.3	138.6	137.6
7	85.6	89.7	88.3	119.5	125.9	127.3
8	86.1	89.4	87.8	108.0	111.9	111.7
9	74.0	78.6	77.6	110.2	114.7	117.1
10	73.4	77.2	74.9	91.3	93.4	94.9

Table 8.2: "Residual resistivities" versus orientation of magnetization $(\widehat{M})$, $\rho_{xx}(r=a_{3D})[\mu\Omega cm]$ in Co and Fe chains. $\delta = 0$ mRy (extrapolated). MAX. and MIN. resistivity values for a given chain are explicitly shown.

Chapter 9

Gold nanocontacts

As mentioned in the Introduction, nanocontacts made of gold are presumably the most studied atomic-sized conductors in the literature both theoretically and experimentally. A dominant peak very close to the conductance quantum, 1 $G_0 = 2e^2/h$, has been reported for gold in the conductance histogram [31, 32], attributed to the highly transmitting sp-channel across a linear monoatomic chain connecting the two electrodes. In this Chapter gold contacts are investigated in different geometries as well as the influence of transition metal impurities on the conductance is studied within the real-space approach described in Sections 4.1 and 4.2.3.

The host system for the embedding is shown in Fig. 9.1. It should be noted that all of the considered sites (Au, vacuum and impurities) refer to the positions of an underlying ideal fcc structure of gold with a lattice constant of $a_{3D} = 7.681$ $a.u.$
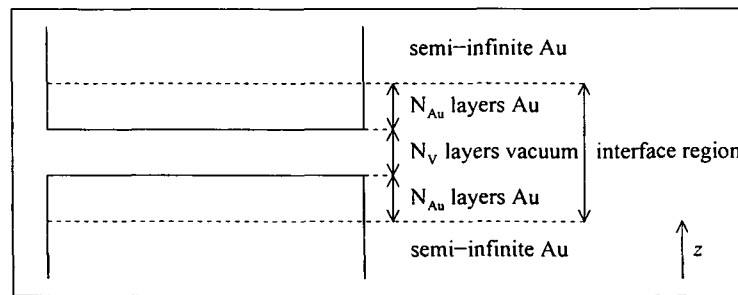
Figure 9.1: Geometrical setup of the studied host Au(001) system. Nanojunction between the two semi-infinite systems is built by embedding Au atoms into the vacuum region, see e.g., Figs. 9.2 and 9.3. The host characterized by N_{Au} and N_V can be different for different contacts.

A schematic view of a typical contact is displayed in Fig. 9.2 with N_V=5 vacuum layers considered in the host system, see Fig. 9.1. As follows from the above, atomic sites refer to layers for which the following notation is used: C denotes the *central layer*, $C-1$ and $C+1$ the layers below and above, etc. For the contact shown in Fig. 9.3a, e.g., the central layer contains 1 Au atom (the rest is built up from empty spheres), layers $C-1$ and $C+1$ contain 4 Au atoms, layers $C-2$ and $C+2$ contain 9 Au atoms and, though not shown, all layers $C-n$ and $C+n$ ($n \geq 3$) are completely filled with Au atoms, i.e., denote full layers.

Non-local conductivities were calculated according to Eq. (4.34) with the side limits in Eq. (4.6), where the SPO of a specific cluster is obtained by the embedding equation, Eq. (2.95). The real space host SPOs were calculated by taking 210 $k_{\parallel}$ points in the 2D IBZ, see Eq. (2.96).
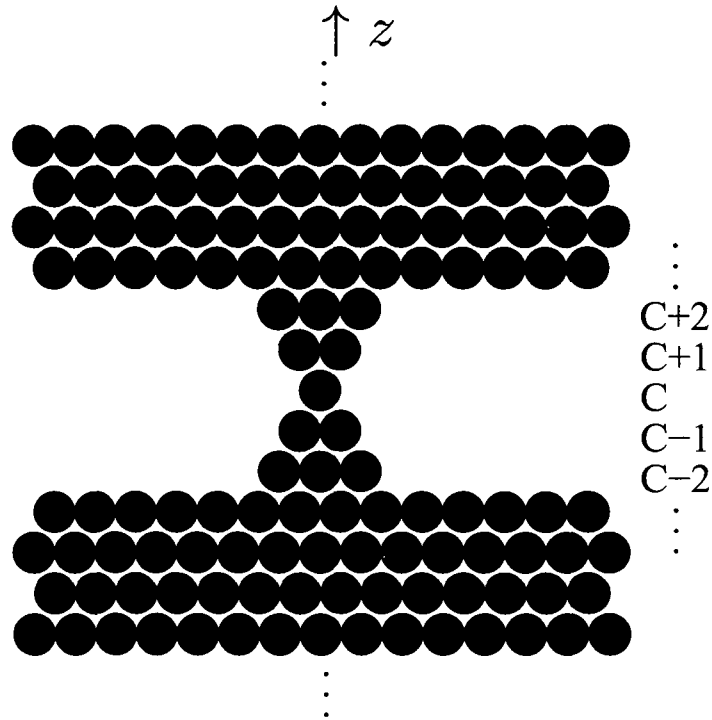
Figure 9.2: Schematic side view of a point contact between two semi-infinite leads embedded into the vacuum region (number of vacuum layers N_V=5). The layers are labelled by C, $C \pm 1$, etc.
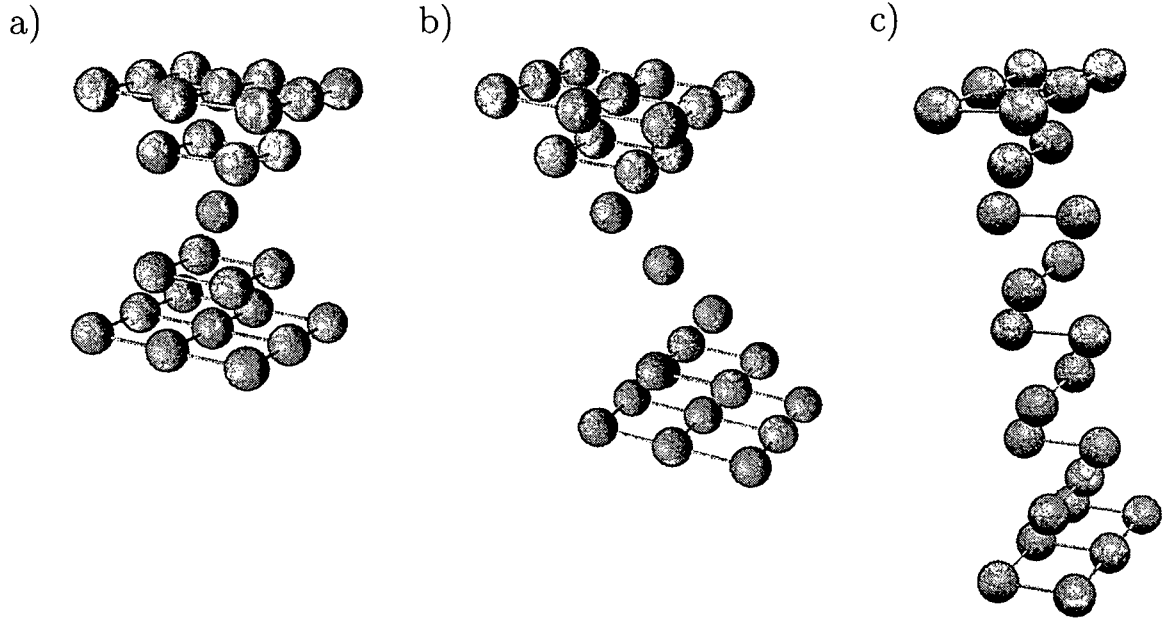
Figure 9.3: Perspective view of some of the studied contacts between two fcc(001) semi-infinite leads. Only the partially filled layers are shown. **a)** point contact (no. of Au layers in the interface region taken from one side: $N_{Au}=5$, no. of vacuum layers between the leads: $N_V=5$, see Fig. 9.1), **b)** slanted linear finite chain ($N_{Au}=7$, $N_V=7$), **c)** 2×2 finite chain ($N_{Au}=6$, $N_V=9$).

9.1 Numerical tests on different gold contacts

As mentioned in Section 4.1 a finite Fermi level broadening, δ, has to be used for non-local conductivity, thus, also for conductance calculations. As an example, for the point contact depicted in Fig. 9.3a, the dependence of the conductance on δ is investigated. The summation in Eq. (4.36) was carried out up to convergence for the first two (symmetric) full layers ($p = C - 3$, $q = C + 3$). As can be seen from Fig. 9.4, the calculated conductances depend strongly but nearly linear on δ. A straight line fitted for $\delta \geq 1.5$ mRy intersects the vertical axis at 2.38 G_0. Assuringly enough, a calculation with $\delta = 1$ μRy resulted in $g = 2.40 G_0$. Although the nearly linear dependence of the conductance with respect to δ enables an easy extrapolation to $\delta = 0$, as what follows all the calculated conductances refer to $\delta = 1$ μRy.
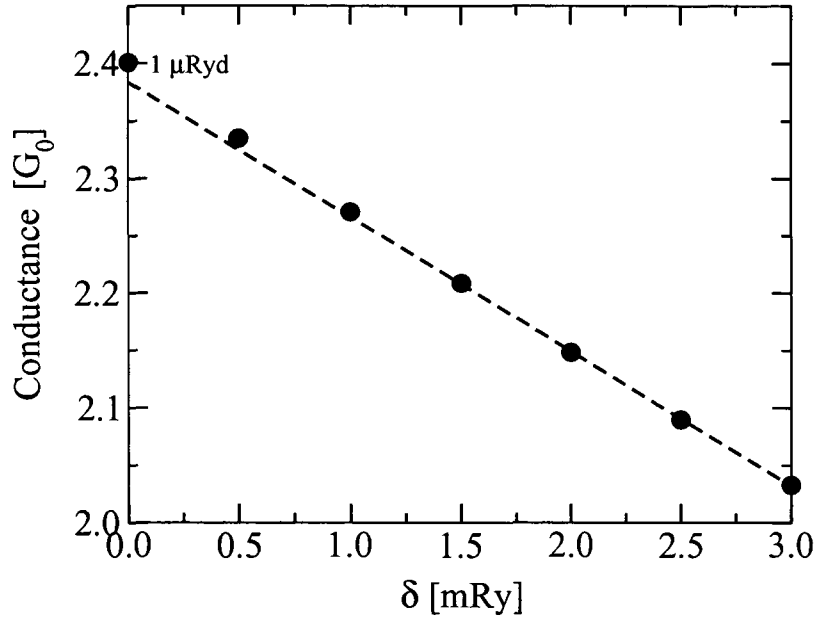
Figure 9.4: Calculated conductance as a function of the Fermi level broadening, δ, for the Au contact shown in Fig. 9.3a. The dashed straight line is a linear fit to the values for δ = 1.5, 2.0, 2.5, and 3.0 mRy.

For the same type of contact (Fig. 9.3a) the convergence of the summation in Eq. (4.36) over the layers p and q was also investigated, whereby different symmetric pairs of full layers were chosen. The convergence with respect to the number of atoms in the layers is shown in Fig. 9.5. Convergence for about 20 atoms can be obtained for the first two full layers ($p = C - 3$, $q = C + 3$), whereas the number of sites needed to get convergent sums gradually increases if one takes layers farther away from the center of the contact. This kind of convergence property is qualitatively understandable since the current flows from the contact within a cone of some opening angle that cuts out sheets of increasing area from the corresponding layers. As all the calculations were performed with $\delta = 1$ μRy, current conservation has to be expected. Consequently the calculated conductance ought to be independent with respect to the layers chosen for the summation in Eq. (4.36). As can be seen from Fig. 9.5 this is satisfied within a relative error of less than 10%. It should be noted, however, that for the pairs of layers, $p = C - n$, $q = C + n$, $n \geq 6$ convergence was not achieved within this accuracy: by taking more sites in the summations even

a better coincidence of the calculated conductance values for different pairs of layers can be expected. Fig. 9.5 also implies that an application of the Landauer-Büttiker approach to calculate the conductance of nanocontacts is numerically more tedious than the present one, since, in principle, two layers situated infinitely far from each other have to be taken in order to represent the leads.
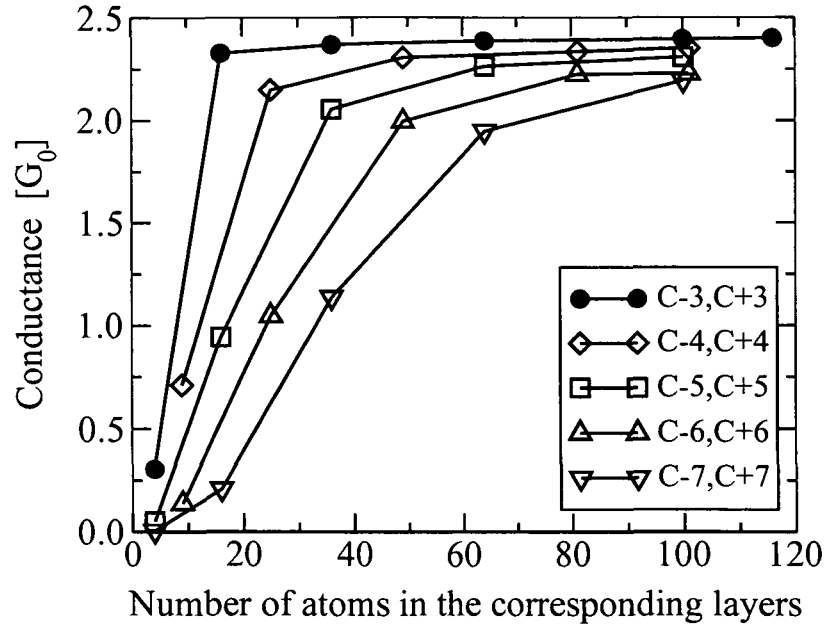

Figure 9.5: Conductance versus the number of sites included in the sum in Eq. (4.36) for the contact in Fig. 9.3a. The different curves show conductances as calculated between different pairs of layers. For a definition of the layer numbering see Fig. 9.2.

Although only one Au atom is placed in the center of the point contact considered above, see Fig. 9.3a, the calculated conductance is more than twice as large as the conductance unit. This is easy to understand since the planes $C - 1$ and $C + 1$, each containing four Au atoms, are relatively close to each other and, therefore, tunneling contributes quite a lot to the conductance through the contact. In order to obtain a conductance around 1 G_0, detected in the experiments, a linear chain has to be considered. The existence of such linear chains is obvious from the long plateau of the corresponding conductance trace with respect to the piezo voltage in the break-junction experiments. Since, as mentioned in Chapter 5, our method at

present can only handle geometrical structures confined to three-dimensional translational invariant simple bulk parent lattices, as the simplest model of such a contact a slanted linear chain was considered as shown in Fig. 9.3b. In here, the middle layer (C) and the adjacent layers $(C \pm 1)$ contain only one Au atom, layers $C \pm 2$ and $C \pm 3$ four and nine Au atoms, respectively, while layers $C \pm 4$ refer to the first two full layers. The sum in Eq. (4.36) was carried out for two pairs of layers, namely for $p = C - 4$, $q = C + 4$ (full layers) and for $p = C - 2$, $q = C + 2$ (not full layers). The convergence with respect to the number of atoms in the chosen layers can be seen from Fig. 9.6. The respective converged values are 1.10 G_0 and 1.17 G_0. In the case of $p = C - 2$, $q = C + 2$ we observed that the contribution coming from the vacuum sites is nearly zero: considering only four Au atoms in the summation already gave a value for the conductance close to the converged one. The small difference between the two calculated values, 0.07 G_0, can most likely be attributed to an error caused by the ASA. Nevertheless, as expected, the calculated conductance is very near to the ideal value of 1 G_0.
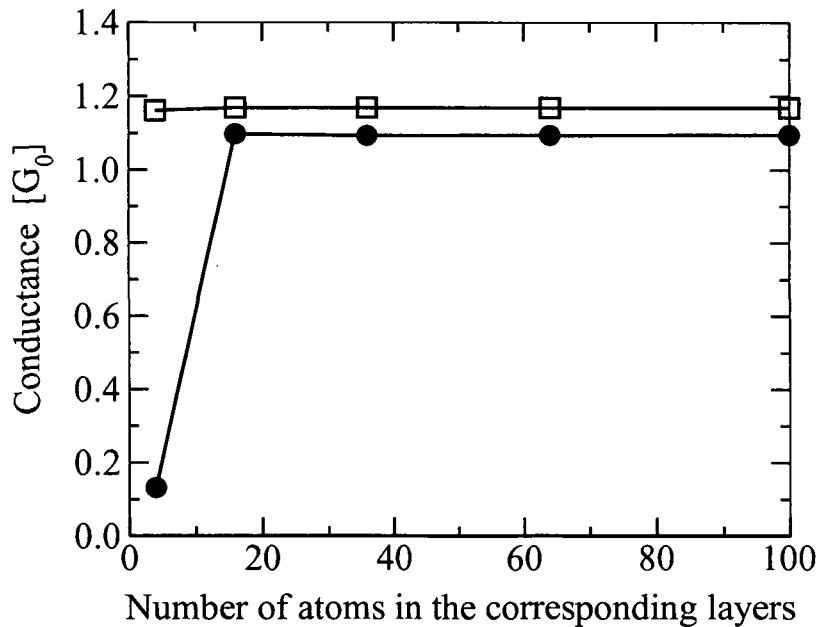

Figure 9.6: Conductance versus the number of sites included in the sum in Eq. (4.36) for the slanted linear chain shown in Fig. 9.3b. Full circles are the results of summing in layers $p = C - 4$ and $q = C + 4$ (first full layers), while squares refer to a summation in layers $p = C - 2$ and $q = C + 2$ (layers containing four Au atoms).

Another interesting structure is the 2×2 chain described in Ref.[38]. Here we considered a finite length of this structure sandwiched between two semi-infinite systems, see Fig. 9.3c. The conductance was calculated by performing the summation for 100 atoms from each of the first two full layers. As a result we obtained a conductance of 2.58 G_0. Papanikolaou et al. [38] got a conductance of 3 G_0 for an infinite Cu wire to be associated with three conducting channels within the Landauer approach. For an infinite wire the transmission probability is unity for all states, therefore, the conductance is just the number of bands crossing the Fermi level. For the present case of a finite chain, the transmission probability is less than unity for all the conducting states. This qualitatively explains the reduced conductance with respect to an infinite wire.

Finally, the dependence of the conductance on the thickness of the nanocontacts was studied. All the investigated structures have C_{4v} symmetry and the central layer of the systems is a plane of reflection symmetry. The set-up of the structures is summarized in Table 9.1. Contact 0 refers to a broken contact which is embedded into a host with $N_{Au}=7$ and $N_V=7$ layers, see Fig. 9.1, while the others have different thicknesses from 1 up to 9 Au atoms in the central layer, and are embedded into a host characterized by $N_{Au}=5$ and $N_V=5$, see Fig. 9.1.

layer	Contact				
position	0	1	4	5	9
C±4	Full	Full	Full	Full	Full
C±3	9	Full	Full	Full	Full
C±2	4	9	16	21	25
C±1	1	4	9	12	16
C	0	1	4	5	9

Table 9.1: Set-up of various nanocontacts. The Table shows the number of Au atoms in the layers as labelled by C, C ± 1, etc., see Fig. 9.2. Contact 1 refers to Fig. 9.3a.

In Fig. 9.7 the calculated conductances are displayed as performed by taking nearly 100 atoms from each of the first two full layers: $p = C - 4$, $q = C + 4$ for the broken contact and $p = C - 3$, $q = C + 3$ for all the other cases, see Table 9.1. It can be seen that the conductance is nearly proportional to the number of Au atoms in the central layer. This finding can qualitatively be compared with the result of

.model calculations for the conductance of a three-dimensional electron gas through a connective neck as a function of its area in the limit of $\vartheta_0 = 90°$ for the opening angle [78]. In the case of the broken contact, the non-zero conductance can again be attributed to tunneling of electrons.
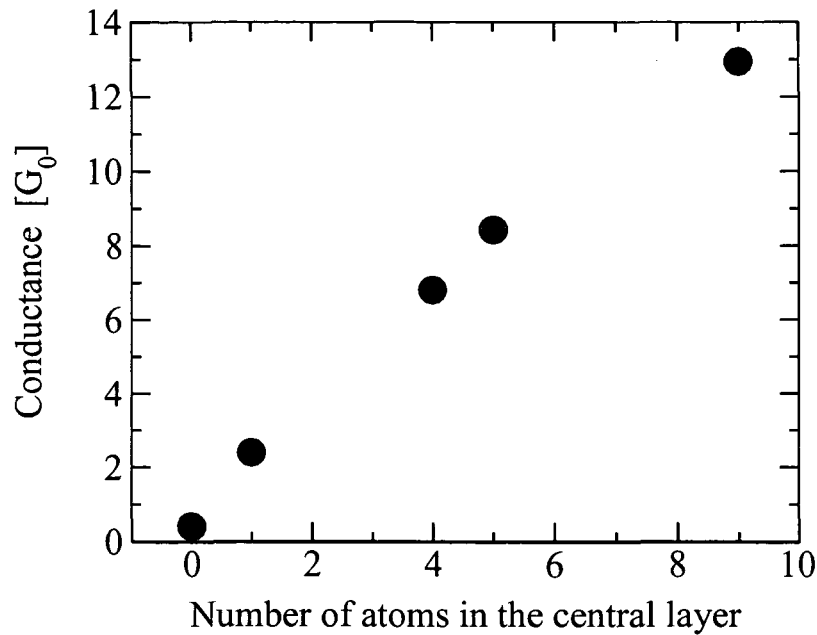

Figure 9.7: Conductance versus the number of Au atoms in the central layer for the Au contacts described in Table 9.1.

9.2 Gold contact with an impurity

In recent break junction experiments [29] remarkable changes of the conductance histograms of nanocontacts formed by AuPd alloys have been observed when varying the Pd concentration. Studying the effect of impurities placed into the nanocontact are, in that context, at least relevant for dilute alloys. The interesting question is whether the presence of impurities can be observed in the measured conductance. For that reason we investigated transition metal impurities such as Pd, Fe, and Co placed at various positions of the point contact as shown in Fig. 9.3a. For the notation of the impurity positions see Fig. 9.8.

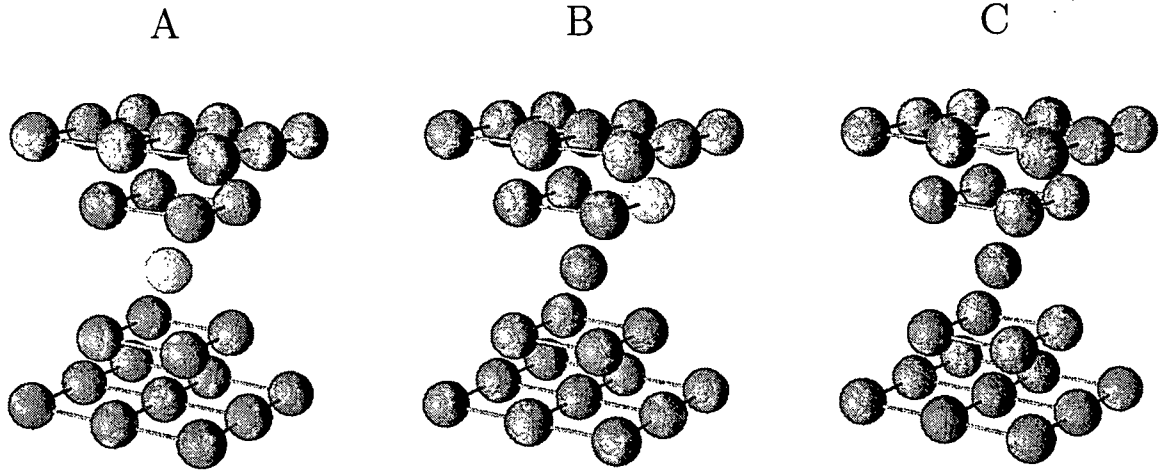A   B   C

Figure 9.8: Impurity positions (light grey spheres) in a Au point contact, see Fig. 9.3a.

The calculated spin and orbital moments of the magnetic impurities are listed in Table 9.2. They were calculated with assuming the direction of magnetization to be parallel to the z axis ($\widehat{\mathbf{M}} = \hat{z}$), i.e., normal to the planes. Additional calculations of the magnetic anisotropy energy confirmed this choice. As usual for magnetic impurities with reduced coordination number [26], both for Fe and Co remarkably high spin moments, and in all positions of a Co impurity large orbital moments were obtained, see also Section 8.1. In particular, the magnitude of the orbital moments is very sensitive to the position of the impurity. This is most obvious in case of Fe, where at positions B and C the orbital moment is relatively small, but at position A a surprisingly high value of 0.47 μ_B was obtained.

position	$S_z[\mu_B]$		$L_z[\mu_B]$	
	Fe	Co	Fe	Co
A	3.36	2.01	0.47	0.38
B	3.46	2.17	0.04	0.61
C	3.42	2.14	0.07	0.22

Table 9.2: Calculated spin and orbital moments of magnetic impurities placed at different positions in a Au point contact, see Fig. 9.8. $\widehat{\mathbf{M}} = \hat{z}$.

The summation over 116 atoms from each of the first two full layers ($p = C - 3$, $q = C + 3$) in Eq. (4.36) has been carried out in order to evaluate the conductance. The calculated values are summarized in Table 9.3.

impurity	Conductance [G_0]		
position	Pd	Fe	Co
A	2.22	2.67	2.97
B	2.24	2.40	2.26
C	2.36	1.95	1.75
pure Au	2.40		

Table 9.3: Calculated conductances of a Au point contact with impurities on different positions, see Fig. 9.8.

A Pd impurity (independent of position) reduces only little the conductance as compared to a pure Au point contact. This qualitatively can be understood from the local density of states (LDOS) of the Pd impurity {calculated by using an imaginary part of the energy of $\delta = 1$ mRy and the real space SPO was obtained by taking 1830 $k_\parallel$ points in the 2D IBZ, see Eq. (2.96)}. The LDOS of site i (n_i) can be calculated by using Eq. (2.21) and integrating over the ith unit cell Ω_i,

$$n_i(\varepsilon) = \mp \frac{1}{\pi} \int_{\Omega_i} d^3 r \, Im \left[G^{\pm}(\varepsilon, \mathbf{r}, \mathbf{r}) \right]. \tag{9.1}$$

In Fig. 9.9 the corresponding LDOS at positions A and C is plotted. Clearly, the change of the coordination number (8 at position A and 12 at position C), i.e., different hybridization between the Pd and Au d bands, results into different widths for the Pd d-like LDOS. In both cases, however, the Pd d states are completely filled and no remarkable change in the LDOS at Fermi level (conducting states) happens.

The case of the magnetic impurities seems to be more interesting. As can be inferred from Table 9.3, impurities at position B change only a little the conductance. Being placed at position A, however, Fe and Co atoms increase the conductance by 11 % and 24 %, while at position C they decrease the conductance by 19 % and 27 %, respectively. In Ref.[38] it was found that single Fe, Co (and also Ni) defects in a 2×2 infinite Cu wire decreased the conductance. By analyzing the DOS it was
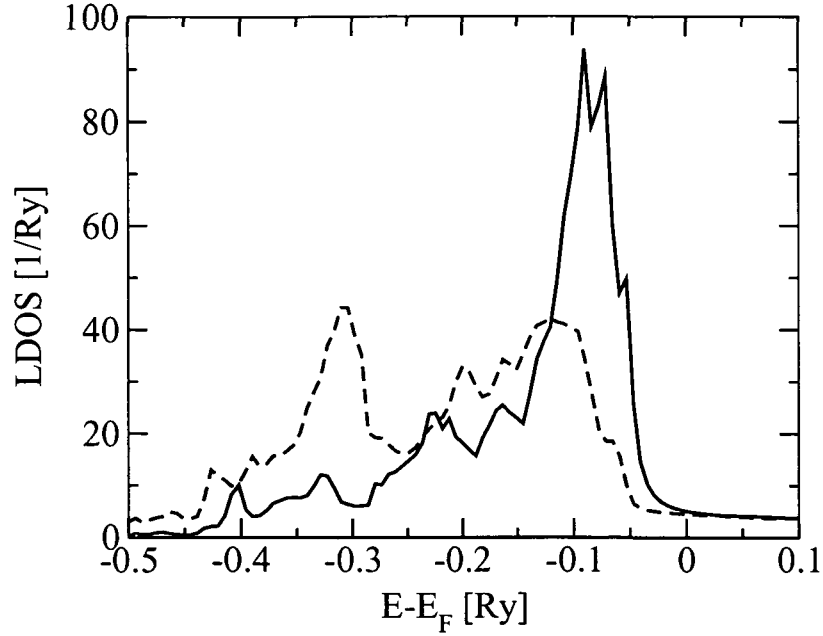
Figure 9.9: Local density of states of a Pd impurity in position A (solid line) and in position C (dashed line) of a Au point contact, see Fig. 9.8.

concluded that the observed reduction of the conductance is due to a depletion of the s states in the minority band. The above situation is very similar to the case of an Fe or Co impurity in position C of the point contact considered, even the calculated drop of the conductance ($\sim$ -20 % for Fe and $\sim$ -28 % for Co) agrees quantitatively well with our present result. Our result, namely, that Fe and Co impurities at position A increase the conductance can, however, not be related to the results of Ref.[38]. In order to understand this feature we have to carefully investigate the LDOS calculated for the point contact.

In Fig. 9.10 the minority d-like LDOS of the Fe and Co impurities in positions A and C are plotted as resolved according to the canonical orbitals $d_{x^2-y^2}$, d_{xy}, $d_{xz,}$, d_{xy} and $d_{3z^2-r^2}$. We have to stress that this kind of partial decomposition, usually referred to as the (ℓ, m, s) representation of the LDOS, is not unique within a relativistic formalism, since due to the spin-orbit interaction the different spin- and orbital components are mixed. However, due to the large spin-splitting of Fe and Co the mixing of the majority and minority spin-states can be neglected.

As can be seen from Fig. 9.10, the LDOS of an impurity in position A is much narrower than in position C. This is an obvious consequence of the difference in the coordination numbers (8 for position A and 12 for positions C). Thus an impurity in position A hybridizes less with the neighboring Au atoms and, as implied by the LDOS, the corresponding d states are fairly localized. Also to be seen is a spin-orbit induced splitting of about 8 mRy (~ 0.1 eV) in the very narrow $d_{x^2-y^2}$-d_{xy} states of the impurities in position A. The difference of the band filling for the two kind of impurities shows up in a clear downward shift of the LDOS of Co with respect to that of Fe.
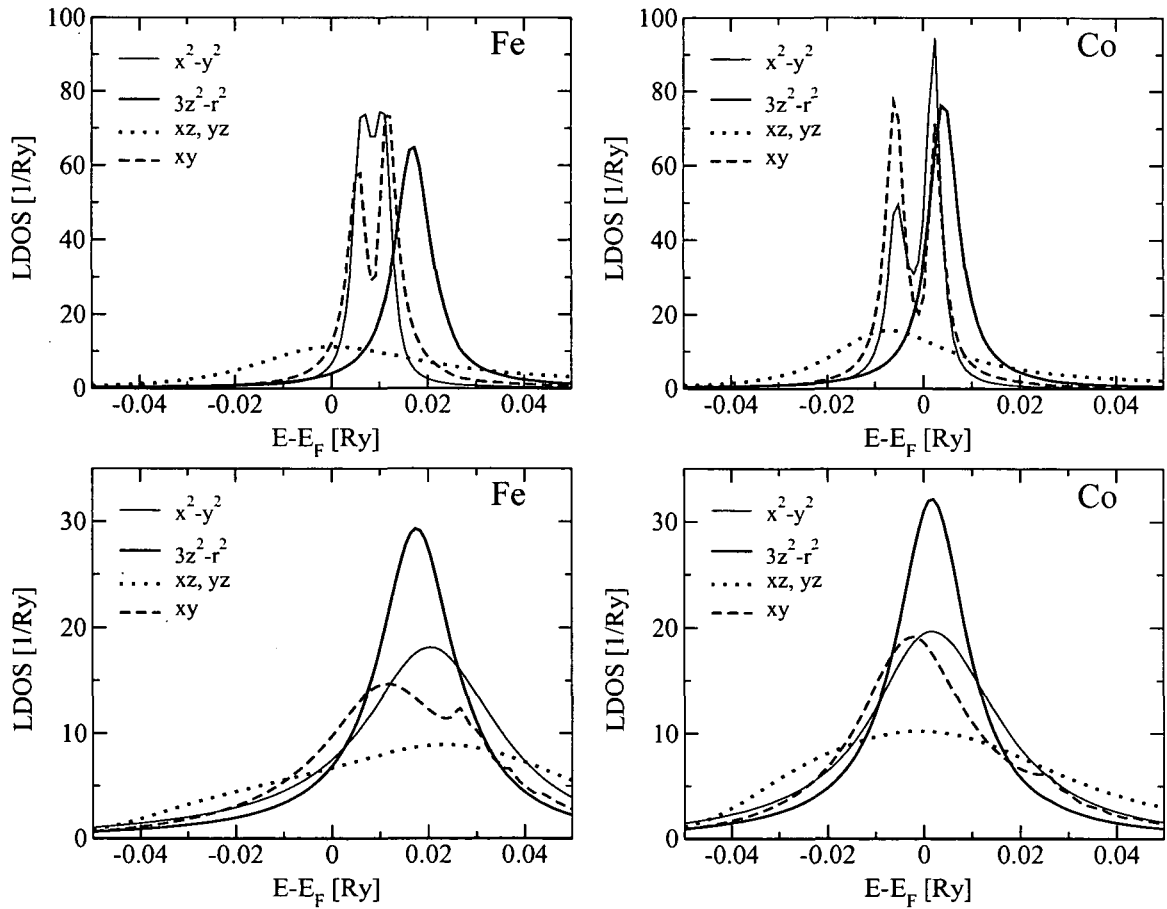

Figure 9.10: Minority-spin orbital-resolved d-like local density of states of Fe and Co impurities in position A (upper panels) and in position C (lower panels) of a Au point contact, see Fig. 9.8.

In Fig. 9.11 the difference between non-relativistic and relativistic calculations are seen. The splitting in the $d_{x^2-y^2}$ and d_{xy} states vanishes by turning off the spin-orbit coupling. Furthermore, the very narrow states can be better observed as well as a 2-1-1-1 splitting of the orbitals is detected which is due to the reduced crystal field symmetry (C_{4v}) of the Co atom in position A. This kind of splitting in the non-relativistic case is in full conformity with group theoretical forecasts [58].
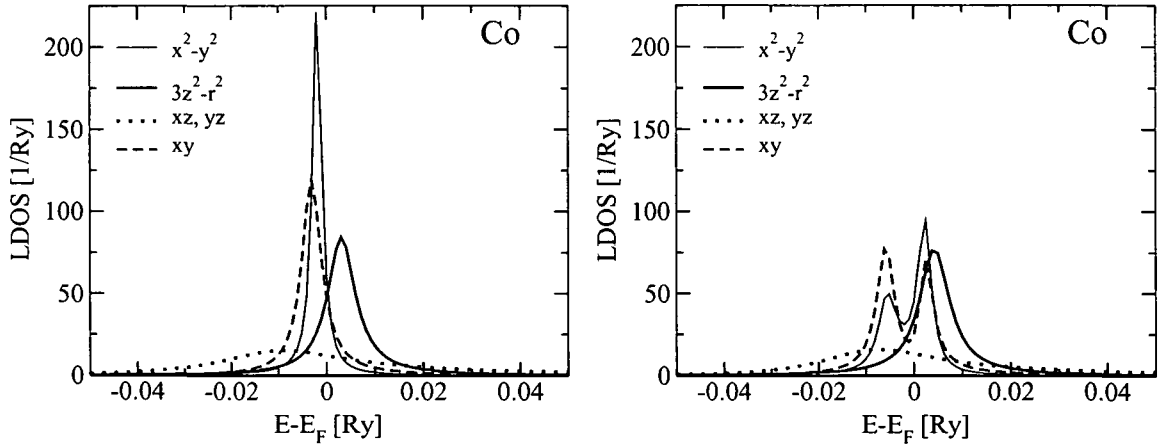

Figure 9.11: Minority-spin orbital-resolved d-like local density of states of a Co impurity in position A, see Fig. 9.8. On the left non-relativistic, on the right relativistic calculations are seen.

In explaining the change of the conductance through the point contact caused by the impurities in positions A and C, the s-like DOS at the center site, i.e., at the narrowest section of the contact, is plotted in the top half of Fig. 9.12. As a comparison the corresponding very flat s-like DOS is shown for a pure Au contact. For contacts with impurities this s-like DOS shows a very interesting shape which can indeed be correlated with the corresponding $d_{3z^2-r^2}$-like DOS at the impurity site, see bottom half of Fig. 9.12. Clearly, the center positions and the widths of the $d_{3z^2-r^2}$-like DOS peaks and those of the respective (anti-)resonant s-like DOS shapes coincide well with each other. This kind of behavior in the DOS resembles to the case studied by Fano for a continuum band and a discrete energy level in the presence of configuration interaction (hybridization) [79]. Apparently, by keeping this analogy, in the point contact the s-like states play the role of a continuum and the $d_{3z^2-r^2}$-like state of the impurity acts as the discrete energy level. Since the

two kinds of states share the same cylindrical symmetry, interactions between them
can occur due to backscattering effects. It should be noted that similar resonant
line-shapes in the STM I-V characteristics have been observed for Kondo impurities
at surfaces [80, 81] and explained theoretically [82].

Inspecting Fig. 9.12, the enhanced s-like DOS at the Fermi level at the center of the
point contact provides a nice interpretation to the enhancement of the conductance
when the Fe and Co impurity is placed at position A. As the peak position of the
$d_{3z^2-r^2}$-like states of Fe is shifted upwards by more than 0.01 Ry with respect to
that of Co, the corresponding resonance of the s-like states is also shifted and the
s-like DOS at the Fermi level is decreased. This is also in agreement with the
calculated conductances. In the case of impurities at position C, i.e., in a position
by $a_{3D} = 7.681$ $a.u.$ away from the center of the contact, the resonant line-shape
of the s-like states is reversed in sign, therefore, we observe a decreased s-like DOS
at the Fermi level, explaining in this case the decreased conductance, see Table 9.3.
Since, however, the s-like DOS for the case of a Co impurity is larger than for an Fe
impurity, this simple picture cannot account correctly for the opposite relationship
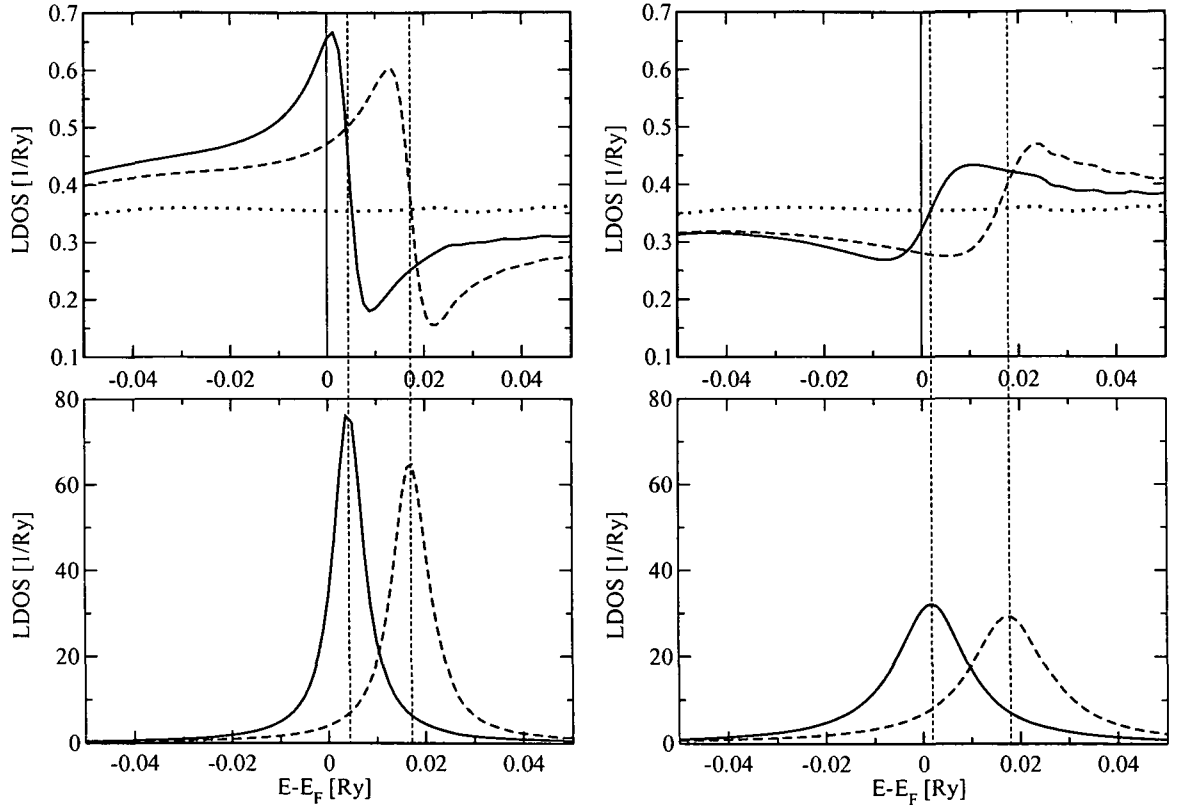we obtained for the corresponding conductances.

Figure 9.12: Top left: minority-spin s-like local density of states at the center site of a Au point contact with an impurity at position A, see Fig. 9.8 (solid line: Co, dashed line: Fe). Top right: the same as before, but with an impuritiy at position C. As a comparison, in both figures the corresponding LDOS for the pure Au contact is plotted by dotted lines. The solid vertical lines highlight the position of the Fermi energy. Bottom: minority-spin $d_{3z^2-r^2}$ local density of states of the impurities (solid line: Co, dashed line: Fe) at positions A (left) and C (right). Vertical dashed lines mark the center positions of the $d_{3z^2-r^2}$-LDOS peaks.

Chapter 10

Conclusions

In Chapter 7, by using the Kubo-Greenwood formula within the fully relativistic spin-polarized Screened KKR-CPA method for disordered layered systems ab-initio calculations of the residual resistivities and anisotropic magnetoresistance ratios of bulk fcc $Ni_{1-c}Fe_c$ alloys in the Ni-rich regime were performed. Resistivities in satisfactory agreement with experiments were obtained. The differences relative to the measured data most likely have to be attributed to the missing vertex corrections within the single-site CPA and/or to additional scattering effects due to imperfections present in the experimental samples. Quite surprisingly, practically in the entire concentration range under consideration, the calculated AMR ratios were found in excellent quantitative agreement with the measurements, indicating that an accurate computational scheme, which includes spin-polarization and relativity on the same level, can indeed account for magnetoresistive effects of alloys with high precision. In addition to the AMR ratios, for two permalloy systems, namely, for $Ni_{0.80}Fe_{0.20}$ and $Ni_{0.85}Fe_{0.15}$, the dependence of the resistivity on the angle between the current and the magnetization was calculated. The results fit well the general phenomenological expression given by Döring for the resistivity of saturated ferromagnetic cubic crystals.

Corresponding to the main topic of this work, a real space method is presented and has been implemented which uses a real-space embedding technique within the KKR Green's function method and the CPA and which is combined with the real-space Kubo-Greenwood formula in order to describe electric transport in nanostructures. In Chapter 6 the reliability of the presented real space method was checked. It can

be stated that the method works well in "large cluster" limit. Good convergence to the surface resistivity was achieved for Ag(001) surface layer by increasing the size of planar clusters, and quite reliable bulk resistivities were obtained in the case of substitutionally disordered binary alloys (CuPt), while the resistivity of pure Ag(001) bulk was calculated with an absolute error of roughly 0.05 $\mu\Omega cm$.

In Chapter 8 in-plane transport properties of the surface layer of Ag(001) were investigated by embedding single impurities and finite chains (length of 2-10 atoms) of Fe and Co along the (110) direction (x) into the surface layer. By defining a "residual resistivity" for finite clusters it was obtained that chains made of Co have less resistivity than those made of Fe. Moreover, by studying the influence of the direction of magnetization on the resistivity, it was found that in most cases the magnetization parallel to the orientation of the chains ($\widehat{\mathbf{M}} = \hat{x}$) provides the least resistivity, while there is not much difference between resistivities calculated with magnetization perpendicular to the chains $\widehat{\mathbf{M}} = \hat{y}$ and $\widehat{\mathbf{M}} = \hat{z}$.

In Chapter 9 the conductance of gold nanocontacts was studied depending on the contact geometry and transition metal impurities placed at various positions. Several numerical tests were performed that proved the efficiency of our method. In good agreement with experiments and other calculations a conductance of 1.1 G_0 was obtained for a finite linear chain connecting two semi-infinite Au leads. The calculated conductance for a thicker 2×2 wire, 2.58 G_0, can be related to a recent result for an infinite 2×2 chain (3 G_0) [38]. Also in agreement with quantum mechanical model calculations [78] a nearly linear dependence of the conductance was found on the "thickness" of the contact. By embedding magnetic transition metal impurities into a point contact both enhancement and reduction of the conductance was found depending on the position of the impurities. On analyzing the local density of states we concluded that the effect of the impurity is mainly controlled by the interaction of the minority d-like and s-like states giving rise to a resonant line-shape (Fano-resonance) in the s-like DOS at the center of contact. We suggest that this line-shape should also be observed in $I - V$ conductance characteristics providing thus an "experimental" tool to detect magnetic impurities (even their position) in a noble metal point contact.

Appendix A

Density Functional Theory

Density Functional Theory (DFT) has the main purpose to investigate ground-state properties of a system of interacting electrons which is shortly discussed in this Appendix.

A.1   The Hohenberg-Kohn theorems

Let us consider an N-electron system in a solid (N is fixed). The Hamilton operator of the electrons within the Born-Oppenheimer approximation can be written as

$$\hat{H} = \hat{T} + \hat{U} + \hat{W} = -\frac{\hbar^2}{2m} \sum_{i=1}^{N} \boldsymbol{\nabla}_i^2 + \sum_{i=1}^{N} u(\mathbf{r}_i) + \frac{1}{2} \sum_{i \neq j} w(\mathbf{r}_i - \mathbf{r}_j), \qquad \text{(A.1)}$$

where m is the electron mass, $\hat{T}$ corresponds to the kinetic energy operator, $\hat{U}$ is the external potential containing the electrostatic potential between the electrons and nuclei, and $\hat{W}$ contains the potentials of the electron-electron interaction of form

$$w(\mathbf{r}_i - \mathbf{r}_j) = \frac{1}{4\pi\varepsilon_0} \cdot \frac{e^2}{|\mathbf{r}_i - \mathbf{r}_j|} . \qquad \text{(A.2)}$$

Let the wavefunctions, $\Psi(\mathbf{r}_1, \mathbf{r}_2, \ldots, \mathbf{r}_N)$ denote the coordinate representations of N-electron states, which are antisymmetric against the permutation of their variables (Pauli's exclusion principle). The density of electrons is defined with wavefunctions as

$$n(\mathbf{r}) = \sum_{\sigma, \sigma_2, \ldots, \sigma_N} \int d^3 r_2 \cdots \int d^3 r_N \cdot |\Psi(\mathbf{r}, \sigma; \mathbf{r}_2, \sigma_2; \ldots; \mathbf{r}_N, \sigma_N)|^2 . \qquad \text{(A.3)}$$

Let us define the so-called class of pure-state *v-representable densities* [83] as

$\mathcal{A}_N = \{n(\mathbf{r}) \mid n$ comes from an N-particle ground-state$\}$.

We can define the class of the proper potentials as well as

$\mathcal{U}_N = \{u(\mathbf{r}) \mid u \in \mathcal{L}^p$ for some p, p$=\infty$ is also allowed, $\hat{H}[u]$ has a ground-state$\}$.

Assuming a fixed form of the interaction operator, $\hat{W}$ as $w(\mathbf{r})$ defined in Eq. (A.2), $\hat{H}$ can be regarded as a function of $u(\mathbf{r})$ like $\hat{H} = \hat{H}[u(\mathbf{r})]$. The ground-state energy can be defined as the lowest expectation value of $\hat{H}$ as

$$E_0[u(\mathbf{r})] = \inf_{\Psi} \left\langle \Psi \left| \hat{H}[u(\mathbf{r})] \right| \Psi \right\rangle, \qquad (A.4)$$

where $|\Psi\rangle$-s are N-electron states with finite kinetic energy. Let $|\Psi_0[u(\mathbf{r})]\rangle$ denote the ground-state of a Hamiltonian with $u(\mathbf{r})$ as

$$\hat{H}[u(\mathbf{r})]|\Psi_0[u(\mathbf{r})]\rangle = E_0[u(\mathbf{r})] |\Psi_0[u(\mathbf{r})]\rangle. \qquad (A.5)$$

We will call two potentials, $u_1(\mathbf{r})$ and $u_2(\mathbf{r})$ physically different from each other if they obey $u_1(\mathbf{r}) - u_2(\mathbf{r}) \neq const.$ in the whole real space. If they differ only in a constant the corresponding ground-states will be the same. Let us now list the Hohenberg-Kohn theorems [84],

Theorem 1: The external potential $u(\mathbf{r})$ is a unique function of the ground-state density $n_0(\mathbf{r})$ apart from a trivial constant. In other words, for a given $n(\mathbf{r})$ there is only one $u(\mathbf{r})$ for which $n(\mathbf{r})$ is the ground-state density.

Theorem 2: The total energy, E is a unique function of $n(\mathbf{r})$ and the exact ground-state electron density $n_0(\mathbf{r})$ minimizes the functional $E[n(\mathbf{r})]$ like $E_0 = E[n_0(\mathbf{r})]$.

Theorem 3: The ground-state expectation value of any observable is a unique function of the exact ground-state electron density $n_0(\mathbf{r})$.

These theorems can be proved by reductio ad absurdum. The so-called Hohenberg-Kohn density functional as the functional Legendre-transformation of the ground-state energy in Eq. (A.4) is defined as

$$F_{HK}[n] = E_0[u[n]] - \int d^3r \cdot u[n(\mathbf{r})]n(\mathbf{r}). \qquad (A.6)$$

Using this functional the ground-state energy can be expressed as

$$E_0[u] = \min_n \left\{ F_{HK}[n] + \int d^3r \cdot u(\mathbf{r})n(\mathbf{r}) \right\}, \qquad (A.7)$$

which, together with the Hohenberg-Kohn theorems follows that the ground-state energy can be written as a functional of the ground-state density, $n_0(\mathbf{r})$ instead of the external potential $u(\mathbf{r})$. There are problems remained, namely neither the classes $\mathcal{U}_N$ and $\mathcal{A}_N$ nor the functional $F_{HK}[n]$ are known explicitly.

A.2 The Kohn-Sham equation

The main trick that Kohn and Sham [85] introduced into DFT is that the ground-state density of an interacting system can be identified as the ground-state density of a non-interacting system with an effective one-particle potential, $u^s(\mathbf{r})$. If this potential is found, only a one-particle problem has to be solved.

In the Kohn-Sham theory the ground-state of an electron (or more generally a fermion) system is written as a Slater determinant of the lowest N one-particle solutions, $\phi_i(\mathbf{r})$ of the Schrödinger equation with total potential $u^s(\mathbf{r})$, as

$$\Psi_0^s(\mathbf{r}_1, \mathbf{r}_2, \ldots, \mathbf{r}_N) = \frac{1}{\sqrt{N!}} \det[\phi_i(\mathbf{r}_k)], \tag{A.8}$$

which implies the form of the electron density,

$$n^s(\mathbf{r}) = \sum_{i=1}^{N} \phi_i^*(\mathbf{r})\phi_i(\mathbf{r}) \tag{A.9}$$

and the kinetic energy,

$$T^s = -\frac{\hbar^2}{2m} \sum_{i=1}^{N} \left\langle \phi_i \left| \boldsymbol{\nabla}^2 \right| \phi_i \right\rangle. \tag{A.10}$$

The Hohenberg-Kohn functional of a non-interacting system ($w(\mathbf{r}) \equiv 0$) is the kinetic energy in the ground-state which is in turn a functional of the ground-state density,

$$T^s[n] = E_0^s[u^s[n]] - \int d^3r \cdot u^s[n(\mathbf{r})]n(\mathbf{r}). \tag{A.11}$$

Even this functional is not explicitly known, but its existence is guaranteed by the Hohenberg-Kohn theorems. We can write the variation of any functional of n with respect to ϕ_i^* according to Eq. (A.9) as

$$\frac{\delta}{\delta\phi_i^*(\mathbf{r})} = \int d^3r' \frac{\delta n(\mathbf{r}')}{\delta\phi_i^*(\mathbf{r})} \frac{\delta}{\delta n(\mathbf{r}')} = \phi_i(\mathbf{r})\frac{\delta}{\delta n(\mathbf{r})}, \tag{A.12}$$

therefore, the variation of T^s in Eq. (A.10) with respect to ϕ_i^* may be compared to that of in Eq. (A.11) and can be written as

$$-\frac{\hbar^2}{2m}\boldsymbol{\nabla}^2\phi_i(\mathbf{r}) = \frac{\delta T^s[n]}{\delta \phi_i^*(\mathbf{r})} = \frac{\delta T^s[n]}{\delta n(\mathbf{r})}\phi_i(\mathbf{r}). \qquad (A.13)$$

If we calculate the variation of $E_0^s[n]$ in Eq. (A.11) with respect to ϕ_i^* we obtain

$$\frac{\delta}{\delta n(\mathbf{r})}\left[T^s[n] + \int d^3r'n(\mathbf{r}')u(\mathbf{r}') - \varepsilon_i\left(\int d^3r'n(\mathbf{r}') - N\right)\right]\phi_i(\mathbf{r}) =$$

$$= \left(-\frac{\hbar^2}{2m}\boldsymbol{\nabla}^2 + u(\mathbf{r}) - \varepsilon_i\right)\phi_i(\mathbf{r}) = 0 , \qquad (A.14)$$

where we introduced Lagrange multipliers, ε_i in order to take into account the constraint of a fixed number of particles, N. If we calculate the expression

$$\int d^3r\phi_i^*(\mathbf{r})\left(-\frac{\hbar^2}{2m}\boldsymbol{\nabla}^2 + u(\mathbf{r}) - \varepsilon_i\right)\phi_i(\mathbf{r}) = 0, \qquad (A.15)$$

we get the ground-state energy of the non-interacting system,

$$E_0^s[u] = \sum_{i=1}^{N}\varepsilon_i , \qquad (A.16)$$

where the summation is over the lowest N eigenvalues. In the interacting case $(w(\mathbf{r}) \neq 0)$ we can decompose the Hohenberg-Kohn functional as

$$F_{HK}[n] = T^s[n] + E_H[n] + E_{xc}[n] \qquad (A.17)$$

with defining the Hartree energy as

$$E_H[n] = \frac{e^2}{8\pi\varepsilon_0}\int d^3r \int d^3r'\frac{n(\mathbf{r})n(\mathbf{r}')}{|\mathbf{r} - \mathbf{r}'|} \qquad (A.18)$$

and the exchange-correlation energy as

$$E_{xc}[n] = F_{HK}[n] - T^s[n] - E_H[n]. \qquad (A.19)$$

Inserting Eq. (A.17) into (A.7) and similar to the non-interacting case, taking the variation with respect to $\phi_i^*(\mathbf{r})$ we get the Kohn-Sham equation,

$$\left(-\frac{\hbar^2}{2m}\boldsymbol{\nabla}^2 + u_{eff}(\mathbf{r})\right)\phi_i(\mathbf{r}) = \varepsilon_i\phi_i(\mathbf{r}) \qquad (A.20)$$

with the effective potential, $u_{eff}(\mathbf{r}) = u(\mathbf{r}) + u_H(\mathbf{r}) + u_{xc}(\mathbf{r})$, where $u(\mathbf{r})$ means the external potential, the Hartree potential is given by

$$u_H(\mathbf{r}) = \frac{\delta E_H[n]}{\delta n(\mathbf{r})} = \frac{e^2}{4\pi\varepsilon_0} \int d^3r' \frac{n(\mathbf{r}')}{|\mathbf{r} - \mathbf{r}'|} \qquad (A.21)$$

and the exchange-correlation potential is defined as

$$u_{xc}(\mathbf{r}) = \frac{\delta E_{xc}[n]}{\delta n(\mathbf{r})} . \qquad (A.22)$$

The exact form of E_{xc} is not known thus some kind of approximations are needed. The uniform electron gas problem resulted the so-called Local Density Approximation (LDA), which was, in the mostly used form, elaborated by Gunnarson and Lundqvist [86]. Despite the fact that LDA is exact only for uniform densities, it works quite well for calculating ground-state properties of atoms, molecules and solids. The exchange-correlation energy and the exchange-correlation potential within LDA can be written as

$$E_{xc}[n] \approx \int d^3r \cdot \varepsilon_{xc}[n(\mathbf{r})]n(\mathbf{r}) \qquad (A.23)$$

and

$$u_{xc}(\mathbf{r}) = \varepsilon_{xc}[n(\mathbf{r})] + \frac{d\varepsilon_{xc}[n(\mathbf{r})]}{dn(\mathbf{r})}n(\mathbf{r}), \qquad (A.24)$$

respectively, where $\varepsilon_{xc}[n(\mathbf{r})]$ is the density of the exchange-correlation energy of a uniform electron gas with density of $n(\mathbf{r})$.

Having an assumption of the form of u_{xc} or ε_{xc}, the Kohn-Sham equation has to be solved and as second step $n(\mathbf{r})$ from the wavefunctions as well as $u_H(\mathbf{r})$ and $u_{xc}(\mathbf{r})$ can be recalculated. Repeating this procedure successively a self-consistent solution to the ground-state of the interacting system is obtained.

A.3 The Kohn-Sham-Dirac equation

A relativistic generalization of DFT is needed in order to be able to treat magnetic systems in a non-perturbative way. The Dirac-Hamiltonian can be written in presence of an external magnetic field as

$$\hat{H} = -ic\hat{\alpha} \cdot \nabla + \hat{\beta}mc^2 - ec\hat{\beta}\gamma_\mu A^\mu , \qquad (A.25)$$

where A^μ (μ=0,1,2,3) is the vector potential, c is the velocity of light and $\hat{\boldsymbol{\alpha}}$, $\hat{\beta}$, γ_μ are the common Dirac matrices,

$$\hat{\alpha}_i = \begin{pmatrix} 0 & \hat{\sigma}_i \\ \hat{\sigma}_i & 0 \end{pmatrix}, \quad \gamma_i = -i\gamma_0\hat{\alpha}_i, \quad (i=1,2,3); \quad \gamma_0 = \hat{\beta} = \begin{pmatrix} I_2 & 0 \\ 0 & -I_2 \end{pmatrix}; \quad I_2 = \begin{pmatrix} 1 & 0 \\ 0 & 1 \end{pmatrix}.$$

The Pauli matrices are $\hat{\sigma}_1 = \begin{pmatrix} 0 & 1 \\ 1 & 0 \end{pmatrix}$, $\hat{\sigma}_2 = \begin{pmatrix} 0 & -i \\ i & 0 \end{pmatrix}$, $\hat{\sigma}_3 = \begin{pmatrix} 1 & 0 \\ 0 & -1 \end{pmatrix}$. (A.26)

It should be noted that in this Section no special units will be used because of the simplicity of the formulas.

Let us now briefly present the Current Density Functional Theory (CDFT), first described by Rajagopal and Callaway [87, 88] and later by MacDonald and Vosko [89] as well as by Vignale and Rasolt [90, 91]. In CDFT new variables are introduced, namely the four-current, $J^\mu = \bar{\psi}(\mathbf{r})\gamma^\mu\psi(\mathbf{r})$, where $\bar{\psi}$ denotes $\psi^+\hat{\beta}$, and the four-density, $(n(\mathbf{r}), \mathbf{M}(\mathbf{r}))$, where the magnetization density is defined by

$$-e\mathbf{J}(\mathbf{r}) = \boldsymbol{\nabla} \times \mathbf{M}(\mathbf{r}) \tag{A.27}$$

with $\mathbf{J}(\mathbf{r})$ being the three-current density, in stationary states of form

$$\mathbf{J}(\mathbf{r}) = \frac{1}{2m}\boldsymbol{\nabla} \times (\mathbf{L}(\mathbf{r}) + 2\mathbf{S}(\mathbf{r})). \tag{A.28}$$

Here $\mathbf{L}(\mathbf{r})$ is the so-called angular momentum density,

$$\boldsymbol{\nabla} \times \mathbf{L}(\mathbf{r}) = \bar{\psi}(\mathbf{r})\left(-i\overleftarrow{\nabla} + i\overrightarrow{\nabla} + 2e\mathbf{A}(\mathbf{r})\right)\psi(\mathbf{r}) \tag{A.29}$$

and $\mathbf{S}(\mathbf{r})$ the spin density,

$$\mathbf{S}(\mathbf{r}) = \frac{1}{2}\bar{\psi}(\mathbf{r})\boldsymbol{\Sigma}\psi(\mathbf{r}) \quad \text{with} \quad \boldsymbol{\Sigma} = \begin{pmatrix} \hat{\sigma} & 0 \\ 0 & \hat{\sigma} \end{pmatrix}. \tag{A.30}$$

It is important to mention that for a homogeneous electron gas the angular momentum density is zero, which, in turn results the total neglection of inter-orbital current-current interactions within LDA. The Kohn-Sham-Dirac equation can be derived by varying the total energy functional with respect to $\bar{\psi}(\mathbf{r})$ and

$$\left[-ic\hat{\boldsymbol{\alpha}} \cdot \boldsymbol{\nabla} + \hat{\beta}mc^2 + u_{ext}(\mathbf{r}) + u_{xc}(\mathbf{r}) + \frac{e\mu_0}{2m}\boldsymbol{\Sigma}(\mathbf{B}_{ext}(\mathbf{r}) + \mathbf{B}_{xc}(\mathbf{r}))\right]\psi_k(\mathbf{r}) = \varepsilon_k\psi_k(\mathbf{r}) \tag{A.31}$$

is obtained, where the exchange-correlation field is defined by

$$\mu_0 \mathbf{B}_{xc}(\mathbf{r}) = \frac{\delta E_{xc}}{\delta S(\mathbf{r})} .$$

(A.32)

Local Spin(-polarized) Density Approximation (LSDA) was elaborated by Vosko et al. [72] and MacDonald et al. [92] in order to approximate $\mathbf{B}_{xc}(\mathbf{r})$. In this approach the independent variables are the spin-projected densities, $n_\uparrow$ and $n_\downarrow$, with them $n(\mathbf{r}) = n_\uparrow(\mathbf{r}) + n_\downarrow(\mathbf{r})$ and $S(\mathbf{r}) = n_\uparrow(\mathbf{r}) - n_\downarrow(\mathbf{r})$ can be easily defined. For collinear spin structures with spin quantization axis pointing along the z-axis, $\mathbf{B}_{xc}$ can be expressed as

$$\frac{e\mu_0}{m} \mathbf{B}_{xc}(n_\uparrow(\mathbf{r}), n_\downarrow(\mathbf{r})) = [u_{xc,\uparrow}(n_\uparrow(\mathbf{r}), n_\downarrow(\mathbf{r})) - u_{xc,\downarrow}(n_\uparrow(\mathbf{r}), n_\downarrow(\mathbf{r}))]\, \mathbf{e}_z .$$

(A.33)

Appendix B

Kubo formalism

In this Appendix, some derivations of equations and proofs of formulas taken from Section 1.3 are presented.

Proof of Kubo's identity, Eq. (1.51):

$$\hat{\varrho} \int_0^\beta d\lambda \, \dot{\hat{X}}_H(t - i\lambda\hbar) = -\frac{i}{\hbar}\hat{\varrho} \int_0^\beta d\lambda \left[e^{\lambda\hat{H}} \hat{X}_H(t) e^{-\lambda\hat{H}}, \hat{H} \right] = \frac{i}{\hbar}\hat{\varrho} \int_0^\beta d\lambda \, \frac{d}{d\lambda}\left(e^{\lambda\hat{H}} \hat{X}_H(t) e^{-\lambda\hat{H}} \right)$$

$$= \frac{i}{\hbar}\left(\underbrace{\hat{\varrho}\, e^{\beta\hat{H}} \hat{X}_H(t) e^{-\beta\hat{H}}}_{\hat{X}_H(t)\hat{\varrho}} - \hat{\rho}\hat{X}_H(t) \right) = \frac{i}{\hbar}\left[\hat{X}_H(t), \hat{\varrho} \right] \ .$$

Derivation of the Kubo formula, Eq. (1.52):

$$Tr\left(\hat{\varrho}_0 \, \dot{\hat{H}}'_H(t' - i\lambda\hbar) \hat{A}_H(t) \right) = Tr\left(\hat{\varrho}_0 \, e^{\frac{i}{\hbar}(t' - i\lambda\hbar)\hat{\mathcal{H}}_0} \, \dot{\hat{H}}'(t') \, e^{-\frac{i}{\hbar}(t' - i\lambda\hbar)\hat{\mathcal{H}}_0} \hat{A}_H(t) \right)$$

$$= Tr\left(\hat{\varrho}_0 \, \dot{\hat{H}}'(t') \, e^{-\frac{i}{\hbar}(t' - i\lambda\hbar)\hat{\mathcal{H}}_0} \, \hat{A}_H(t) \, e^{\frac{i}{\hbar}(t' - i\lambda\hbar)\hat{\mathcal{H}}_0} \right) = Tr\left(\hat{\varrho}_0 \, \dot{\hat{H}}'(t') \, \hat{A}_H(t - t' + i\lambda\hbar) \right) \ .$$

Derivation of Eq. (1.63) starting from Eq. (1.61):

$$\int_0^\beta d\lambda \, Tr\left(\hat{\varrho}_0 \, \hat{J}_\nu(-\mathbf{q}, 0)\hat{J}_\mu(\mathbf{q}, t + i\lambda\hbar) \right) = \int_0^\beta d\lambda \frac{1}{\mathcal{Z}} Tr\left(e^{-\beta\hat{\mathcal{H}}_0} \, \hat{J}_\nu(-\mathbf{q}, 0) \, e^{-\lambda\hat{\mathcal{H}}_0} \, \hat{J}_\mu(\mathbf{q}, t)e^{\lambda\hat{\mathcal{H}}_0} \right)$$

$$= \int_0^\beta d\lambda \frac{1}{\mathcal{Z}} Tr\left(e^{-\lambda\hat{\mathcal{H}}_0} \, \hat{J}_\mu(\mathbf{q}, t) \, e^{(\lambda - \beta)\hat{\mathcal{H}}_0} \, \hat{J}_\nu(-\mathbf{q}, 0) \right)$$

$$= \int_0^\beta d\lambda \, Tr \left(\hat{\varrho}_0 \, e^{(\beta-\lambda)\hat{\mathcal{H}}_0} \, \hat{J}_\mu(\mathbf{q},t) \, e^{(\lambda-\beta)\hat{\mathcal{H}}_0} \, \hat{J}_\nu(-\mathbf{q},0) \right)$$

$$= \int_0^\beta d\lambda \, Tr \left(\hat{\varrho}_0 \, e^{\lambda\hat{\mathcal{H}}_0} \, \hat{J}_\mu(\mathbf{q},t) \, e^{-\lambda\hat{\mathcal{H}}_0} \, \hat{J}_\nu(-\mathbf{q},0) \right) = \int_0^\beta d\lambda \, Tr \left(\hat{\varrho}_0 \, \hat{J}_\mu(\mathbf{q},t-i\lambda\hbar) \, \hat{J}_\nu(-\mathbf{q},0) \right)$$

$$= \frac{i}{\hbar} \int_t^{t-i\hbar\beta} d\tau \, Tr \left(\hat{\varrho}_0 \, \hat{J}_\mu(\mathbf{q},\tau) \, \hat{J}_\nu(-\mathbf{q},0) \right)$$

$$= \frac{i}{\hbar} \int_t^\infty dt' \, Tr \left\{ \hat{\varrho}_0 \, \left(\hat{J}_\mu(\mathbf{q},t')\hat{J}_\nu(-\mathbf{q},0) - \hat{J}_\mu(\mathbf{q},t'-i\hbar\beta)\hat{J}_\nu(-\mathbf{q},0) \right) \right\}$$

$$= \frac{i}{\hbar} \int_t^\infty dt' \, Tr \left\{ \hat{\varrho}_0 \, \left(\hat{J}_\mu(\mathbf{q},t')\hat{J}_\nu(-\mathbf{q},0) - \hat{J}_\nu(-\mathbf{q},0)\hat{J}_\mu(\mathbf{q},t') \right) \right\}$$

$$= \frac{i}{\hbar} \int_t^\infty dt' \, Tr \left(\hat{\varrho}_0 \, \left[\hat{J}_\mu(\mathbf{q},t'), \hat{J}_\nu(-\mathbf{q},0) \right] \right) \,,$$

where it was assumed that the integrand is analytical.

Derivation of Eq. (1.65) starting from Eq. (1.63):

Integration by part yields,

$$\sigma_{\mu\nu}(\mathbf{q},\omega) = \frac{1}{\hbar V \varpi} \int_0^\infty dt \, \frac{d e^{i\varpi t}}{dt} \int_t^\infty dt' \, Tr \left(\hat{\varrho}_0 \, \left[\hat{J}_\mu(\mathbf{q},t'), \hat{J}_\nu(-\mathbf{q},0) \right] \right) =$$

$$\frac{1}{\hbar V \varpi} \left(\left[e^{i\varpi t} \int_t^\infty dt' \, Tr \left\{ \hat{\varrho}_0 \, \left[\hat{J}_\mu(\mathbf{q},t'), \hat{J}_\nu(-\mathbf{q},0) \right] \right\} \right]_0^\infty + \int_0^\infty dt \, e^{i\varpi t} \, Tr \left\{ \hat{\varrho}_0 \, \left[\hat{J}_\mu(\mathbf{q},t), \hat{J}_\nu(-\mathbf{q},0) \right] \right\} \right)$$

$$= \frac{1}{\hbar V \varpi} \left(\int_0^\infty dt \, e^{i\varpi t} \, Tr \left\{ \hat{\varrho}_0 \, \left[\hat{J}_\mu(\mathbf{q},t), \hat{J}_\nu(-\mathbf{q},0) \right] \right\} - \int_0^\infty dt' \, Tr \left\{ \hat{\varrho}_0 \, \left[\hat{J}_\mu(\mathbf{q},t'), \hat{J}_\nu(-\mathbf{q},0) \right] \right\} \right)$$

$$= \frac{\Sigma_{\mu\nu}(\mathbf{q},\varpi) - \Sigma_{\mu\nu}(\mathbf{q},0)}{\varpi}$$

with definition of the current-current correlation function, $\Sigma_{\mu\nu}(\mathbf{q},\varpi)$ taken from Eq. (1.64).

Derivation of Eq. (1.71):

$$Tr\left(\hat{\varrho}_0\left[\hat{J}_\mu(\mathbf{q},t'),\hat{J}_\nu(-\mathbf{q},0)\right]\right) = \sum_{nmp}\langle n|\hat{\varrho}_0|p\rangle\langle p|e^{\frac{i}{\hbar}\hat{H}_0t'}\hat{J}_\mu(\mathbf{q})e^{-\frac{i}{\hbar}\hat{H}_0t'}|m\rangle\langle m|\hat{J}_\nu(-\mathbf{q})|n\rangle$$

$$-\sum_{mnp}\langle m|\hat{\varrho}_0|p\rangle\langle p|\hat{J}_\nu(-\mathbf{q})|n\rangle\langle n|e^{\frac{i}{\hbar}\hat{H}_0t'}\hat{J}_\mu(\mathbf{q})e^{-\frac{i}{\hbar}\hat{H}_0t'}|m\rangle$$

$$=\sum_{nm}f(\varepsilon_n)e^{\frac{i}{\hbar}\varepsilon_nt'}J_\mu^{nm}(\mathbf{q})e^{-\frac{i}{\hbar}\varepsilon_mt'}J_\nu^{mn}(-\mathbf{q}) - \sum_{mn}f(\varepsilon_m)J_\nu^{mn}(-\mathbf{q})e^{\frac{i}{\hbar}\varepsilon_nt'}J_\mu^{nm}(\mathbf{q})e^{-\frac{i}{\hbar}\varepsilon_mt'}$$

$$=\sum_{nm}\{f(\varepsilon_n)-f(\varepsilon_m)\}\,e^{\frac{i}{\hbar}(\varepsilon_n-\varepsilon_m)t'}\,J_\mu^{nm}(\mathbf{q})J_\nu^{mn}(-\mathbf{q})\,.$$

Derivation of Eq. (1.97) using Eq. (1.94):

$$\operatorname{Re}\Sigma_{\mu\nu}(\omega) \equiv \frac{1}{2}\left(\Sigma_{\mu\nu}(\omega)+\Sigma_{\mu\nu}(\omega)^*\right) = -\frac{1}{4\pi V}\int_{-\infty}^{\infty}d\varepsilon\,f(\varepsilon)$$

$$\times\left\{Tr\left(\hat{J}_\mu\hat{G}^+(\varepsilon+\hbar\omega)\hat{J}_\nu\left[\hat{G}^+(\varepsilon)-G^-(\varepsilon)\right]\right) + Tr\left(\hat{J}_\mu\left[\hat{G}^+(\varepsilon)-G^-(\varepsilon)\right]\hat{J}_\nu\hat{G}^-(\varepsilon-\hbar\omega)\right)\right.$$

$$\left.+Tr\left(\hat{J}_\mu\hat{G}^-(\varepsilon+\hbar\omega)\hat{J}_\nu\left[\hat{G}^-(\varepsilon)-G^+(\varepsilon)\right]\right) + Tr\left(\hat{J}_\mu\left[\hat{G}^-(\varepsilon)-G^+(\varepsilon)\right]\hat{J}_\nu\hat{G}^+(\varepsilon-\hbar\omega)\right)\right\}$$

$$=-\frac{1}{4\pi V}\int_{-\infty}^{\infty}d\varepsilon\,f(\varepsilon)\left\{Tr\left(\hat{J}_\mu\left[\hat{G}^+(\varepsilon+\hbar\omega)-\hat{G}^-(\varepsilon+\hbar\omega)\right]\hat{J}_\nu\left[\hat{G}^+(\varepsilon)-G^-(\varepsilon)\right]\right)\right.$$

$$\left.-Tr\left(\hat{J}_\mu\left[\hat{G}^+(\varepsilon)-G^-(\varepsilon)\right]\hat{J}_\nu\left[\hat{G}^+(\varepsilon-\hbar\omega)-\hat{G}^-(\varepsilon-\hbar\omega)\right]\right)\right\} = \frac{1}{\pi V}\int_{-\infty}^{\infty}d\varepsilon\,f(\varepsilon)$$

$$\times\left\{Tr\left(\hat{J}_\mu\operatorname{Im}\hat{G}^+(\varepsilon+\hbar\omega)\hat{J}_\nu\operatorname{Im}\hat{G}^+(\varepsilon)\right) - Tr\left(\hat{J}_\mu\operatorname{Im}\hat{G}^+(\varepsilon)\hat{J}_\nu\operatorname{Im}\hat{G}^+(\varepsilon-\hbar\omega)\right)\right\}$$

$$=\frac{1}{\pi V}\int_{-\infty}^{\infty}d\varepsilon\,(f(\varepsilon)-f(\varepsilon+\hbar\omega))\,Tr\left(\hat{J}_\mu\operatorname{Im}\hat{G}^+(\varepsilon+\hbar\omega)\hat{J}_\nu\operatorname{Im}\hat{G}^+(\varepsilon)\right)\,,$$

where the last step was obtained by shifting the argument of integration by $\hbar\omega$ in the second term of last but one row.

Derivation of Eq. (1.105) starting from Eq. (1.101):

$$
\sigma_{\mu\nu} = -\frac{\hbar}{2\pi V} \int_{-\infty}^{\infty} d\varepsilon \, f(\varepsilon)
$$

$$
\times Tr\left(\hat{J}_\mu \frac{\partial \hat{G}^+(\varepsilon)}{\partial \varepsilon} \hat{J}_\mu \left[\hat{G}^+(\varepsilon) - \hat{G}^-(\varepsilon) \right] - \hat{J}_\mu \left[\hat{G}^+(\varepsilon) - \hat{G}^-(\varepsilon) \right] \hat{J}_\mu \frac{\partial \hat{G}^-(\varepsilon)}{\partial \varepsilon} \right)
$$

$$
= -\frac{\hbar}{2\pi V} \int_{-\infty}^{\infty} d\varepsilon \, f(\varepsilon) Tr\left(\hat{J}_\mu \frac{\partial}{\partial \varepsilon} \left[\hat{G}^+(\varepsilon) - \hat{G}^-(\varepsilon) \right] \hat{J}_\mu \left[\hat{G}^+(\varepsilon) - \hat{G}^-(\varepsilon) \right] \right)
$$

$$
= -\frac{\hbar}{4\pi V} \int_{-\infty}^{\infty} d\varepsilon \, f(\varepsilon) \frac{\partial}{\partial \varepsilon} Tr\left(\hat{J}_\mu \left[\hat{G}^+(\varepsilon) - \hat{G}^-(\varepsilon) \right] J_\mu \left[\hat{G}^+(\varepsilon) - \hat{G}^-(\varepsilon) \right] \right)
$$

$$
= \underbrace{\left[-\frac{\hbar}{4\pi V} f(\varepsilon) \, Tr\left(\hat{J}_\mu \left[\hat{G}^+(\varepsilon) - \hat{G}^-(\varepsilon) \right] J_\mu \left[\hat{G}^+(\varepsilon) - \hat{G}^-(\varepsilon) \right] \right) \right]_{-\infty}^{\infty}}_{=0}
$$

$$
- \frac{\hbar}{4\pi V} \int_{-\infty}^{\infty} d\varepsilon \left(-\frac{df(\varepsilon)}{d\varepsilon} \right) Tr\left(\hat{J}_\mu \left[\hat{G}^+(\varepsilon) - \hat{G}^-(\varepsilon) \right] \hat{J}_\mu \left[\hat{G}^+(\varepsilon) - \hat{G}^-(\varepsilon) \right] \right) .
$$

Bibliography

[1] P. Weinberger, Physics Reports **377**, 281 (2003).

[2] J. Smith, Physica **16**, 612 (1951).

[3] M.C. Cadeville and B. Loegel, J. Phys. F **3**, L115 (1973).

[4] I.A. Campbell, A. Fert, and O. Jaoul, J. Phys. C **3**, S95 (1970).

[5] I.A. Campbell, J. Phys. F **4**, L181 (1974).

[6] L. Berger and S.A. Friedberg, Phys. Rev. **165**, 670 (1968).

[7] C. Blaas, P. Weinberger, L. Szunyogh, P.M. Levy, and C.B. Sommers
Phys. Rev. B **60**, 492 (1999).

[8] C. Blaas, L. Szunyogh, P. Weinberger, C. Sommers, and P.M. Levy
Phys. Rev. B **63**, 224408 (2001).

[9] P. Weinberger, L. Szunyogh, C. Blaas, and C. Sommers, Phys. Rev. B **64**, 184429 (2001).

[10] H.C. Herper, P. Weinberger, A. Vernes, L. Szunyogh, and C. Sommers,
Phys. Rev. B **64**, 184442 (2001).

[11] H.C. Herper, P. Weinberger, L. Szunyogh, and C. Sommers,
Phys. Rev. B **66**, 064426 (2002).

[12] J. Bahnhart and H. Ebert, Europhys. Lett. **32**, 517 (1995).

[13] J. Banhart, A. Vernes, and H. Ebert, Solid State Comm. **98**, 129 (1996).

[14] H. Ebert, A. Vernes, and J. Banhart, Solid State Comm. **113**, 103 (2000).

[15] P. Grünberg, Physics Today **54/5**, 31 (2001).

[16] D.J. Schiffrin, MRS Bulletin **26/12**, 1015 (2001).

[17] L. Szunyogh, B. Újfalussy, P. Weinberger, and J. Kollár
Phys. Rev. B **49**, 2721 (1994).

[18] P. Weinberger: "*Electron Scattering Theory for Ordered and Disordered Matter*", Oxford (1990).

[19] P. Weinberger and L. Szunyogh, Comp. Mat. Sci. **17**, 414 (2000).

[20] R. Kubo, M. Toda, N. Hashitsume, "*Statistical physics II: Non-equilibrium Statistical Mechanics*", Springer, Berlin (1985);
R. Kubo, J. Phys. Soc. Jpn. **12**, 570 (1957).

[21] D.A. Greenwood, Proc. Phys. Soc. London **71**, 585 (1958).

[22] W.H. Butler, Phys. Rev. B **31**, 3260 (1985).

[23] P. Weinberger, P.M. Levy, J. Banhart, L. Szunyogh, and B. Újfalussy
J. Phys.: Cond. Mat. **8**, 7677 (1996).

[24] J. Banhart, H. Ebert, P. Weinberger, and J. Voitländer
Phys. Rev. B **50**, 2104 (1994).

[25] R. Zeller, P.H. Dederichs, B. Újfalussy, L. Szunyogh, and P. Weinberger
Phys. Rev. B **52**, 8807 (1995).

[26] B. Lazarovits, L. Szunyogh, and P. Weinberger, Phys. Rev. B **65**, 104441 (2002).

[27] B. Lazarovits: "*Electronic and magnetic properties of nanostructures*"
Dissertation, TU Vienna (2003).

[28] L. Dulca, J. Banhart, and G. Czycholl, Phys. Rev. B 61, 16502 (2000).

[29] A. Enomoto, S. Kurokawa, and A. Sakai, Phys. Rev. B **65**, 125410 (2002).

[30] J.W.T. Heemskerk, Y. Noat, D.J. Bakker, J.M. van Ruitenbeek, B.J. Thijsse, and P. Klaver, Phys. Rev. B **67**, 115416 (2003).

[31] J.M. Krans, I.K. Yanson, Th.C.M. Govaert, R. Hesper, and J.M. van Ruitenbeek, Phys. Rev. B **48**, 14721 (1993).

[32] M. Brandbyge, J. Schiøtz, M.R. Sørensen, P. Stoltze, K.W. Jacobsen, J.K. Nørskov, L. Olesen, E. Laegsgaard, I. Stensgaard, and F. Besenbacher, Phys. Rev. B **52**, 8499 (1995).

[33] R.H.M. Smit, C. Untiedt, A.I. Yanson, and J.M. van Ruitenbeek, Phys. Rev. Lett. **87**, 266102 (2001).

[34] N. Agraït, A.L. Yeyati, and J.M. van Ruitenbeek, Phys. Rep. **377**, 81 (2003).

[35] M. Brandbyge, N. Kobayashi, and M. Tsukada, Phys. Rev. B **60**, 17064 (1999).

[36] A.K. Solanki, R.F. Sabiryanov, E.Y. Tsymbal, and S.S. Jaswal, J. Magn. Magn. Mat., in press.

[37] V.S. Stepanyuk, P. Bruno, A.L. Klavsyuk, A.N. Baranov, W. Hergert, A.M. Saletsky, and I. Mertig, Phys. Rev. B **69**, 033302 (2004).

[38] N. Papanikolaou, J. Opitz, P. Zahn, and I. Mertig, Phys. Rev. B **66**, 165441 (2002).

[39] J. Opitz, P. Zahn, and I. Mertig, Phys. Rev. B **66**, 245417 (2002).

[40] R. Landauer, IBM J. Res. Dev. **1**, 223 (1957); Z. Phys. B **21**, 247 (1975); Z. Phys. B **68**, 217 (1987); IBM J. Res. Dev. **32**, 306 (1988); J. Phys. Cond. Matter **1**, 8099 (1989).

[41] M. Büttiker, Phys. Rev. Lett. **57**, 1761 (1986); IBM J. Res. Dev. **32**, 317 (1988).

[42] J.M. Luttinger, in *"Mathematical Methods in Solid State and Superfluid Theory"* (Oliver and Boyd, Edinburgh) Chap. 4, pp. 157 (1962).

[43] H.U. Baranger and A.D. Stone, Phys. Rev. B **40**, 8169 (1989).

[44] A. Halbritter, Sz. Csonka, O. Yu. Kolesnychenko, G. Mihály, O.I. Shklyarevskii, and H. van Kempen, Phys. Rev. B **65**, 045413 (2002); Sz. Csonka, A. Halbritter, G. Mihály, E. Jurdik, O.I. Shklyarevskii, S. Speller, and H. van Kempen, Phys. Rev. Lett. **90**, 116803 (2003).

[45] C.J. Muller, J.M. van Ruitenbeek, and L.J. de Jongh,
Phys. Rev. Lett. **69**, 140 (1992).

[46] M.F. Crommie, C.P. Lutz, and D.M. Eigler, Science **262**, 219 (1993).

[47] J.K. Gimzewski and R. Möller, Phys. Rev. B **36**, 1284 (1987).

[48] N.F. Mott, Adv. Phys. **13**, 325 (1964).

[49] J. Korringa, Physica **13**, 392 (1947).

[50] W. Kohn and N. Rostoker, Phys. Rev. **94**, 1111 (1954).

[51] A. Gonis: *"Green Functions for Ordered and Disordered Systems"*
North Holland (1990).

[52] G.A. Korn and T.M. Korn: *"Mathematical handbook for scientists and engineers"*, McGraw-Hill, New York (1961).

[53] E. Badralexe and A.J. Freeman, Phys. Rev. B **36**, 1401 (1987).

[54] P. Lloyd, Proc. Phys. Soc. **90**, 207 (1967).

[55] P. Lloyd and P.V. Smith, Advances in Physics **21**, 69 (1972).

[56] M.E. Rose: *"Relativistic Electron Theory"*, Wiley, New York (1961).

[57] A. Messiah: *"Quantum Mechanics"*, North Holland, Amsterdam (1969).

[58] S.L. Altmann and P. Herzig: *"Point Group Theory Tables"*, Oxford (1994).

[59] B.L. Györffy and M.J. Stott: *"Band structure spectroscopy of metals and alloys"* (ed. D.J. Fabian and L.M. Watson), Academic Press, London (1973).

[60] M. Abramovitz and I.A. Stegun: *"Handbook of mathematical functions"*
Dover Publications, New York (1972).

[61] L. Szunyogh, B. Újfalussy, and P. Weinberger, Phys. Rev. B **51**, 9552 (1995).

[62] R. Podloucky, R. Zeller, and P.H. Dederichs, Phys. Rev. B **22**, 5777 (1980).

[63] P. Weinberger, R. Dirl, A.M. Boring, A. Gonis, and A.J. Freeman
Phys. Rev. B **37**, 1383 (1988).

[64] P.H. Dederichs and R. Zeller, Phys. Rev. B **28**, 5462 (1983).

[65] D.D. Johnson, Phys. Rev. B **38**, 12807 (1988).

[66] H. Ehrenreich and L.M. Schwartz, Solid State Physics **31**, 149 (1976).

[67] J.S. Faulkner and G.M. Stocks, Phys. Rev. **B23**, 5623 (1981).

[68] P. Soven, Phys. Rev. **156**, 809 (1967).

[69] R. Mills, L.J. Gray, and T. Kaplan, Phys. Rev. B **27**, 3252 (1983).

[70] B. Ginatempo and J.B. Staunton, J. Phys. F: Met. Phys. **18**, 1827 (1988).

[71] P. Mavropoulos, N. Papanikolaou, and P.H. Dederichs
Phys. Rev. B **69**, 125104 (2004).

[72] S.H. Vosko, L. Wilk, and M. Nusair, Can. J. Phys. **58**, 1200 (1980).

[73] J. Alvarez, E. Lundgren, X. Torrelles, and S. Ferrer,
Surf. Sci. **464**, 165 (2000).

[74] W. Döring, Ann. Physik **32**, 259 (1938).

[75] P. Weinberger, L. Szunyogh, C. Blaas, C. Sommers, and P. Entel
Phys. Rev. B **63**, 094417 (2001).

[76] T.R. McCuire and R.I. Potter, IEEE Trans. Mag. **11**, 1018 (1975).

[77] B. Lazarovits, L. Szunyogh, and P. Weinberger, Phys. Rev. B **68**, 024433 (2003).

[78] J.A. Torres, J.I. Pascual, and J.J. Sáenz, Phys. Rev. B **49**, 16581 (1994).

[79] U. Fano, Phys. Rev. **124**, 1866 (1961).

[80] V. Madhavan, W. Chen, T. Jamneala, M.F. Crommie, and N.S. Wingreen,
Science **280**, 567 (1998).

[81] H.C. Manoharan, C.P. Lutz, and D.M. Eigler, Nature **403**, 512 (2000).

[82] O. Újsághy, J. Kroha, L. Szunyogh, and A. Zawadowski,
Phys. Rev. Lett. **85**, 2557 (2000);
O. Újsághy, G. Zaránd, and A. Zawadowski, Solid State Comm. **117**, 167 (2001).

[83] H. Eschrig: *"The fundamentals of Density Functional Theory"*
Teubner, Leipzig (1996).

[84] P. Hohenberg and W. Kohn, Phys. Rev. **136**, B864 (1964).

[85] W. Kohn and L.J. Sham, Phys. Rev. **140**, A1113 (1965).

[86] O. Gunnarson and B.I. Lundqvist, Phys. Rev. B **13**, 4274 (1976).

[87] A.K. Rajagopal and J. Callaway, Phys. Rev. B **7**, 1912 (1973).

[88] A.K. Rajagopal, J. Phys. C: Solid State Phys. **11**, L943 (1978).

[89] A.H. MacDonald and S.H. Vosko, J. Phys. C: Solid State Phys. **12**, 2977 (1979).

[90] G. Vignale and M. Rasolt, Phys. Rev. Lett. **59**, 2360 (1987).

[91] G. Vignale and M. Rasolt, Phys. Rev. B **37**, 10685 (1988).

[92] A.H. MacDonald, J.M. Daams, S.H. Vosko, and D.D. Koelling
Phys. Rev. B **25**, 713 (1982).

List of publications

Publications in refereed journals connected to my PhD work

1. K. Palotás, B. Lazarovits, L. Szunyogh, and P. Weinberger
   Ab initio studies of electric transport in terms of the real space Kubo-Greenwood equation
   Phys. Rev. B **67**, 174404 (2003)

2. S. Khmelevskyi, K. Palotás, L. Szunyogh, and P. Weinberger
   Ab initio calculation of the anisotropic magnetoresistance in $Ni_{1-c}Fe_c$ bulk alloys
   Phys. Rev. B **68**, 012402 (2003)

3. K. Palotás, B. Lazarovits, P. Weinberger, and L. Szunyogh
   Electric transport in nanostructures: real space ab initio investigations
   J. Magn. Magn. Mat., in press (contribution to ICM 2003)

4. K. Palotás, B. Lazarovits, L. Szunyogh, and P. Weinberger
   Ab initio studies of electric transport in gold nanocontacts
   submitted to Phys. Rev. B, manuscript number: BQ9186 (2004),
   cond-mat/0403282 (2004)

Further publications

1. L. Udvardi, L. Szunyogh, K. Palotás, and P. Weinberger
   First principles fully relativistic study on low energy magnetic excitations in thin films
   Bull. Am. Phys. Soc., **48**, 521 (2003)

2. L. Udvardi, L. Szunyogh, K. Palotás, and P. Weinberger
   First principles relativistic study on spin waves in thin magnetic films
   Phys. Rev. B **68**, 104436 (2003)

3. L. Udvardi, L. Szunyogh, K. Palotás, and P. Weinberger
   First principles fully relativistic study on low energy magnetic excitations of thin films
   J. Magn. Magn. Mat., in press (contribution to ICM 2003)

Conferences, seminars

1. Poster *'Magnon spectra of bulk and layered materials by means of fully relativistic KKR method'*
   European Graduate School of Condensed Matter, June 9-15, 2001, Prague, Czech Republic

2. Talk *'Transport properties of magnetic nanostructures using real-space Kubo-formalism'*
   Evaluation of the CMS-Science College, January 7, 2002, Vienna, Austria

3. Poster *'Electric transport in nanostructures: real space ab-initio investigations'*
   International Conference of Magnetism, July 27-Aug.1, 2003, Rome, Italy

4. Talk *'Electrical transport properties of nanostructures using the real space Kubo-Greenwood equation'*
   CMS-Science College Seminar, November 10, 2003 Vienna, Austria

Acknowledgements

Curriculum Vitae

Personal data

Name:	Krisztián Palotás
Birthdate, place:	December 16, 1977 ; Békéscsaba (Hungary)
Nationality:	Hungarian
Family status:	single
Permanent address:	H-5600 Békéscsaba, Fövenyesstr. 12., Hungary
Mailing address:	Center for Computational Materials Science (CMS), Gumpendorferstrasse 1A/4.OG., A-1060 Vienna, Austria
Phone:	+43/1/58801-15841
Fax:	+43/1/58801-15898
E-mail:	kp@cms.tuwien.ac.at, h0027589@wu-wien.ac.at

Education

1984-1992   Elementary school in Békéscsaba

1992-1996   Ferenc Rózsa Secondary School, Békéscsaba (special Mathematics)

Studies

Sept.1996-June 2001	Engineering Physics study at the Budapest University of Technology and Economics, Hungary (specialization: condensed matters)
July 24-Aug.3, 2000	Internship in CMS
March-June 2001	Fellowship in CMS, writing diploma thesis 'Magnon-spectra in bulk Fe. A relativistic approach', supervisor: Dr. László Udvardi, collaboration with Univ.-Prof. Dr. Peter Weinberger
June 25, 2001	diploma degree (MSc. in Engineering Physics)
since October 2001	Doctorate study of Technical Sciences at the Vienna University of Technology, Austria, supervisor: Univ.-Prof. Dr. Peter Weinberger, collaboration with Dr. László Szunyogh
since March 2003	Information Systems study at the Vienna University of Economics and Business Administration, Austria

Computer skills

Windows/Linux/DOS // Java/Fortran/Pascal/Basic/C // HTML/XML //
Data modelling/UML // MS-Office/LaTeX, etc.

Language skills

Hungarian (native)
German (fluent)
English (good)
Polish (basic level)